Bee Gustatory Neurons Encode Sugar Concentration as a Coherent Temporal Pattern of Spiking

Ashwin Miriyala

Thesis submitted to the Faculty of Medical Sciences,
Newcastle University
In partial fulfilment of the requirements for the degree of
Doctor of Philosophy

April 2017

Newcastle University

Abstract

Individual peripheral gustatory neurons in insects encode stimulus category (e.g. sweet, bitter) and concentration as a tonic rate of spiking that adapts with prolonged stimulation. While individual chemosensory neurons have been shown to interact through mutual inhibition, this interaction does not affect stimulus coding by the activated neuron. Here, I report the first evidence of a coherent, temporal pattern of spiking produced by the interaction of the gustatory receptor neurons (GRNs) within sensilla present on the mouthparts of bumblebees (*Bombus terrestris*) that encodes information about sugar concentration. Stimulation of gustatory sensilla with sucrose concentrations >10 mM elicited bursts of spikes riding on an oscillation in voltage of ~20 Hz. The concentration response function of spiking and bursting was sugar-identity specific, and only concentrations that produced bursting in the GRNs elicited the bee's feeding reflex. Bursting bee GRNs exhibited a low rate of adaptation (0.002 s adaptation after 1 s of stimulation) compared to rates measured from other insect species' GRNs. These data are the first to show that primary chemosensory neurons encode stimulus features such as concentration as a coherent temporal pattern of spiking produced as an interaction between two neurons. I propose that 1) the silent period between bursts is driven by the spike after-hyperpolarization of one neuron, which inhibits spiking of its neighboring neuron through an inhibitory lateral interaction, and 2) bursting is a novel mechanism evolved to allow persistent high frequency spiking during fluid consumption. Finally, I show that neural activity can be monitored from the bee's central nervous system, which allows future experiments to question the function of this coherent and structured GRN activity in driving post-synaptic responses.

Acknowledgements

I'd like to start by thanking my project supervisors, both past and present, who have made this PhD possible. Jeri, one of the main reasons I'm still in science is because I get to explore questions that I find interesting, and you've let me do just that throughout my PhD. It's been amazing nurturing this project with you for so many years, and I really hope we get a chance to push it even further. Also, thanks to Mark Stopfer and the members of his lab, the techniques I learned from each one of you was fundamental for me to progress through this PhD. And of course Joby, I don't think you'll ever really stop being a supervisor for me for as long as I stay in research. Your approach to scientific deduction is still reflected in my work after all these years.

I'd also like to thank my family for supporting my decision to stay in research. Also, the amount of trust you have in me means a lot to me, and I can tell that you're proud of me every time I talk to you. And my room mate Shrinivas, I'm glad that someone got to see me grow both as an individual and as a researcher. Thanks for all the conversations and laughs bro. Finally, I'd like to extend this thanks to the members of Jeri's lab, for the endless entertainment and support that you've provided.

Table of contents

Abbreviations

µm	micrometer
mm	millimeter
mM	millimole
s	seconds
Hz	Hertz
AHP	After-Hyperpolarization
AL	Antennal Lobe
ARP	Absolute Refractory Period
ET	Esophageal Tract
FLD	Fisher’s Linear Discriminant
GR	Gustatory Receptor
GRN	Gustatory Receptor Neuron
IR	Ionotropic Receptor
ISI	Inter Spike Interval
Lb	Labia
LbN	Labial Nerve
Md	Mandible
MdN	Mandibular Nerve
Mx	Maxilla
MxN	Maxillary Nerve
OR	Olfactory Receptor
ORN	Olfactory Receptor Neuron

PCA	Principal Component Analysis
SEZ	Sub-Esophageal Zone
TEM	Transmission Electron Microscopy
TRP	Transient Receptor Potential

Chapter 1. General Introduction

1.1 Abstract

One of the primal instincts of any living animal is to feed. To identify palatable food, animals ranging from insects to vertebrates have developed efficient neural circuits that mediate the sense of taste, known as gustation. The gustatory circuit functions to encode taste stimuli into information that can be interpreted by the brain. The brain then coordinates behaviors that enables the location of food and quick avoidance of potentially harmful compounds. Given that taste is such a fundamental sense, exploring its structural and functional organization can help reveal the basic principles underlying sensory coding and behavior.

A large contribution to understanding the mechanisms of gustation comes from studies in insects. In this chapter, I describe the organization, structure and function of the insect gustatory neurons at the periphery and their first synaptic relay within the sub-esophageal zone (SEZ) of the brain. In particular, I will focus on the coding strategies used by the GRNs and will compare them to the well studied olfactory circuitry, which like gustation is mediated by chemosensory neurons. I will then describe what is known about gustatory coding within the insect SEZ. Finally, I will discuss how the bumble bee could be used as a model for studying the principles of gustation.

1.2 Introduction

Insects detect food using peripheral gustatory receptor neurons (GRNs). The dendrites of 4-5 GRNs are housed within hair-like structures called contact chemoreceptor sensilla (figure 1.1 a), which are distributed on the mouthparts, antennae, feet, wings and ovipositor (for reviews see [1]–[3]. When the sensillum comes in contact with a tastant, the tastant molecules activate receptors present on the GRN dendrites, which evokes a train of action potentials (spikes) from the GRN soma [4]–[6]. The GRN spike train encodes for concentration as well as the taste category to which the stimulus belongs to, i.e. bitter (and other aversive compounds), sweet, water (or solutions with low osmolarity), and salt [1], [7]–[11].

The GRN axons project onto post-synaptic neurons in the SEZ (figure 1.1 b), which is the first region of gustatory processing in the insect brain [11]–[13]. Several interneurons separate these GRN axons from the motor neurons that are located in the SEZ [14], [15]. These interneurons integrate GRN input, along with input from other senses such as olfaction [12] and internal cues such as satiety [16]–[19]. They then synapse onto motor neurons to drive the initiation, continuation or cessation of feeding.

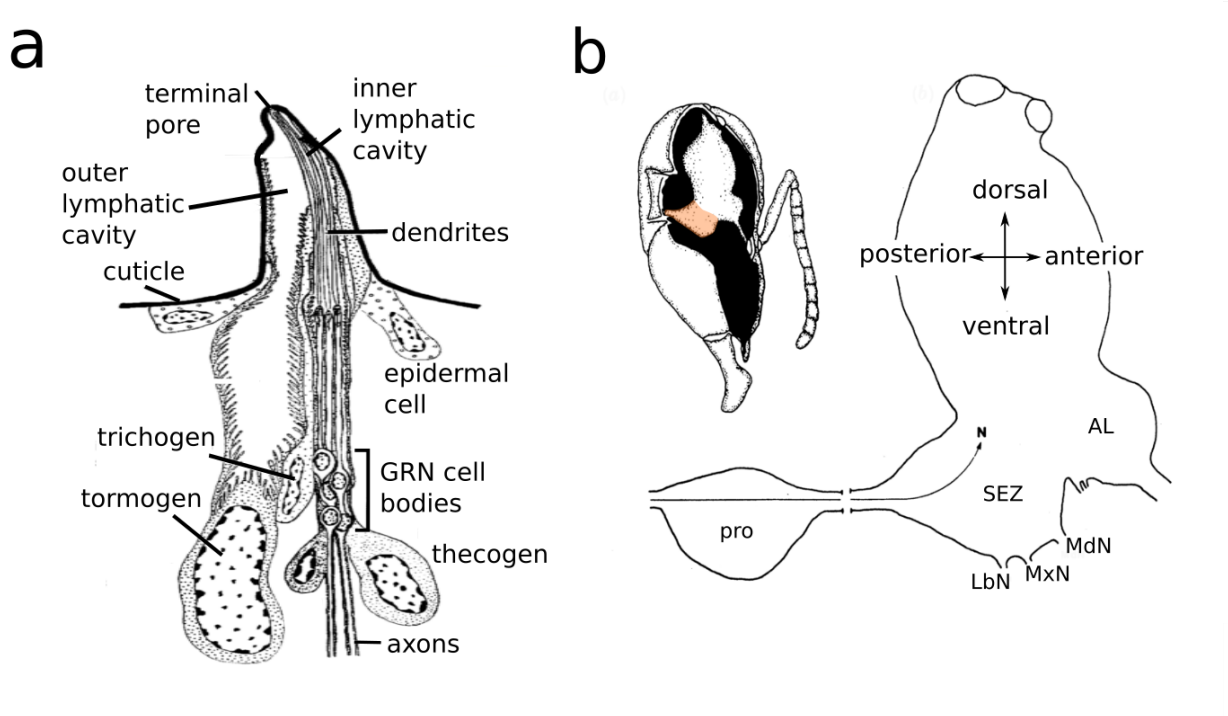

Figure 1. Insect gustatory machinery. a) *Diagram of a typical insect contact chemosensillum (figure modified from [20]), showing accessory cells and GRNs.* ***b)*** *Side-view of the brain of a honey bee (modified from Snodgrass 1956). GRN axons enter the SEZ, which is located below the esophagus. The SEZ is fused to the brain in bees [22], flies [12], [15] and lepidopterans [20]. In comparison, insects such as cockroach [23] and locusts [24] have circumesophageal connectives that separates the brain and the SEZ.*

1.2.1 Structure and function of GRNs

The sense of taste starts within the sensilla. When the sensillum comes in contact with a chemical compound, the molecules enter its terminal pore and activate receptors present on the GRN dendrites. Imaging and genetic studies in *Drosophila* have revealed a variety of receptor types that interact with tastants. Most sweet compounds, as well as some pheromones and cuticular hydrocarbons, bind to gustatory receptors (Grs) [25], [26]. Grs are suggested to form ligand-activated cation channels [27][28], similar to olfactory receptors (ORs, [29], [30]). However, some reports suggest that Grs could also be G-protein coupled receptors [27]. GR5a, GR64a and GR64f are required by *Drosophila* for sensing most sugars except for fructose [31], [32], whereas GR43a responds specifically to fructose [33]. Gustatory receptors are also responsible for detection of aversive bitter compounds such as caffeine, and in *Drosophila* include Gr 32a, Gr33a, Gr39a, Gr66a and Gr89a [34]. Some aversive compounds such as aristolochic acid [35] and camphor [36] activate transient receptor potential (TRP) cation channels via a transduction pathway involving phospolipase C [37]. TRP channels are largely permeable to Ca^{2+}. Another class of receptors, the ionotropic receptors (IRs), are activated by ligands such as Na^{+} ions and signal the presence of low concentrations of salt [38] as well as pheromones [39]. The ppk28 receptor, which belongs to the family of pickpocket receptors, mediates the detection of pure water or low osmolarity solutions [40].

When a receptor is activated, it initiates an intracellular signal transduction mechanism that involves a combination of secondary messengers [41], [42] and cation channels [28], [37]. Ca^{2+} imaging in *Xenopus* oocyte cells that expressed *Bombyx mori* Gr9 revealed that they responded to fructose with an influx of extracellular Ca^{2+} [28]. Using electrophysiology techniques that allow for monitoring neural activity extracellular to the GRNs within individual sensilla [4], [43], it was revealed that the signal transduction process generates a low frequency (<10 Hz) receptor potential across the dendritic membrane [44]. The receptor potential is passively transmitted along the dendrite towards the GRN soma, located some tens of microns below the base of the sensillum [20], [45], where it evokes a train of spikes [46]. The spike train encodes stimulus relevant information.

Each GRN within a sensillum expresses receptors that are activated by molecules belonging to individual taste categories. For instance, the GRs and TRP receptors that are activated by bitter molecules and certain aversive compounds are expressed on the 'bitter-sensing' GRN [47], [48]. Similarly, sugar binding GRs are expressed on a 'sweet-sensing' GRN [26], [31], [49], and IRs that are activated by low salt concentrations are expressed on the 'low-salt concentration' sensing' GRN. There is also a GRN responsive to water (low osmolarity; for review see [2]).

1.2.2 Coding at the periphery

Peripheral chemosensory neurons in insects, such as GRNs and olfactory receptor neurons (ORNs), encode quality and quantity of chemical stimuli through a train of action potentials. The coding problem faced by ORNs tend to be quite complex; odours are often composed of hundreds of volatile compounds [50], and changes in odour concentration can lead to changes in perceived qualities (for review see [51]). To deal with this complexity, ORNs use efficient coding strategies (figure 1.2 a). They encode odours through temporally structured spike responses, with structures varying from inhibition of baseline spiking activity to brief periods of excitation and inhibition, and responses outlasting the stimulation period [52], [53]. These temporally diverse responses are spatially distributed across the population of ORNs [53]. Further, ORNs represent concentration in part through the intensity of spike firing [54].

As for odours, the foods insects feed on can be complex with regards to number of constituent tastant molecules. For example, the nectar bees feed on can contain hundreds of individual components [55]. However, GRNs exhibit a different coding strategy as compared to ORNs for dealing with this large stimulus space (figure 1.2 b). As described in section 1.2.1, the activity of each GRN encodes a specific taste category. This has given rise to a 'labeled line' model for gustatory coding, which is suggested to allow for the gustatory system to drastically reduce the complexity arising from a large stimulus space. In fact, early studies suggested that GRNs reduce the stimulus space even further, by classifying all compounds as either 'stimulating' or 'deterrent' [56]. For example, the bitter GRN would be 'deterrent' since it responds to unfavorable high salt concentrations [38] and repellent pheromones [9].

In comparison to ORNs, GRNs exhibit simple patterns of spiking (figure 1.2 b ii). GRN spike trains are typically characterized by a ~0.1 s phasic increase in spiking frequency that gradually adapts to tonic firing over the course of stimulation [7], [57]–[60]. Further, the intensity of the spiking response is found to be concentration dependent [25], [59], [61]–[66]. Ultimately, the activity of GRNs encode taste category, while the rate of firing of action potentials encodes concentration.

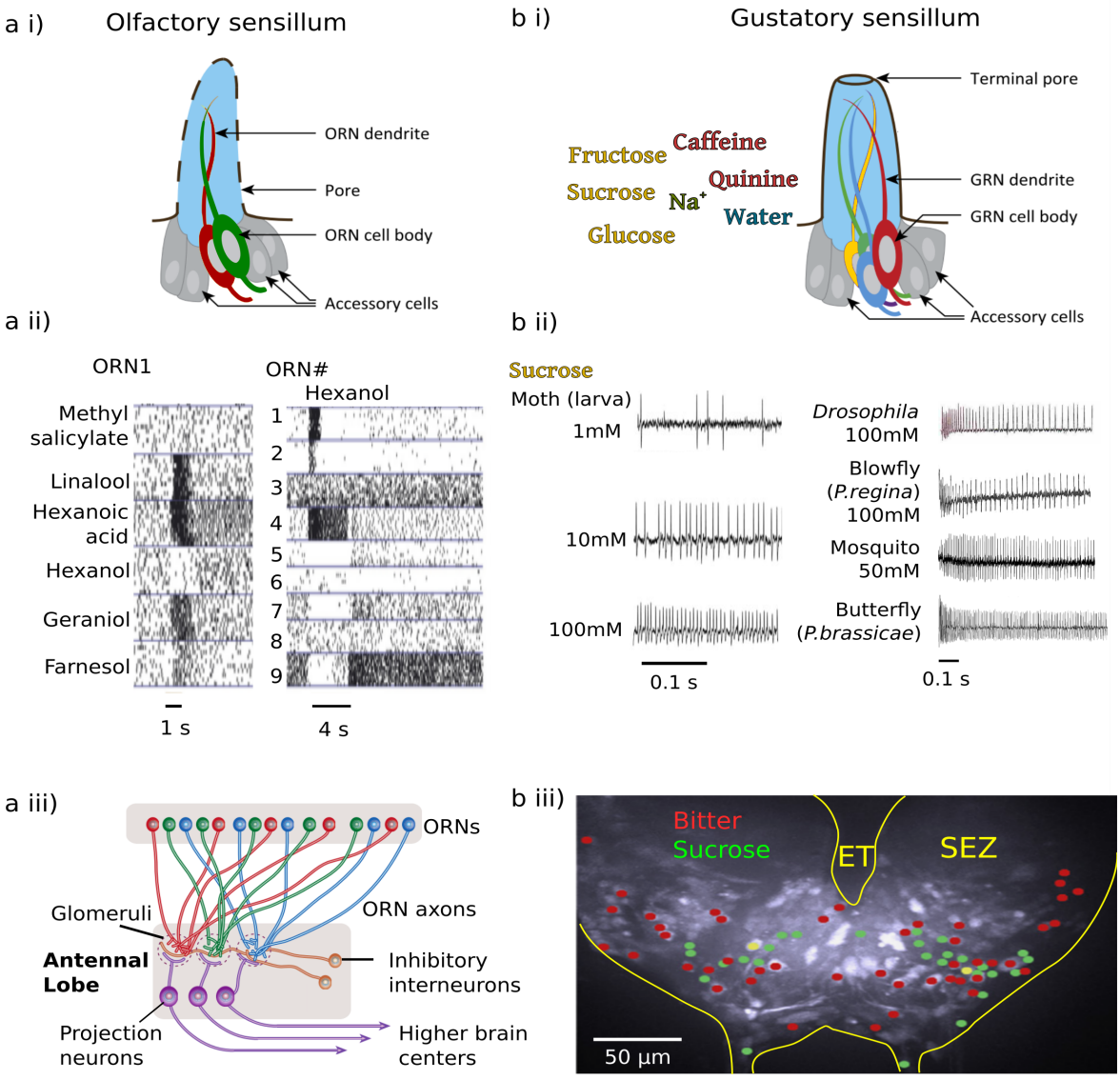

Figure 1.2 (legend on next page)

Figure 1.2 : Olfactory and gustatory coding. a i) *ORNs are located in groups, with two or four units per sensillum [67]. Odour molecules enter the sensillum through pores, and bind to olfactory receptors (ORs). Each ORN expresses one or only a few ORs [68].* ***a ii left)*** *Raster plots for multiple odours (separated by horizontal lines) presented over multiple trials (rows) shows that ORN responses are temporally heterogeneous.* ***a ii right)*** *ORN responses are spatially distributed. Figures modified from [53]* ***a iii)*** *Glomeruli within the AL receive axons of ORNs that express the same OR (indicated by color).* ***b i)*** *Similar to ORNs, the GRNs within a sensillum are tuned to specific groups of tastant chemicals based on the receptors (GRs) they express (represented by colours).* ***b ii left)*** *GRNs encode concentration through rate of firing (recordings from moth, H. virescens [65]).* ***b ii right)*** *Unlike ORN spike responses, GRN responses are not heterogeneous, as shown in Drosophila [8], blowfly (P. regina) [69], mosquito (A. gambiae) [70], butterfly (P. xuthus) [71] and honey bee (A. mellifera) [72].* ***b iii)*** *Sucrose and bitter GRNs synapse onto distinct populations of downstream neurons, similar to the wiring in the olfactory circuit. However, these postsynaptic neurons are spatially distributed in the SEZ (figure from [73]) ET: esophageal tract. Top row of* ***a*** *and* ***b*** *from [3].*

1.2.3 Interactions between chemosensory neurons that could participate in coding

In olfaction, there is evidence that the spiking responses of neighboring ORNs are not completely independent of each other [74]–[76]. For example in a *Drosophila* sensillum, the spiking activity of one ORN appeared to inhibit the activity of its neighboring ORN, and was predicted to do so through a non-synaptic interaction between the two neurons, since there is no evidence for synapses at the level of the chemosensory sensilla [15], [75]. Instead, the interaction was suggested to be driven by a lateral ephaptic interaction. In an ephaptic interaction, the electric field associated with the activity of one neuron affects the excitability of neurons that are in close proximity of it [76]–[78]. In vertebrates, ephaptic coupling between neurons has been shown to inhibit spiking for a few milliseconds [79], or even mediate transmission of spikes between axons of neurons which do not have a myelin sheath [80]. The close proximity of the ORNs within the sensillum environment along with the fact that insect neurons are unmyelinated makes ephaptic coupling possible between these neurons. This suggests that interactions between the ORNs could contribute to olfactory coding at the periphery, which is referred to as an ‘across-fiber’ model for coding.

There are a few inconclusive studies that suggest lateral interactions could occur between GRNs of a sensillum as well. White *et al*. [81] found that the tarsal gustatory sensilla of grasshoppers possess a GRN responsive to nicotine hydrogen tartarate, whose spiking activity inhibited for a brief period of time (order of 0.01 s) by the occasional spontaneous activity of a second GRN. This suggests that the second GRN drives an inhibition that prevents spiking from the first GRN.

White *et al*. suggested that a gap junction could mediate this inhibition. Gap junctions are protein channels that connect neighboring neurons and allow flow of electric current [82], and can therefore mediate transmission of a depolarizing or hyperpolarizing potential between neurons to modulate activity [83]–[86]. Only a few studies report evidence for gap junctions in insect chemosensory neurons. One detailed study of contact chemosensilla in the inner cavity of the cockroach hypopharynx identified gap-junction like articulations among its GRN dendrites (a.k.a inedite jonction intercellulaire, [87]. Similarly, Ma [66] reported connections like gap junctions among the ciliary connective tissues of the GRN dendrites of the maxillary sensillar styloconicum of larvae of the cabbage moth, *Pieris brassica*. These are the only studies I know of where gap-junction like connections have been reported among the dendrites of GRNs. Whether or not this is a general feature of GRNs in insects, therefore, remains uncertain.

The activity of a sugar responsive GRN can also be inhibited by mixing a toxic compound such as quinine with the stimulating solution [70], [88]–[90]. In the same way, the activity of bitter responsive GRNs can be inhibited by the presence of sugars or acids [57]. While this form of inhibition could also convey stimulus relevant information, it arises from direct interaction of the ligand with the signal transduction mechanisms of the sugar-sensing neuron [89]. Overall, peripheral gustatory coding is considered to be driven by ‘labelled lines’, with little cross-talk between GRNs.

1.2.4 Taste integration downstream to the GRNs

The central nervous system integrates input from the peripheral neurons to coordinate behavior. Coding has been well studied in the insect antennal lobe (AL), which receives the

axonal projections of ORNs (figure 1.2 a iii). As described above, the ORNs represent quantity and quality of stimuli through spatially distributed and temporally structured trains of action potentials [53], [54]. ORN axons are organized into glomeruli within the antennal lobe, in accordance to the receptors they express [91]. This structured and organized input along with feedback inhibition from interneurons [92], [93] drives coherent activity from neural ensembles, which aids in stimulus discrimination [94], drives activity in higher brain regions involved in learning and memory [95], and is finally reflected in behavior [74].

Like the AL, the insect SEZ exhibits a certain level of organization of gustatory input. The SEZ receives GRN axonal projections from across the insect's body into specific zones, which reflect their organ of origin [9], [22], [96]. For example, studies in the bee have shown that the majority of the SEZ is divided into the labial, maxillary and mandibular neuromeres, that receive input from those respective mouthpart organs [22]. Further, studies in *Drosophila* have revealed that the axonal projections of the GRNs exhibit a certain level of functional organization as well : sweet, bitter and low-salt responsive GRNs synapse onto mostly non-overlapping (yet spatially distributed) subsets of post-synaptic neurons [31], [38], [48], [73], [97] (figure 1.2 b iii). The activity of sweet-responsive and bitter-responsive GRNs evokes attractive and aversive behaviors, respectively [47].

Studies in *Drosophila* have shown that GRN axons synapse onto interneurons within the SEZ [15]. These interneurons coordinate motor neuron activity which control the various groups of muscles that drive proboscis extension and ingestion [15], [98]. An early study in blowflies suggested that, based on the time taken for muscle activity to be evoked after stimulating a gustatory sensillum, there were at least two orders of interneurons that the GRN input passed through before synapsing onto motor neurons. It was shown in *Drosophila* as well that GRNs do not directly synapse onto motor neurons [15].

Studies in *Drosophila* have revealed the roles of some of these interneurons in integrating GRN input and in controlling feeding motor programs. One such set of GABAergic interneurons was found to drive a selective presynaptic inhibition of sweet GRN axonal input but not bitter GRN input, which could function as a gain mechanism to ensure toxic bitter compounds are not

consumed [92]. A set of four inhibitory GABAergic neurons were discovered which keeps feeding behaviors under inhibition unless they receive excitatory input [99]. A set of 12 cholinergic interneurons were found to be activated by sweet GRN input and modulated by satiety, and functioned to control ingestion [100]. Another set of feeding interneurons were found to control the initiation of feeding [101].

The internal state of the insect plays a role in controlling these feeding circuits as well. For example, thirst in *Drosophila* can convert water avoidance into water seeking behaviors [102]. Hunger can make insects more tolerant to toxins (such as bitter compounds) in food [17], [18]. The internal state could be under neuromodulatory control [17], [18] or even under the control of gustatory receptors that function as nutrient sensors in the brain [33].

The features of the GRN spike train that are important for driving downstream responses are still unknown. Studies in blowfly show that the intensity of GRN spiking activity within the first 0.03 s of stimulation is enough to drive muscle activity [14]. Studies in the blowfly and *Drosophila* suggest that the interneurons retain information regarding the strength of the GRN input, and ultimately drive graded activity from the motor neurons [14], [15]. This suggests that a population of GRNs spiking close to their thresholds is important for driving downstream activity [103]. Recordings from moth GRNs suggest that tastant specific information is initially encoded by spatio-temporal patterns of GRN activity, and that this information is temporally transformed over synapses [103], similar to that observed in the olfactory circuit. The mechanisms driving this transformation of GRN input are yet to be answered.

1.2.5 Gustation in bees

Taste plays an important role in the life cycle of a bee. Worker bees are bestowed with the task of foraging for nectar and pollen, which they convert into honey and bee bread. Bees belong to the order Hymenoptera, along with ants, wasps and sawflies. Like ants and termites, bees are social insects, and therefore the food they collect is used to sustain their entire colony. Honey bees have been shown to pass on information regarding quality and profitability of the

food source to other workers so return trips can be planned, through behaviors like the waggle dance [104].

Nectar and pollen are made up of hundreds of components, including water, carbohydrates, proteins, amino acids, salts, fats, vitamins and minerals [55], [105]. Carbohydrates are of particular importance as they provide the main source of energy for sustained flight and other metabolic processes [106]. In floral nectar, one of the main foods of bees, sucrose, glucose and fructose make up the major carbohydrate constituents to which bees exhibit strong behavioral preferences [107], [108].

The proboscis of bees is specialized for acquiring nectar from flowers. It is comprised of the labium which includes the labial palps and glossa, and the maxillae which includes the maxillary palps and the galea (figure 1.3) [21], [109], [110]. The movement of the proboscis is controlled by several sets of muscles, which have been described in detail by Snodgrass [21]. In particular, the M17 pair of muscles are responsible for the retraction of the entire proboscis, and are commonly recorded from to track feeding behaviors [111], [112]. While feeding nectar, the galea and labial palps form a tube around the glossa through which liquids can be sucked into the mouth through the action of cibarial muscles [21]. The back and forth movement of the glossa functions to draw nectar into the proboscis.

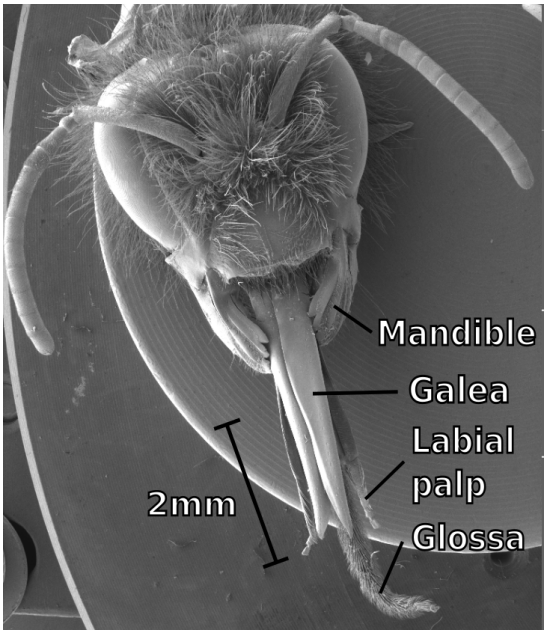

Figure 1.3: Mouthparts of the bumble bee B. terrestris.

Contact chemoreceptor sensilla are distributed on the surface of the bee's mouthparts [45]. Bees have a very small repertoire of functional GRs with which they detect tastants, with 12 in *A. mellifera* and 23 in *B. terrestris* [113], [114]. In comparison, this count is much higher for *D. melanogaster* and *A. gambiae* which have 68 and 76 functional GRs, respectively [115]. This suggests that the bee's gustatory machinery is limited and could be tuned for detecting the subsets of tastants that are essential for their survival.

Studies in honey bees have helped understand how gustatory input is integrated with higher brain regions involved in learning and memory. Classic Pavlovian conditioning shows that bees can form strong associations between a gustatory reward and an olfactory or visual stimulus (for review see [116]). An early study revealed a neuron within the maxillary neuromere of the SEZ (VUMmx1 neuron) that mediates the reward value during this learning process [117]–[119].

Recent behavioral experiments have shown that bumble bees exhibit complicated behaviors that are unique even among insects. For example, they have been shown to learn an operant learning task to acquire sugars [120], [121]. Like honey bees, bumble bees are able to associate an odour with a sugar reward [122] as well. Unlike honey bees, bumble bees do not communicate information about nectar sources through a waggle dance, nor do they exhibit trophollaxis; instead, foragers unload their nectar into honey pots that other foragers can taste to plan foraging trips [123]. Carbohydrates are particularly important for bumble bees as they have a very high metabolic rate for flight [124], and travel for distances up to 3km on each foraging trip [125]. Of the carbohydrates, *B.terrestris* exhibits most preference for sucrose, glucose and fructose [126], [127]. Due to this necessity for carbohydrates, it would not be surprising if bumble bees developed a specific advantage when it comes to detecting them in nectar.

1.3 Future of insect taste study

Insects have been shown to exhibit elegant coding strategies to deal with environmental stimuli to coordinate rapid and complex behaviors. They are by no means a simple model for understanding the coding mechanisms used by sensory circuits. However, they do present a

system that can be manipulated using genetic and electrophysiological techniques which allows for understanding the fundamentals underlying sensory coding. In particular for gustation, it is easier to access individual neurons at different levels of processing using intracellular recording techniques, which allows for studying the coding strategies that occur at the millisecond time scale. *Drosophila* possesses a powerful genetic tool-kit that allows for observing the contribution of specific subsets of neurons. Insects like the honey bee present robust feeding behaviors such as the proboscis extension response (PER) that allows for comparison of qualities of different stimuli.

The principles of gustation in insects are somewhat similar to those of mammals [108], [128]. For example, the mammalian taste receptor cells that express the receptors to which tastants bind are grouped in taste buds [129], with each cell tuned to different taste categories : salt, sweet, bitter, sour and umami (i.e meaty taste, mediated by cells expressing receptors that bind to glutamate) [130]. These taste receptor cells activate primary afferent neurons that carry the information towards several taste processing regions within the brain [1], [2]. Further, the sweet and bitter pathways are found to evoke attractive and aversive behaviors, respectively [131], [132]. Therefore, discoveries made in the insect gustatory system can help elucidate how animals have solved the problem of the coordination of feeding and the representation of taste stimuli in the brain.

Finally, while the coding strategies used by the peripheral taste neurons have been well documented, there are still many questions that remain to be answered regarding how taste is integrated at downstream regions. Studies in *Drosophila* are starting to unravel the function of the neurons within the SEZ, and experiments in bees are revealing the complexity of the involvement of learning and memory in driving decisions to feed. Future research will reveal whether the gustatory circuitry has evolved to reduce the vast tastant stimulus space into only a few perceived taste categories, or whether the brain has a role in reconstructing the input based on spatially and temporally structured activity. The latter case would allow for an expansion in the number of perceived tastes, or allow for a more detailed discrimination between quality and quantity of different tastant chemicals, similar to what is found in olfaction.

Chapter 2.0 Spike Sorting and Burst Detection in Sensillum Recordings

2.1 Abstract

In insects, gustatory receptor neurons (GRNs) are responsible for encoding taste information through trains of action potentials. The activity of groups of GRNs within individual sensilla can be recorded using the tip and tungsten extracellular recording techniques. These recordings can then be coupled with spike sorting and analyses of spike timing to understand how the population of GRNs encodes taste information. However, existing spike sorting methods available for sensillum recordings produces an output that is limited in interpretation, primarily because they sort spike waveforms from single channels of recording, rely on manual detection of superpositions, and do not have methods to estimate the quality of sorting. For detecting burst positions in a spike train, available methods are designed for higher-order neurons which exhibit spontaneous activity, rather than an increase in ISI that reflects adaptation as in GRNs. In this chapter, I describe 1) a spike sorting technique for sensillum recordings based on methods developed by Pouzat *et al*. [133] and Hill *et al*. [134] that covers for the aforementioned limitations in sorting spikes from sensillum recordings, and 2) a method for detecting burst positions that takes adaptation into account by using a time-varying inter-spike interval (ISI) threshold. These methods will be used to analyze data in Chapter 3.

2.2 Introduction

Neural activity is accompanied by the movement of ions across neuronal membranes, resulting in a potential difference at a given location within the extracellular medium relative to a far away electrode. To a first approximation, the potentials of all nearby neurons will summate at this location, and the difference between this summed potential with respect to a far away reference potential can be monitored by an extracellular electrode [134]–[136]. The resulting local field potential (LFP) varies over different time scales, i.e., frequencies, which range between 1 and 7000 Hz [137], [138]. For example, graded currents contribute to the LFP below 300 Hz [139]. Such currents, for example those associated with the receptor potential, are generated by the signal transduction mechanisms either due to ligand binding [44], [76] or activation of subthreshold ion channels [28]. Action potentials on the other hand typically

contribute to the LFP in the 300-7000 Hz range [136], [137]. However, action potentials can also be associated with low frequency components, such as after-hyperpolarizations (AHPs) that can contribute to the LFP below 300 Hz [135], [140]–[142].

Both receptor potential- and action potential-associated components contribute to the LFP measured from first order of gustatory neurons (gustatory receptor neurons, GRNs) in insects [5], [44], [60]. GRNs are organized in groups of 2-5 units, and their dendrites are housed in hair-like sensilla [10], [20], [45], [66], [70], [71], [143]–[145]. When the sensillum comes in contact with a tastant, the molecules enter through the terminal pore and bind to gustatory receptors (GRs) present on the dendrites. This generates a receptor potential at the level of the dendrite [44], that is passively transmitted to the GRN soma where it evokes action potentials [5], [46]. The LFP evoked by GRN activity can be studied using extracellular electrodes such as the tip electrode [43], as well as the tungsten and side-wall electrodes.

In the tip recording method [43], a glass capillary electrode is filled with a tastant solution and is positioned onto the hair-like sensillum. Along with the receptor potential, the tip electrode monitors 'return currents', which are currents associated with action potentials generated near the cell body that are transmitted back into the sensillum via its outer lymphatic cavity [5]. Some studies also show that the dendrites possess ion channels, which could allow active anti-dromic propagation into the sensillum via the dendrites [146]. The tip recording technique has been used to reveal that GRNs encode tastant stimuli through trains of action potentials [6], [44], [60], [147], that different compounds can either activate or inhibit GRN activity [7], [63], [89], and that individual GRNs respond to tastant stimuli through a phasic increase in spiking frequency that adapts over time [25], [59], [61]–[66].

In the tungsten recording method, a sharpened tungsten wire is pushed a few microns into the socket at the base of the sensillum [148]–[150], and allows for monitoring GRN activity before, during and after stimulating the sensillum with a tip electrode. This is similar to the 'side-wall' recording technique, where a glass capillary tube filled with electrolyte is either pushed into the base of the sensillum [146] or is touched to the wall of the sensillum [6], [44], [60]. A side-wall electrode offers lower impedance (and thus lower noise in a recording) at the

expense of a fragile electrode. These methods have been used in *Drosophila* [150] and *S. littoralis* [149] to monitor GRN activity beyond the stimulation period, and in several other insects to characterize the contribution of different currents distributed along the length of the sensillum to the generation of action potentials [5], [46], [146].

Sensillum recordings measure the LFP contributed by the activity of all GRNs within a sensillum. There are several analysis techniques for isolating the activity of individual GRNs from this measured LFP. These techniques make use of the fact that the action potentials of each GRN will have unique waveforms on the recording electrodes, depending on factors such as the distribution of ionic channels generating the spikes, the distance of these ion channels from the recording electrode, and resistance of the extracellular medium [135], [137], [138], [151]. Filtering methods can be used to extract the higher frequency action potentials. This is done by removing the lower frequency graded potentials as well as 'noise' frequencies i.e frequencies that are not contributed by neural activity. Once the action potentials are isolated, a process known as spike sorting can be used to attribute the spikes to the GRNs that generate them [133], [134], [152], [153].

2.2.1 Introduction to spike sorting

Spike sorting involves two separate steps: 1) clustering and 2) classification. During clustering, spike waveforms are first extracted from the recording channels. Then, specific features (parameters) of the spike waveforms are chosen to compare across the dataset. The spikes are then divided into separate clusters based on these parameters. Spike templates are then generated from each cluster, and finally the quality of clustering was estimated using statistical techniques.

During classification, superposition waveforms are first isolated from the dataset. Superposition waveforms are generated when two or more neurons fire within a small time window, such that their individual waveforms add up (i.e are superposed). The time window is described by the absolute refractory period (ARP) for a neuron, which is defined as the minimum time required for a single neuron to fire two sequential action potentials. The ARP is generated due to the fact that the voltage gated Na^+ channels that contribute to the rising phase of an action

potential need time to recover before firing another action potential. In addition, the delayed closing of K^+ channels generates a spike after-hyperpolarization (AHP) that lasts for a short period of time, and which makes it difficult for the voltage gated Na^+ channels to get re-activated. For most neurons, the ARP is > 2 ms [133], [136], [152]. Then, all spike waveforms are classified to either the cluster templates or superposition templates. Finally, the quality of classification is quantified through statistics. Many programs have been developed that implement these sorting techniques using different statistics and analyses.

Spike sorting programs such as DbWave [154] and AutoSpike (Syntech) have specifically been developed to sort spike waveforms from sensillum recordings. These programs have been designed to sort spikes obtained from single channels of recording. To cluster spikes, user-selected parameters such as amplitude and width are first obtained. These parameters are plotted against each other to visually split the dataset into separate clusters and to visually detect outliers that arise from superpositions. Each cluster is assumed to belong to a separate neuron, and hence there is no further classification or estimation of cluster quality done on the dataset. This describes a very basic spike sorting algorithm, which works for most sensillum recordings due to the fact that individual neurons appear with distinct amplitudes on the recording channels [155], [156]. Further, there are only between 2-4 neurons within each sensillum, of which only a few are activated by stimulation [7].

Sorting spikes from recordings made from the brain are more complicated, since there are a larger number of neurons and spike shapes from each neuron are not as distinct. Further, it is often required to accurately classify superpositions, particularly when studying the temporal structure of spiking activity of individual neurons. Several spike sorting programs have been developed for such recordings, such as PouzatSort [133], UltraMegaSort2000 [134] and WaveClust [153]. In comparison to the spike sorting programs available for sensillum recordings as described above, these programs compare spike waveforms obtained from multiple extracellular electrodes that simultaneously monitor neural activity. This sorting technique makes use of the fact that spike waveforms will have different shapes on each electrode based on the proximity of the neuron to the electrode. Entire segments of these spike waveforms are used as parameters for sorting and generating templates to which spikes and superpositions are classified.

Finally, these programs allow for quantifying the quality of clustering and classification. While the analysis techniques used for sorting vary between these programs, they all share a common procedure, which I will briefly describe below.

In the first step of clustering, spike waveforms are extracted from each filtered recording channel. For each spike, only those segments that exhibit the most variance across the dataset are chosen. Each datapoint along these segments are used as a parameters for comparison. The number of parameters can be reduced through a principal component analysis (PCA) [133], [152], [153], [157] or via a Kolmogrov-Smirnov test [153], [158]. In PCA, data is plotted into new coordinates such that the first dimension describes the most variance, the second dimension the next most variance and so on. In this way, only a few dimensions that describe most of the variance can be used and the rest can be ignored. The Kolmogrov-Smirnov test selects only those parameters across the dataset that are not normally distributed, as is the noise.

These reduced number of parameters are then used for clustering waveforms. For smaller datasets, K-means clustering can be used, in which the parameters are clustered based on their distances from a user-defined number of centroids [159]. Another method is to decide the number of clusters based on the lowest Bayesian Information Criterion (BIC, [159]). The BIC includes a penalty term that increases when data is overfitted due to increasing the number of parameters in the model. For larger datasets, the expectation maximization algorithm can be used, which generates the 'best' model from a given number of units in a dataset, and is also useful for incomplete datasets [160]. Fee *et al*. [137] use a method to calculate 'interface energy' that produces large values when two different clusters are very close to each other. Blatt *et al*. [161] describe a method to calculate cluster 'temperature', which describes a cluster as consisting of neighboring points that have a high probability of simultaneously changing their state (considering a limited number of possible state changes).

Once spikes have been sorted into different clusters, their separation is quantified. This can be done by observing if the residuals of each cluster exhibit large, apparently non-random variations, which could indicate the presence of multiple units in the cluster. Another method is to measures the distance between clusters using a joint Fisher's Linear Discriminant Analysis

(LDA), which projects data onto the axis that is best for separation of different clusters [133], [134]. These clusters are then used to generate spike templates.

In the first stage of classification, superposition waveforms are detected. This can be done by calculating the Mahalanobis distance of every spike waveform from the median spike waveform, and then setting a distance threshold; any spike waveform having a distance greater than this threshold is considered as a superposition [133]. The Mahalanobis distance is a multi-dimensional generalization of the idea of finding how many standard deviations that a datapoint is from the mean of the dataset; this is done along each principal component axis. This method takes into account the co-variance of the dataset, which accommodates, for example, drift in spike shape (for example due to movement of the recording electrode). Finally, all spikes are classified to a superposition template or the cluster templates. This can be done by obtaining the minimum Euclidean distance between a spike and each template (Euclidean distance is obtained from the Mahalanobis distance after rescaling each principal component axis to have unit variance) [133], [134].

Once the spikes are classified, the quality of classification is estimated. This can be done by calculating the percentage of false positives arising from refractory period violations, false positives and false negatives in classification due to overlap between two clusters, and determining false negatives due to spikes falling below the set threshold for detecting spikes [134]. Further visual estimates of classification quality can be done by observing the distribution of ISIs for each unit. For sensory neurons like GRNs, the distribution of ISIs of a response is often well described by an exponential distribution [10].

2.2.2 Burst detection

Once spikes have been sorted, the contribution of individual neurons to the spike train can be studied. Most insect GRNs can be characterized by a brief (order of ~0.1 s) increase in the rate of firing of action potentials that gradually adapts over time [25], [59], [61]–[66]. For sensory neurons like GRNs that exhibit adaptation, the ISIs over time can typically be represented by a fitted non-linear function, such as a logarithmic [162], power [163] or exponential fit [164]. Deviations from these fits would then be indicative of processes other than

adaptation that are involved in driving neural activity. For example, ISIs at a time point that are several multiples greater than that estimated by the fit could indicate that spikes are organized in bursts, with long periods of silence between bursts.

In this chapter, I present a method for spike sorting sensillum recordings using methods developed by [133] and [134]. These techniques were required to accurately characterize the burst spiking evoked when stimulating gustatory sensilla in *B. terrestris*. I also describe a time-varying burst detection method for detecting burst positions in neurons such as GRNs that exhibit adaptation in spike frequency over time. In the discussion, I compare these methods to existing methods for spike sorting sensillum recordings and to existing methods for detecting bursts in spike trains. Additionally, I have included the details of how to implement these methods in the MATLAB environment.

2.3 Methods

2.3.1 Symbols and terminology

For the following section, MATLAB script will be written in font `UbuntuMono`. The term *PouzatSort* will refer to all the methods and scripts that were adapted from [133], [134] and adapted to the MATLAB platform by the lab of Dr. Stopfer (for examples of use in locust and moth see [103], [165]

2.3.2 Physiological preparation

B. terrestris were caught as they emerged from their colony. Colonies were provided by Koppert Biological Systems, NATURPOL, Netherlands. Bees were immobilized on ice and then fixed in a restraining harness as described in [116]. To avoid mouthpart movements, the M17 muscles [21] and the labial, maxillary and mandibular nerves were severed. The base of the galea were then held down in dental wax with 'U' shaped wire pins.

2.3.3 Dual tip-tungsten recording

A dual tip-tungsten recording method was used to measure the responses of 100 mM sucrose from the A-type sensilla present on the galea of *B. terrestris*. To fabricate the tungsten electrode, a 0.05 mm outer diameter (OD) uninsulated tungsten wire was sharpened by electrolysis. A 15 mm length of tungsten wire was attached to the positive lead of a 3 V AC power supply, and set on a vertical manipulator. Below it, a 1000 mM solution of KOH was placed in a petri dish, and a carbon electrode (made from pencil lead) dipped in it acted as a connection to the negative terminal of the power supply. A horizontally placed microscope was used to view the tungsten wire. The wire was sharpened by repeatedly dipping into the KOH solution. For the first dip, approximately 50% of the wire was submerged, and for the second dip onwards, 25% of the wire was submerged. The wire was dipped for varying durations, until a suitable tip sharpness was obtained (tip sharpness <1 µm).

The tip electrode was a 1.5 mm outer diameter capillary tube, pulled to a tip size of ~3 µm. A chlorinated silver wire (0.5 mm outer diameter) acted as a connection between the solution in the tip electrode and the headstage. Another chlorinated silver wire was placed in the

head capsule, which served as the ground wire. Wires were chlorinated by leaving them in a flask of bleach overnight. The electrode and amplifier setup is described in figure 2.1 a.

For a typical recording procedure, both headstage amplifiers were attached to two different Sutter manipulators (MPC-200, Sutter Instrument,USA). The preparation was viewed under a microscope (M205C, Leica, Germany) at a magnification of 256X. The tungsten electrode approached the base of an A-type sensillum at approximately a 30º angle, and was pushed ~1 mm into the cuticle. Typically, if the electrode was positioned properly, a few spikes (probably from the sensillum's mechanoreceptor) could be seen in the recording trace.

Channel data from both the tip and tungsten electrodes were imported into the MATLAB environment for analysis. Data from each channel was stored as a vector of samples, with each sample being a voltage measurment at a specific timestamp (time of arrival of that spike, with respect to stimulus onset). These channel data are referred to as $R_w(t)$ and $R_c(t)$ for the tungsten and tip channels, respectively.

2.3.4 Spike sorting

Generating initial variables

The function designed in PouzatSort were implemented in the MATLAB environment. All scripts were modified to run with tip-tungsten data. Spike sorting starts with the function `pouzatsort()`, which takes input as:

```
pouzatsort(opts);
```

Or, the function adapted to specifically deal with tip-tungsten recordings (which is used in this analysis) is:

```
pouzatsortASH(opts);
```

`opts` is a structure that contains several fields, each which carries information about the experiment for the spike sorting process. The tip-tungsten data is first stored in the `opts` structure, which is then saved as a specific file format that can be run with `pouzatsortASH(opts)`. The contents of the `opts` structure is described below:

step#	Function/Variable	Description
1	`opts.chdata(1,:)=`R_{Nc}`*pow2(16)/1000` ; `opts.chdata(2,:)=`R_{Nw}`*pow2(16)/1000`;	%converting channel data to 16-bit signed integer format (meaning values are set to range between -2^{15}:2^{15}-1), and scaling to an amplitude range $<10^4$ (data gets clipped otherwise!). R_N is filtered and normalized channel data, see below.
2	`opts.prefix= 'suc';`	%setting the title of the file, based on what stimulus was tested
3	`opts.spkchan=[1 2];`	%setting how many channels that are being used

4	`writeOneChannel(opts.chdata(1,:), …`
	`opts.prefix,opts.spkchan(1));`
	`writeOneChannel(opts.chdata(2,:), …`
	`opts.prefix,opts.spkchan(2));`
		%generating the file type that can be run with `pouzatsortASH()`

The function `writeOneChannel()` generates the following file types that can be run with `pouzatsortASH()`:

suc_t01.01
suc_t01.02

The folder in which these files are saved has to be the current working directory when calling `pouzatsortASH()`. Once this is done, the `opts` structure is built further:

Step#	Variable	Description
1	`opts.fs=fs;`	%sampling rate
2	`opts.bndx= ‘ ’;`	%has to be set empty for tip-tungsten recordings
3	`opts.ntrials=1;`	%since only one stimulus trial was made
4	`opts.mf=1;`	%multiplication factor, set as 1 if detecting peaks, -1 if detecting troughs
5	`opts.bandlims = [300 3000];`	%setting the pass band for filtering, which is implemented by a 2nd order butter filter

At this stage, the function `pouzatsortASH()` is called. Calling this function starts the spike sorting process, and takes the user through a series of thresholding stages. This is called as:

`spikes=pouzatsortASH(`*`opts`*`)`

where `spikes` is the output of the clustering process. The different stages of the spike sorting process are detailed below.

Filtering

In the first step of sorting in `pouzatsortASH()`, the channel data is filtered using a 2nd order Butterworth filter. The pass-band used is set in the field `opts.bandlims`:

`opts.bandlims` = [300 3000]; %setting the pass band for filtering

A description of how this filter works and how it is implemented is described as follows. $R_w(t)$ and $R_c(t)$ were first filtered to preserve only those frequencies that contribute to the spike waveforms. To observe the frequency components in a trace, a power spectral density (PSD) estimate was calculated using the Welch’s averaged, modified periodogram method via the `pwelch()` function in MATLAB, using a 6000 sample window with a 300 sample overlap.

`Wn`=[300 3000]; % *pass-band for filtering*
[B,A]=`butter(N,Wn/(fs/2), ‘bandpass’)` *%building a Butterworth filter with order N*

R_{filt}=filtfilt(B,A,R(t)); *% applying the filter on* R_w(t) *or* R_c(t)

Where fs is the sampling rate. The function filtfilt() is a forward reverse filter that maintains the phase of the signal, which is required as the Butterworth filter in this pass band is non-zero and non-linear. I wrote a function ashfilt() that uses a 2nd order butter filter, and allows the user to select the pass-band, and the 'type' of filter i.e lowpass, highpass, bandpass or bandstop:

```
ashfilt(R(t),Wn, 'type', fs)
```

An additional filter type is the tolerance zone filter , which preserves frequencies near the edges of the pass-band to produce a more stable filter. This is built as follows:

Tolerance zone filter:

```
Wp = [ 700 8000]/(fs/2);          %pass band for filtering
Ws  = [ 500 10000]/(fs/2);        %transition zone
[N,Wn] = buttord(Wp, Ws, 3, 20);  %determining filter parameters: 3dB tolerance in the
                                  pass band, and at least 20dB attenuation in the stop-
                                  zone
[B,A]=butter(N,Wn)                %building the tolerance zone filter
Rfilt=filtfilt(B,A,Data);         % applying the filter
```

Filtered data is then normalized to the median absolute deviation (MAD) of the channel data. The MAD is a measure similar to the standard deviation (SD), but is not sensitive to the presence of outliers in the dataset. Normalization is implemented as follows:

R_N=R_{filt}/[1.48*mad(R_{filt})]; *%Normalizing data to MAD of stimulation period*

where 1.48 is a constant that is used when the distribution is normal, as is the case for the distribution of noise frequencies.

Spike detection

`pouzatsortASH()` requires a vertical threshold `Vt` to be selected for each recording. It then applies three fixed thresholds `thr1`, `thr2` and shadow to detect spike positions. An index is considered as a spike if it crosses both the lower threshold `thr1=[2/3*Vt]/ std(`R_N`)` and upper threshold `thr2=Vt/ std(`R_N`)`. A subsequent index had to drop below `thr1` before exceeding `thr2` and had to be separated by a minimum distance of `shadow`=2/3 s. This spike detection method was advantageous as it required a single vertical user defined threshold for each trace. These thresholds can be set in the opts structure as follows:

```
opts.rthresh=Vt;
opts.thr1=thr1;
opts.thr2=thr2 ;
opts.shadow=shadow;
```

The way these thresholds are applied are described as follows. The function `schmidttriggerZA_auto()` applies the two vertical thresholds `thr1` and `thr2` to R_N and uses `findpeaks()` to apply the `shadow` threshold. These functions are called as follows:

Step#	Function	Description
1	[*sp sizes*]=schmidttriggerZA_auto(R_N, ... []`,thr1,thr2`)	*%To get initial timestamps (`sp`) and amplitudes (`sizes`) of spikes in R_N using thresholds `thr1` and `thr2`*

2	`spikeArray=zeros(1,max(sp)+1)`
	`[sp indices]=sort(sp)`
	`spikeArray(sp)=sizes(indices);`
		%creating the vector spikeArray, which will contain the sizes of the spikes detected in their corresponding time indexes

3	[*~,ind*]=findpeaks(*spikeArray*, … 'minpeakdistance',ceil(shadow*fs/1000)	*using `findpeaks()` to remove the smaller peaks that are within the shadow period. fs=sampling rate*

Outside `pouzatsortASH()`, I created a function `ashpeaks()` that automatically does all these steps. This function opens a window for each channel that is given as input, so that the user can select a vertical threshold `Vt` for each channel.

Spike sorting

Once spikes were detected in both channels, spike timestamps that have the maximum amplitude from both channels are chosen to form the vector of spike times `ind`. `ind` is then used to extract the waveforms of the spikes for each channel, by using a window 0.0035 s to the left and right of each index. This results in two matrices of waveforms, one for each channel, having *`ind`* rows and 0.0035*`fs` columns. For every pair of corresponding spike waveforms from both channels, only the one with the maximum amplitude is taken for each spike time index to form a matrix `spkmax` of waveforms. These waveforms are used for thresholding, to choose which segments of the spike waveforms will be used for comparison in the sorting procedure. Only those segments of `spkmax` that exhibit the most variation are used for the sorting process. Choosing these segments involves 3 thresholding steps: choosing a window `spwin` where spikes in `spkmax` exhibit the most variation, removing the portions of the waveforms around the peak using a vertical threshold `threshv2` to prevent high amplitude artifacts, and setting an envelope around `spkmax` to remove noisy spikes and superpositions.

To choose `spwin`, a figure is presented of the median `spkmax` waveform, along with the MAD (median average deviation) of `spkmax` and the MAD of all data outside of spiking events, i.e channel noise. `spwin` is then chosen as the window where the MAD separates from the channel noise. Next, a figure is presented to choose threshold `threshv2` as a multiple of the SD of `spkmax` to ignore the central peak of spikes that have high amplitudes. Then, a figure is presented to select the envelope threshold `threshv` around `spkmax` to remove noisy waveforms that exceed the envelope.

The resulting length of the segments that are used for comparison is referred to the dimensionality of the dataset. The next step involves principal component analysis (PCA) on these segments to reduce the number of dimensions even further. The user chooses a reduced number of dimensions (`ndim`) to use for sorting. Using too many dimensions should be avoided,

since noisy dimensions affect clustering. Next, the first three dimensions are plotted in a 3d graph, and the user chooses a range of cluster sizes (`nclusts`) that the data should be split into, depending on how separated the clusters appear in the plot. The cluster number that gives the lowest BIC value is used for sorting spikes.

To skip these user selection steps, the variables can be defined in the opts structure as:

```
opts.spwin=[0.001 0.003];
opts.threshv2=5;
opts.threshv1=4;
opts.ndim=5;
opts.nclusts=2;
```

The output of `pouzatsortASH()` is the `spikes` structure which has the following fields:

#	Variable	Description
	`spikes.info`	*%Contains info used to generate the files during `writeOneChannel()`*
	`spikes.opts` `spikes.params`	*%Contains all the info used in the sorting steps described above*
	`spikes.waveforms`	*%Waveforms (`spk`) of the spikes detected*
	`spikes.spiketimes`	*%timestamps (`ind`) of the spikes*
	`spikes.assigns`	*%To which cluster each `ind` and `spk` belong to*

Once this stage of sorting is complete, the clusters are estimated for separation. The data that is used for these estimations are the `ndim` dimensions obtained from PCA. The functions that are useful for this are:

#	Function	Description
1	`fldplot_tot(spikes)`	*%joint fisher linear discriminant. The pairwise distance for each cluster is plotted, and a separation value 'd' is calculated. d>4 is a good indication of well separated clusters*
2	`plot_clustmodwaves(spikes,1)`	*%plots all waveforms of each cluster*
3	`plot_clustmodres(spikes1)`	*%plots the residuals of each cluster on top of the channel MAD.*
4	`plot_cluschan(spikes, … opts.ch(n,:),opts.fs)`	*%plots the channel data with detected spike timestamps as dots, with different colored dots referring to different clusters.*

If any changes had to be made for the clusters, the following functions can be used:

#	Function	Description
1	`removeoutliers_aut(spikes,val)`	*% removes outliers for each cluster that are* `val` *Euclidean distance away from the dataset*
2	`removeoutliers_aut(spikes,'',n,'')`	*% to manually select a threshold val by visualizing the Euclidean distance distribution of cluster* `n`*, to remove outliers*
3	`removeoutliers_man(spikes,n)`	*%to manually remove individual waveforms from cluster* `n`
4	`mergeclusts(spikes,c1,c2)`	*% to merge two clusters* `c1` *and* `c2` *into one cluster*
5	`splitclusts(spikes,c,n)`	*% to split cluster* `c` *into* `n` *clusters*

The final clusters are saved in the structure `spikes1`.

Spike Classification

This stage uses the same `opts` structure that was used for sorting, and any thresholds that need to be varied should be updated. For instance, if during sorting it was found that `opts.rthresh` was set too high resulting in undetected spikes, the value should be changed before continuing. Classification is then called as:

```
sz=pouzatclassASH(spikes1,opts);
```

Where the output `sz` will contain the fields describing the classification. The first step of classification is to detect superposition features, which occur when two spikes fire within a small time interval of each other. This is done based on a threshold distance measure (Fig. 2.8). First, the Mahalanobis distances of the spikes for each cluster are calculated from their median spike shapes. Then, a threshold (`xval`) is automatically generated using the covariance of noise. The noise covariance is calculated by randomly choosing segments in the data trace that are not near spike features and constructing a matrix of these segments, and then taking the covariance of this matrix. Next, The PCA of this noise covariance is calculated, and the number of dimensions (`r`) that describes 90% of the variance of this dataset is found. Finally, the inverse chi-squared cumulative distribution function with `r` degrees of freedom is calculated at 99% probability to determine the distance threshold:

```
xval=chi2inv(0.99,r); %calculating superposition threshold
```

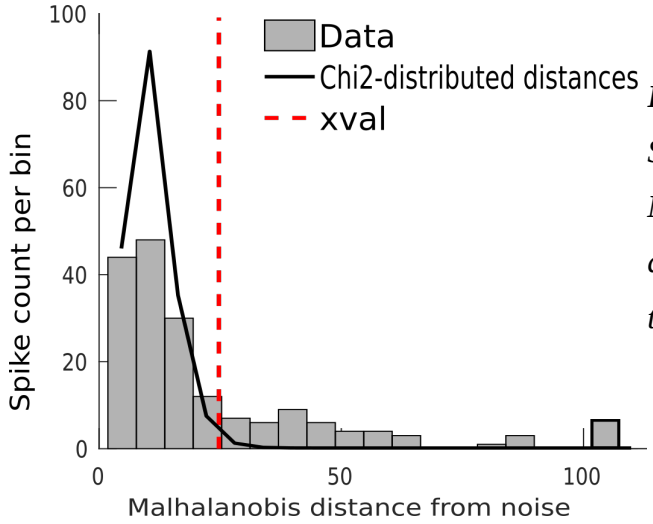

Figure 2.1 : Detecting superposition features*. Superpositions are detected as spikes whose Mahalanobis distances (bars) are greater than a threshold `xval` (dashed line) calculated from the noise estimate from the trace.*

Spikes with distances >xval are classified as superposition spikes. Spikes within the `xval` threshold are matched to one of the templates that was generated for each cluster. This is done by calculating the Euclidean distance of the spike to each cluster template, and attributing the spike to the cluster to which it has the minimum Euclidean distance. Next, superposition templates are constructed using templates from each cluster, and the spikes with distances greater than `xval` are matched to them, using the minimum Euclidean distance criterion.

Estimating quality of classification

Errors that arise due to refractory period violations, overlaps between clusters and missed spikes due to thresholding are estimated to determine the quality of classification. These error percentages are calculated using the function:

```
[fpos,fneg,fres1,fres2,fres3]= toterr_rt(sz);
```

`fres1` is the percentage of false positives due to refractory period violations, which occur when two spikes of the same cluster fall within 0.002 s of each other. `fres2` is the percentage of false positives and false negatives due to the overlap between two clusters. This is calculated by first running a PCA on the waveforms and obtaining the number of dimensions that describe 98% of the variance. Multivariate gaussians are then fit to each cluster to obtain the overlap. For example, the false positive percentage in cluster 1 would refer to the waveforms of neuron 2 that were classified to neuron 1, while the false negative percentage in cluster 1 would refer to the waveforms of neuron 1 that were assigned to neuron 2. `fres3` is the false negatives due to spikes falling below the set `Vt` threshold, which are calculated by plotting the differences of each spike peak from the `Vt` threshold, and estimating how many spikes were missed from the distribution of these distances. `fpos` and `fneg` calculate the cumulative false positives and false negatives from these errors for each cluster.

This completes the sorting and classification by PouzatSort.

2.3.5 Burst detection

Burst detection was done by plotting a fit to the ISI of each spiking event. The ISI for a spike was calculated as the duration following the spike before another spike is seen. The spike timestamps were stored in the vector `ind` and the ISIs were stored in the vector `isi`. A minimum of 4 spikes / s was required for fitting. For a logarithmic fit, the equation `y=a*log(b*x+c)` was used, where `y` is the independent variable (*`isi`*) and `x` is the dependent variable (*`ind`*). `a`, `b` and `c` were set to take values between 0 and infinity (Inf). Values greater than zero were chosen due to the adaptive nature of neural firing, which results in an increase in `isi` and `ind` over time. To give greater weight to smaller ISIs, a weight vector `wt` was set as `1/isi`. After constructing the fit, the `isi` values that exceed a threshold of two times the fit at their corresponding time points are considered as ISIs belonging to end of burst spikes. These curve fitting steps were done in MATLAB as:

#	Function/variable	Description
	Setting fit parameters:	
1	`ft.type=('a*log(b*x+c)', …` `'independent','x','dependent','y')`	*%specifying the fit type*
2	`ft.opts=fitoptions(ft.type)`	*%generating the options for the desired fit type*
3	`ft.opts.Lower=[0 0 0];`	*%set the lower thresholds for the variables*
4	`ft.opts.Higher=[Inf Inf Inf];`	*%set the upper thresholds for the variables*
5	`ft.opts.StartPoint=[0.2 0.6 0.9];`	*%setting a starting point for variables of the fit*
6	`ft.opts.Robust=LAR;`	*%using robust least squares regression*
7	`ft.win=[0:0.01:1];`	*%time intervals over which to evaluate the fit*
	Implimenting Fit:	
8	`ft.out=fit(ind,isi,ft.type,ft.opts)`	*%calculating the fit for each timepoint specified in `ind`*
	Evaluating Fit:	
9	`ft_eval=feval(ft_out,ft.win);`	*%calculating the fit for each timepoint specified in ind*

	Finding Outliers:	
10	`out_ind=find(isi./ft.out>2);`	*%find the indexes where the isi is greater than 2 times the fit that was calculated for each ind corresponding to the isi.*

The function `ash_logfit()` implements the above steps and outputs the end of burst ISIs, and is called as:

```
[save_fit, marker,eob]=asheob(ind,win);
```

where `save_fit` is the saved logarithmic evaluated over the time intervals in `win`, `marker` gives a 0 or 1 depending on whether the fit was successful or not, and `eob` gives the end of burst timestamps.

Reference [166] developed a method for detecting inter-burst intervals using a static ISI threshold. In this method, all ISIs less than the mean ISI are taken to give a vector *Lt.* *S*equential spikes having a mean value less than the mean of *Lt* are considered as the spikes within a burst.

2.4 Results

2.4.1 Dual channel (tip + tungsten electrode) sensillum recordings

The activity of GRNs were monitored from the longer (~20 µm) A-type galeal contact chemoreceptor sensilla in the buff-tailed bumble bee *Bombus terrestris* using two extracellular electrodes: a glass capillary electrode filled with the tastant solution placed at the sensillum tip, and a tungsten electrode inserted about 1 mm into the base of the sensillum. This allowed for monitoring activity at two separate locations along the length of the sensillum. The diagram for this setup and the amplifier connections are shown in figure 2.2 a (see methods for details).

Using 100 mM sucrose as the stimulant, the GRNs were found to respond with bursts of spiking activity along with a low frequency oscillation in potential that were measurable by both electrodes (figure 2.1 b). The response starts when the tip electrode makes contact with the sensillum and ends when it loses contact. This contact is associated with a high amplitude deflection in potential in both recordings (contact artifact), which lasts approximately 0.1 s from stimulus onset. During this time, spikes waveforms are distorted in both channels. The potentials associated with each spiking event lasted approximately 0.005 s (figure 2.1 b right).

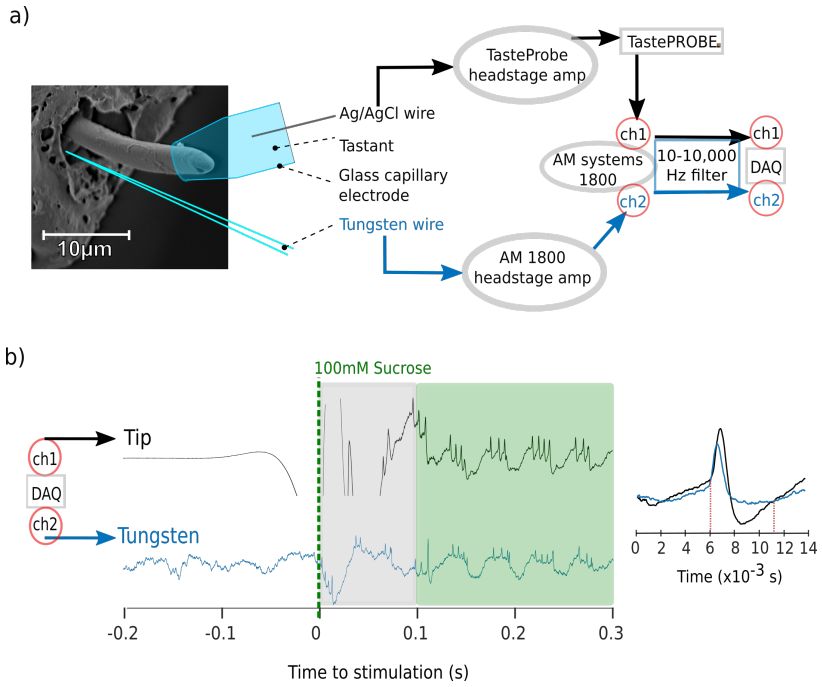

Figure 2.2 *(legend on next page)*

Figure 2.1: Dual tungsten- tip recording setup. a) left *Positions of tip and tungsten electrodes (schematized), as shown on a TEM of a galeal A-type sensillum.* ***Right****) A chlorinated silver wire connects the tastant solution within the tip electrode to a headstage-amplifier (Syntech, Germany), which in turn is connected to a TastePROBE (Syntech, Germany). The tungsten electrode is connected to the positive input of an A-M systems 1800 headstage amplifier, while the negative and ground terminals were shorted and fixed to the ground wire. The ground wire was an Ag/AgCl wire inserted into the head capsule of the bee. The output of these two channels (ch1 and ch2) are amplified (10X) and filtered (10-10,000 Hz) using an AC amplifier (AM-systems 1800) , and acquired (digital acquisition,DAQ) at 30,000 Hz (DataTranslations)* ***b)*** *100 mM sucrose stimulation shows that the first 0.1 s (gray window) is associated with a contact artifact. The spiking and low frequency oscillations can be observed after the initial 0.1 s (green window). The median spike waveforms show that the action potentials last approximately 0.005 s (starting with the sharp depolarization and ending with the after-hyperpolarization; dotted red lines).*

To characterize the spiking component of the GRN response, recordings were filtered between 300-3000 Hz (figure 2.3 a ; see methods and next section for filtering). Spikes in the tip recording could not be detected in a 0.5 s time window after stimulus onset and before stimulus offset, due to the influence of the contact artifact. However, spikes in these durations can still be detected in the tungsten recording.

There were two observable differences in the spike waveforms from both channels (figure 2.3 b). First, the spikes from the tip electrode reached peak amplitude $0.30 \pm 0.03 \times 10^{-3}$ s (mean ± SD; n=5 recordings, 5 animals obtained from 1s stimulations) after the spikes in the tungsten recording. Second, spikes from the tungsten recording had a shorter width (half height width, hhw=0.6×10^{-3} s) in comparison to the spikes from the tip electrode (hhw= 0.8×10^{-3}s; n=5 recordings, 5 animals, obtained from 1 s stimulations).

The longer width of the spikes in the tip recording resulted in a poor resolution for detecting superpositions (figure 2.3 c), with the minimum time required for two subsequent spike peaks to be detected being greater than 0.001 s for the tip recording. In comparison, tungsten

electrode recorded spike peaks could be detected when spikes were separated by as little as 0.0005 s. GRN spiking activity was also associated with a decrease in spike amplitude over the course of stimulation (figure 2.2 d). This amplitude decrease was larger in the tip recording as compared to the tungsten recording over a 1 s duration.

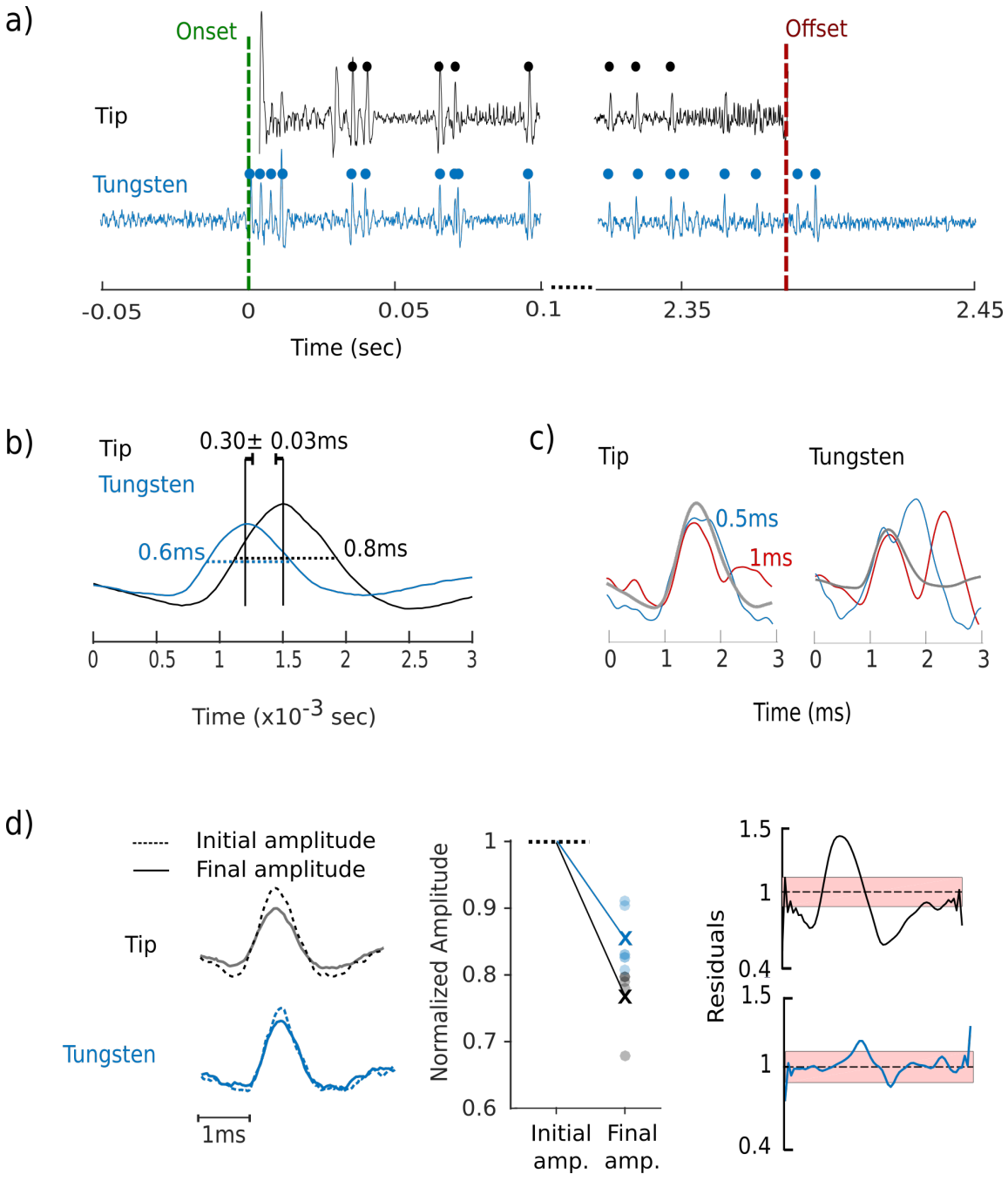

Figure 2.2 *(legend on next page)*

***Figure 2.3**: **Dual channel recording for studying GRN responses**. **a)** 300-3000 Hz band-pass filtered tip and tungsten recordings show that contact artifact distorts spike waveforms around the stimulus onset (left) and offset (right) in the tip recording, but not in the tungsten recording. **b)** Median spike waveforms from both channels reveal differences in time to spike peak and spike width. **c)** Example superpositions show that the tip recording allows less temporal resolution for detecting separate peaks of superpositions as compared to the tungsten recordings. Labels refer to the time interval between the peaks of each superposed spike (blue, 0.5 ms; red, 1ms). Median spike waveform (grey) is shown for comparison. **d left)** Median waveforms from the initial (0.1-0.3 s duration) and final (0.9-1.1 s duration) durations of the recordings show that the amplitude decreases over the course of stimulation. **d middle)** Average decrease in amplitude (crosses) for tungsten spikes (blue dots) and tip spikes (black dots) over recordings. Amplitude normalized to the initial amplitude (n=5 recordings, 5 animals). **d right)** The residuals of the spike waveforms from the tip channel (normalized to the standard deviation of the waveforms) exceed a 95% confidence interval (pink region) set around the noise estimate for the channels (dashed line) near the spike peak, indicating a strong influence of the decreasing spike amplitude. Waveforms are centered at 1 because they have been normalized to the channel noise.*

2.4.2 Optimal filtering for tip and tungsten recordings

To determine the pass-band for filtering the tip and tungsten recordings to extract spike waveforms, I plotted a Welch's power spectral density estimate using the acquired channel data (figure 2.4 a). The most prominent frequency components (those having the largest magnitude) lie within the first 1000 Hz for both channels. The first 10-50 Hz form the oscillatory component. The 100-300 Hz components on the other hand contribute to the slow time scale components associated with each action potential, e.g the spike after-hyperpolarization or the passive currents associated with each action potential (figure 2.4 b). The 100-300 Hz frequencies are prominent in the tip recording but are mostly absent in the tungsten recording. Since frequencies below 300 Hz do not reflect the conductances that generate the spiking events [137], [138] they can safely be removed.

A pass-band for filtering was set between 300-3000 Hz. I applied several filter designs on the dataset (figure 2.4 c; see methods for filter implementation). A 2nd order Butterworth filter was found to work adequately in the chosen pass-band, and hence was used for all filtering purposes. This filter functioned similarly to a 3rd order Butterworth filter used in [133]. While a tolerance zone filter (Fee, Mitra, and Kleinfeld 1996) was better at preserving frequencies near the pass-band cutoffs (300 and 3000 Hz), this was not found to change the outcome during spike sorting (data not shown). The Butterworth filter in this pass-band was non-zero and non-linear (figure 2.4 d). Sample filtered traces are shown in figure 2.4 e.

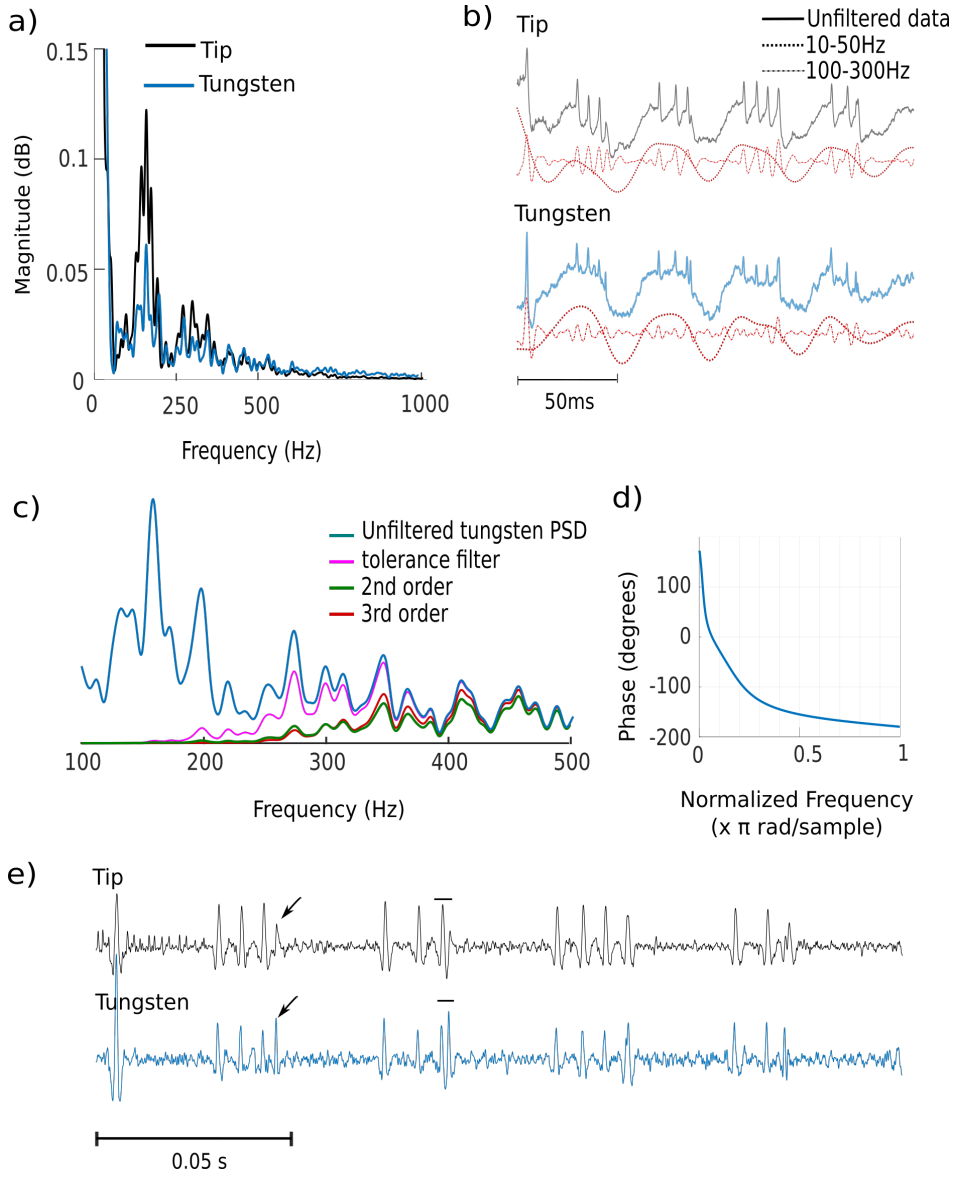

Figure 2.4 *(legend on next page)*

Figure 2.4 : Filtering tip and tungsten recordings. a) *A Welch's power spectral density (PSD) estimate shows that the prominent frequency components lie in the first 1000 Hz for both channels.* ***b)*** *10-50 Hz components (dotted line) and 100-300 Hz components (dashed line) contribute to the low frequencies associated with the 100 mM sucrose response, as seen against the unfiltered tip and tungsten recordings.* ***c)*** *PSD of different types of filters in the bandwidth range of 300-3000 Hz, plotted against the PSD of the unfiltered trace. The 2nd order filter was used for remainder of the analysis.* ***d)*** *A Butterworth filter in the 300-3000 Hz range has a non-zero, non-linear phase response.* ***e)*** *Filtered trace after applying the 2nd order Butterworth filter in the 300-3000 Hz band-pass range. Traces reveal superpositions (horizontal bars) and distinct spike waveforms (arrows), suggesting the presence of multiple active GRNs.*

2.4.3 Sorting

Spikes from filtered tip and tungsten recordings obtained from 100 mM sucrose stimulation (figure 2.4 e) were sorted using a method developed by Pouzat *et al*. [133] and Hill *et al*. [134] (adapted to the MATLAB platform by the lab of Dr. Mark Stopfer, see methods) which shall henceforth be referred to as PouzatSort. These techniques have never been applied to sensillum recordings before, and hence had to be standardized to account for the specific features of the spike waveforms from the tip and tungsten recordings.

For the clustering stage of spike sorting, spike timestamps (time points where spikes are located) were first detected from the filtered tip and tungsten recordings. This was done by setting a single user-defined horizontal threshold line for each recording channel (see methods). As a result, a vector (sequence) of spike timestamps (time point defining the arrival of the spike, in relation to the stimulus onset) were obtained, such that each spike timestamp had a corresponding waveform from each channel. These timestamps were used to extract the corresponding spike waveforms from each channel. Only those spikes in a 0.1-1.1 s duration after stimulus onset were used for sorting, since the first 0.1 s after stimulus onset was associated with a large deflection in potential that distorted spike shapes.

PouzatSort uses entire segments of the waveforms for comparisons; each datapoint along these segments is used as a parameter for clustering. This involves choosing those segments that

exhibit the most variance across the tip and tungsten spike waveforms, which is done in three steps. First, the median absolute deviation (MAD) of the spike waveforms is plotted (figure 2.5 a). This showed that most of the variance between waveforms is observed in a 0.001s-0.003 s window to the left and right of the spike peak, and hence spike waveforms were truncated to this window. Second, a horizontal threshold line delimiting 4*SD of the waveforms was used to remove segments of the spike waveforms that lie above this threshold (figure 2.5 b). This was required since the spike amplitudes in both the tip and tungsten electrodes decreased over the course of the recording. Third, waveforms falling outside a 5*SD envelope set around the spike waveforms were removed (figure 2.5 c). This functions to get rid of superposition waveforms and noise artifacts before generating spike templates.

The segments defined by these three thresholds were applied to all the spike waveforms. Each corresponding waveform from each channel was then concatenated (linked together side-by-side) to form one continuous waveform per spike timestamp. These thresholds could be applied to all recordings, making any user input unnecessary during this stage of sorting. Finally, a principal component analysis (PCA) on the set of concatenated waveforms revealed that the first five principal components accounted for more than 95% of the variance (figure 2.5 d). Therefore, instead of using the entire length of the concatenated waveforms, only the first five principal components per waveform were used as parameters for comparison.

Next, the first five principal components obtained as described above were used to split the spike waveform dataset into two clusters. Two clusters were chosen since the 100 mM sucrose recordings exhibited superpositions and visually distinguishable spike shapes that suggest at least two separate active GRNs (figure 2.4 e). The concatenated waveforms for each cluster and from both channels are shown in figure 2.5 e.

To estimate for cluster quality, the residuals were plotted for each cluster (figure 2.5 e). If the residuals fell within 1.5 * the standard deviation of the noise estimate for each channel (see methods), the spike waveforms of that cluster are similar to each other and likely belong to the same GRN. 1.5*SD was used as a threshold to accommodate for the decrease in spike amplitude over the course of the recording. To observe whether the each cluster was well

separated from each other, a Fisher's Linear Discriminant Analysis (LDA) was done on the first five principal components obtained from PCA. Recordings were only used for classification if the Fisher's LDA revealed a separation greater than 4 (figure 2.5 f); which is considered to be a cutoff for well separated clusters [134]. Sorting was efficient for the dual-channel recordings, with 10 out of 11 recordings yielding well separated clusters (N=11 animals). The median spike shape from each cluster was used as a template.

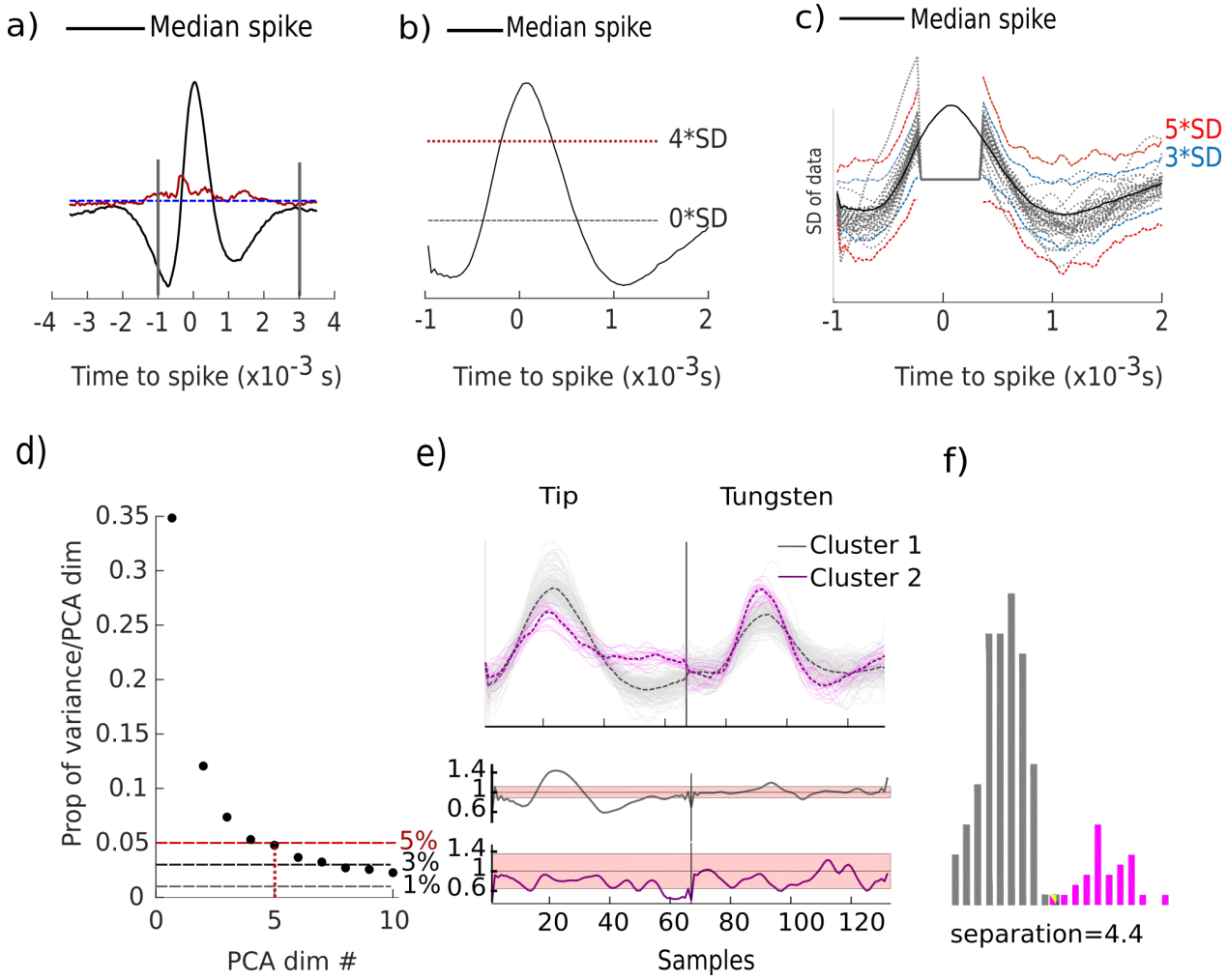

Figure 2.5 : Sorting spikes from 1 s stimulation with 100 mM sucrose. a) *Median absolute deviation (MAD; red trace) of the spike waveforms against the channel noise (horizontal dashed line). Spike waveforms were restricted to the window enclosed by vertical grey lines.* ***b)*** *Horizontal thresholds lines (in multiples of SD of the waveforms) plotted on the median spike*

waveform. ***c)*** *Envelope thresholds plotted around the spike waveforms (dotted grey waveforms).* ***d)*** *Proportion of total variance accounted by each of the 10 largest eigenvectors of the covariance matrix of all detected waveforms.* ***e top)*** *Spike waveforms from each channel after clustering.* ***Middle and bottom)*** *Residuals of both clusters, along with the noise estimate (dashed line) and 95% confidence interval around the noise estimate (pink box).* ***f)*** *A joint Fisher's LDA using the 5 dimensions obtained from PCA.*

2.4.4 Classification

In the first step of classification, superposition waveforms are identified by setting a Mahalanobis distance threshold from each spike template derived from the channel noise [133] ; see methods). Spike waveforms from the dataset that have a distance greater than this threshold are labeled as superposition waveforms. All spikes were then classified to either the cluster templates or the superposition templates, using a minimum Euclidean distance measure.

To estimate the quality of classification, the error percentages arising from 1) false positives due to refractory period violations, 2) false positives and false negatives in classification due to overlap between two clusters, and 3) false negatives due to spikes falling below the set threshold for detecting spikes were measured, using methods developed by [134] (see methods). If all errors fell under 10% of the dataset for the 1 s recordings, the recording was considered well sorted and was used for further analysis. Using this procedure, 5 of the 10 recordings yielded two separate clusters with less than 10% errors. Visually estimating the accuracy of classification by looking for missed superpositions and incorrect classifications revealed an accurate detection of superpositions and classification in these 5 recordings (Table 2.1 i). As a result, spike sorting revealed the presence of two classes of spikes, termed as Class 1 and Class 2 (spike timestamps shown in figure 2.6 a).

2.4.5 PouzatSort using single channel recordings

The sections above described sorting (section 2.4.3) and classification (section 2.4.4) when two channels were used (i.e tip and tungsten channels). I next compared the efficiency of sorting when single channels of recording (either the tip channel or the tungsten channel) were used for sorting spikes. Using the 5 recordings that yielded low errors after classification when

both channels were used (section 2.4.4), I found that using spikes from only the tungsten electrode yielded a much higher error percentage from false positives and false negatives associated with overlap between the two clusters, with < 71% errors across the 5 recordings (Table 2.1 ii). This indicates that the spike waveforms between clusters are not very different. As a result, there were a high number of visually detected errors; over the 5 recordings, I found on average 3 errors due to misclassification and on average 2 errors due to missed superpositions (Table 2.1 ii, figure 2.6 b).

In comparison, using spikes from only the tip electrode recording yielded lower error percentages, with < 26% errors across recordings (Table 2.1 iii). While the visually detected errors due to misclassification were negligible when using the tip recordings, there was a high error count for missed superpositions (6 errors on average over recordings; Table 2.1 iii, figure 2.6 c). Together, these data show that sorting spike waveforms using both the tip and tungsten electrodes results in a more efficient spike sorting and classification, as compared to when sorting is done using either the tip or the tungsten channels in isolation.

	Cluster1,Cluster2 Recording #	Refractory period violations fpos (%)	Overlap between clusters fpos, fneg (%)	Spikes falling below threshold Fneg (%)	Missed super-positions	Misclassi-fication
i) **Channels**	1	0,0	2,0 ; 0,4	0,0	0	0
	2	0,0	0,0 ; 0,0	0,0	0	0
	3	0,0	1,1 ; 4,5	0,0	0	0
	4	0,0	0,0 ; 1,0	0,0	0	0
	5	3,0	0,0 ; 0,10	0,0	0	0
ii) **Tungsten channel**	1	0,23	24,55 ; 11,5	0,0	3	11
	2	0,0	15,0 ; 0,3	0,0	2	2
	3	0,0	1,35 ; 9,0	0,0	2	0
	4	0,0	9,71 ; 14,2	0,0	2	2
	5	0,0	2,0 ; 0,0	0,0	0	0
iii) **Tip channel**	1	0,0	1,5 ; 19,4	0,0	11	0
	2	0,0	1,1 ; 8,10	0,0	4	1
	3	0,0	0,0 ; 5,1	0,0	8	0
	4	0,0	5,2 ; 10,26	0,0	5	0
	5	0,0	1,1 ; 11,18	0,0	0	0

Table 2.1 (*legend on next page)*

Table 2.1. Comparison of errors from sorting and classification when using individual vs both channels. *Sorting done using spikes from i) both tip and tungsten recordings, ii) only the tungsten recording or iii) only the tip recording channel. False positive (fpos) and false negative (fneg) rates contributed by refractory violations, overlap between clusters, and missed spikes due to incorrect thresholding, for the Class1 (black) and Class2 (magenta) spikes are shown for all three scenarios. The last two columns show the number of visually detected errors due to missed superpositions and misclassification.*

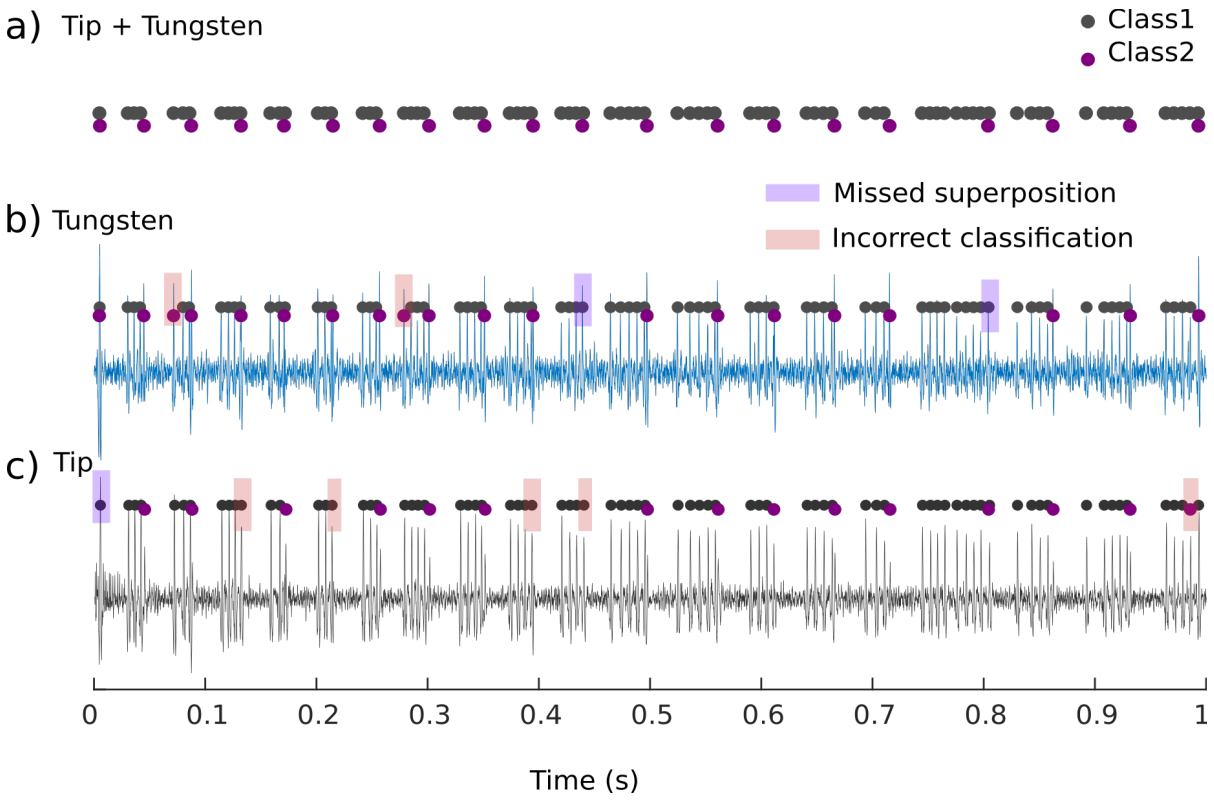

Figure 2.6. Classification using dual-channel vs single channel recordings. ***a)*** *Using spikes from both the tip recording (trace in* ***[b]****) and the tungsten recording (trace in* ***[c]****), spikes were classified as Class1 and Class2.* ***b)*** *Sorting and classification using spike waveforms from only the tip channel and* ***c)*** *using waveforms only from the tungsten channel. Boxes indicate visually detected errors (in comparison to* ***[a]****) which arise from missed superpositions (purple boxes) or misclassification of spikes (pink boxes).*

2.4.6 End of burst detection

Tip recordings made from galeal GRNs show that sucrose evokes a dose-dependent increase in spiking and bursting (figure 2.7). In order to quantify the bursting nature over concentration and determine whether the two GRNs revealed from spike sorting fell at specific positions within the burst structure, it was necessary to detect the burst positions from these recordings. A plot of the ISI histograms over concentration (figure 2.7 a) shows that for lower concentrations, the histogram is more spread out which reflects the more random spike firing of GRNs. The absence of any structure in spike timing is also observed in a scatterplot of the n^{th} vs $(n+1)^{th}$ ISI (figure 2.7 b) .

However, as the concentration is increased, the ISI histogram becomes progressively bimodal, which reflects the structure burst firing of spikes. The shorter mode represents the ISIs of the spikes within bursts (within-burst intervals) and the longer mode represents the inter-burst intervals. Similarly, the scatterplot shows that data points cluster into four separate quadrants, where the third quadrant represents within-burst intervals and the first and fourth quadrants represent the inter-burst intervals. Adaptation in spiking frequency will cause the ISI distribution to spread diagonally across the first quadrant and into the second quadrant. The easiest way to detect burst positions from these traces would be to choose an ISI threshold which separates the two modes of the ISI histogram, or which separates the different clusters in the scatterplots. However, it is immediately apparent that a single ISI threshold cannot be used over recordings from different concentrations. Therefore, an ISI threshold has to be generated for each trace.

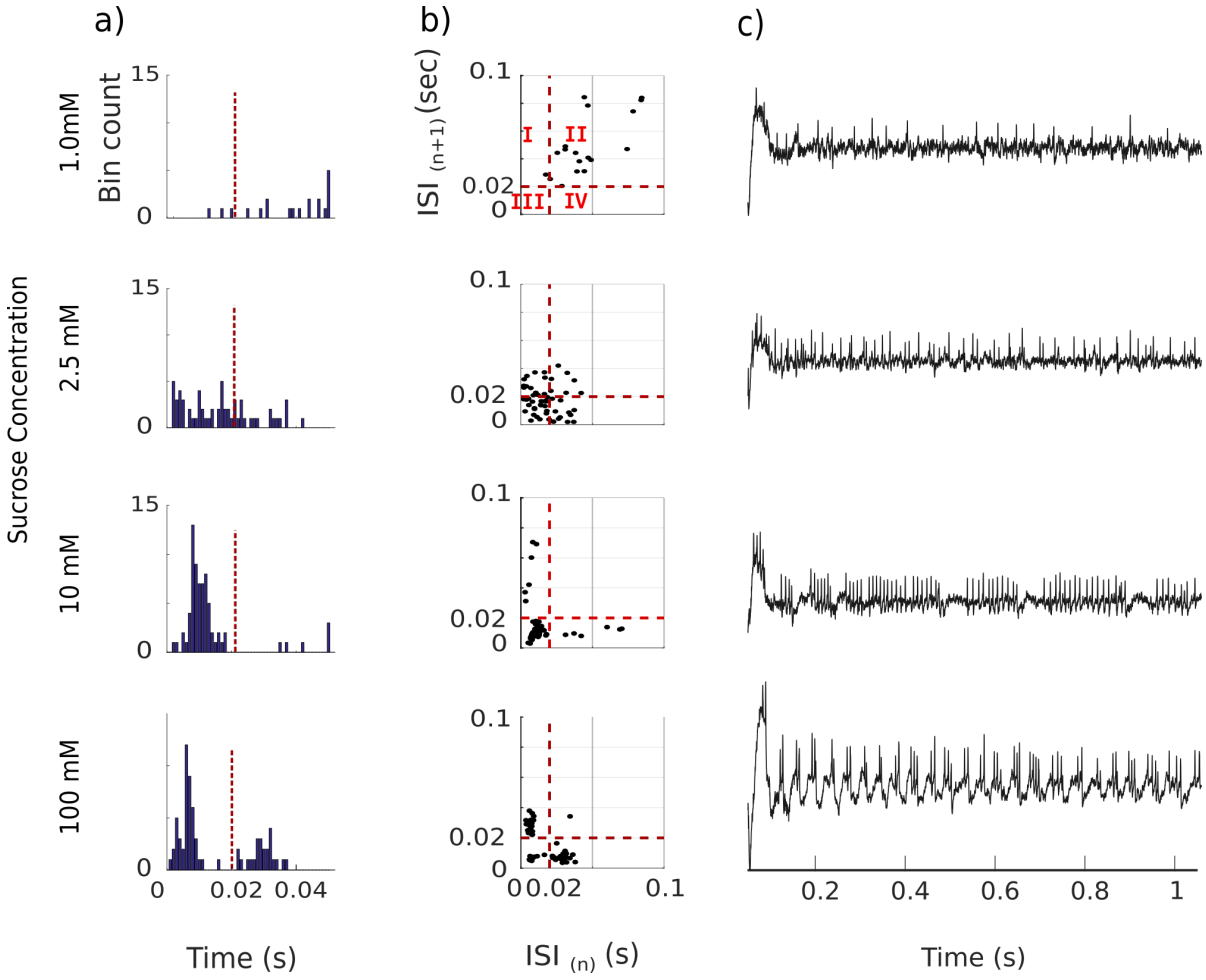

Figure 2.7: A single ISI threshold cannot be used across recordings from different concentrations. ***a)*** *ISI histograms made from 1 s recordings to increasing concentrations of sucrose. Bimodal distribution at higher concentrations is indicative of burst firing.* ***b)*** *Plotting the ISIs as a scatterplot of the n^{th} vs $(n+1)^{th}$ ISI shows that at higher concentrations, datapoints cluster in the third and fourth quadrants, which is indicative of bursting.* ***c)*** *Corresponding recordings obtained from the tip electrode.*

One way to generate an ISI threshold per trace would be to use a static ISI threshold (a threshold that remains constant over time) for each recording, either selected manually or derived from the ISI dataset for the recording. While a static ISI threshold would work well for recordings whose ISI modes are well separated (e.g figure 2.7 row 4), it becomes difficult to

obtain an efficient threshold for longer recordings due to the effect of adaptation in spike firing, which can be observed as an increase in ISI over the course of the recording (figure 2.8a). This causes the separate modes of the ISI histogram to be less distinguishable (figure 2.8 b). Due to adaptation, a threshold derived from the mean ISI for each trace as described by reference [166] was not efficient for detecting burst positions (figure 2.8 a red dots).

In order to account for this increase in ISI as GRN activity adapted, I applied a time-varying threshold to detect the longer inter-burst intervals from the population of ISIs (figure 2.8 c). This was done by constructing a fit to the spike time vs ISI data and using a multiple of this fit to detect inter-burst intervals. ISIs were calculated as the time following a spike event until a subsequent spike event. The fit was weighted towards the shorter within-burst intervals by using weights proportional to 1/ISI and using least absolute residuals fitting to minimize the influence of outliers. Using a three-term logarithmic fit having equation `a*log(b*x+c)` and a threshold of two times this fit was efficient in detecting inter-burst intervals for up to 5 s from stimulus onset for 100 mM sucrose recordings (example for detected bursts shown in figure 2.8 a, green circles). A similar efficiency was observed with a two-term power fit having equation `a*x^b;` while the logarithmic fit detected 67±33 bursts from 11 recordings, the power fit detected 66±32 bursts from the same recordings. Both the two term power fit and three term logarithmic fit were efficient at detecting bursts from 1 s recordings obtained from different concentrations of sucrose as well (data not shown).

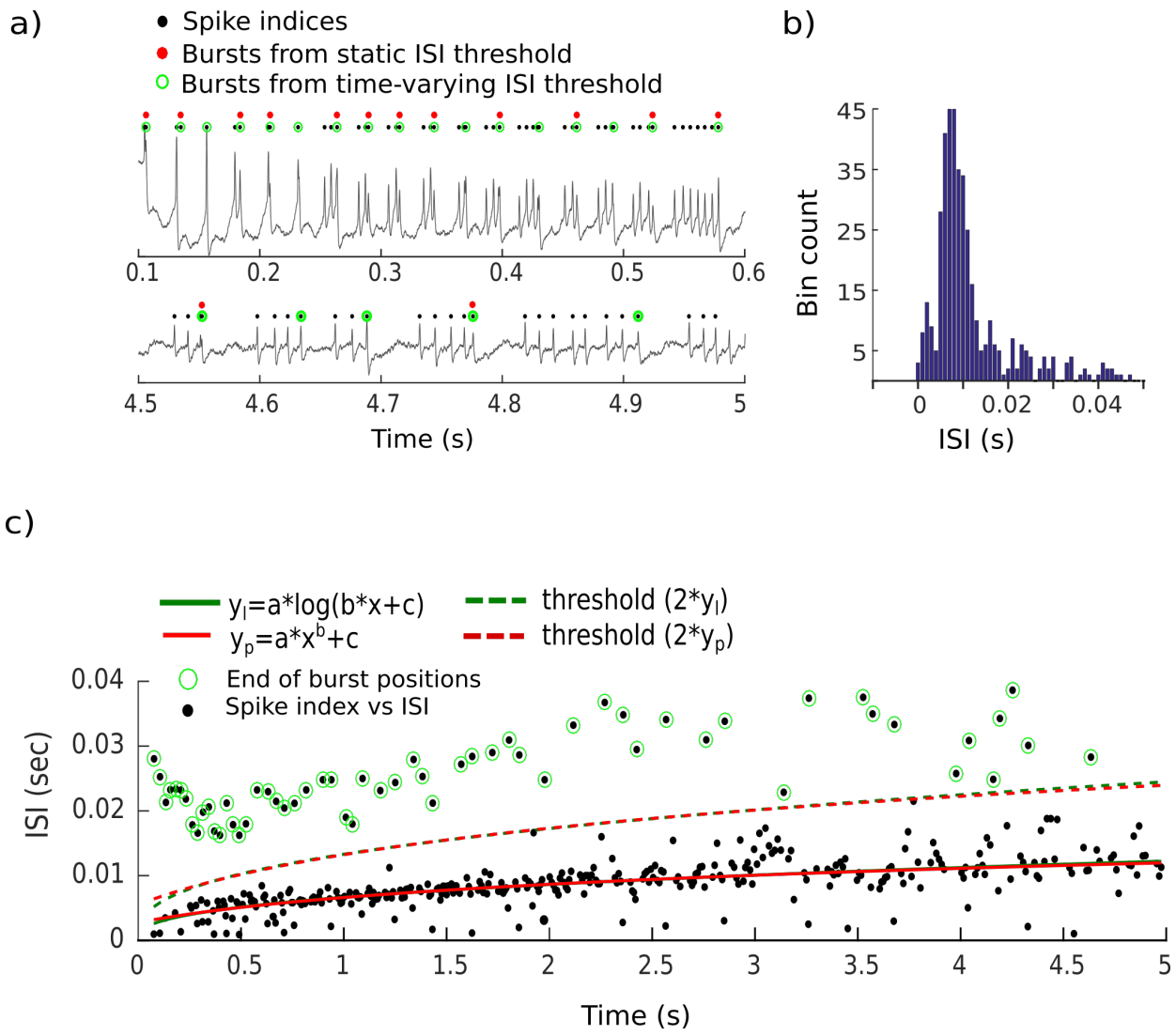

Figure 2.8 : End of burst detection using time-varying threshold. ***a)*** *Segments of a sample recording from a 5 s stimulation with 100 mM sucrose. Detecting end of burst positions using a static threshold (red dots; [166] is inefficient. This is due to the increase in ISI over time as GRN spiking adapts.* ***b)*** *Histogram of ISIs for the 5 s recording shown in (a). Due to adaptation, there is no clear bi-modal structure in the histogram which would normally be indicative of burst spiking.* ***c)*** *Time varying burst detection, by fitting either a three-parameter logarithmic (solid red line) or a three-parameter power (solid green line) equation to the ISIs as a function of the spike timestamps (black dots) and using a threshold of two times these fits (dashed lines) as a threshold for detecting inter-burst intervals (green circles). Burst positions detected using a logarithmic fit are shown in (a) (green circles).*

2.5 Discussion

The tip and tungsten recording methods are widely used for monitoring activity of GRNs within gustatory sensillia. Current spike sorting programs that are available for sensillum recordings are designed to sort spikes obtained from single channels of recording. In this chapter, I present the first spike sorting method (adapted from methods developed by Pouzat *et al*. [133] and Hill *et al*. [134] for sensillum recordings, which uses spike waveforms obtained from both tip and tungsten electrodes that simultaneously monitor sensillum activity. Further, I develop a new burst detection method for detecting bursts in traces that exhibit adaptation over the course of stimulation.

2.5.1 Sorting spiking activity from GRNs

The existing spike sorting programs available for sensillum recordings, such as DbWave [154] and AutoSpike (Syntech), are generally adequate for sorting tip or tungsten recordings. This is because each GRN within a sensillum has a distinct spike amplitude that is apparent on tip or tungsten recordings [8], [89], [156], which allows for using simple sorting procedures to detect them. Further, each sensillum contains a small population of 2-5 GRNs [10], [20], [45], [66], [70], [71], [144], with each GRN responding to a largely non-overlapping set of tastant molecules [7]–[10]. Finally, most studies are interested in detecting the presence or absence of GRN activity [18], [34], and hence accuracy of sorting is not of primary concern. For example, visual thresholds are used to detect clusters and superpositions are often manually detected [8], [72].

However, the responses exhibited by GRNs within galeal sensilla in *B. terrestris* were unlike those exhibited in most other insect species. Stimulating these sensilla with 100 mM sucrose evoked a burst spiking response from the GRNs. Tip and tungsten recordings revealed two visually distinct spike shapes as well as superpositions in these recordings, each of which appeared to fire at a specific position within the burst structure. Therefore, in order to accurately characterize this response, I needed a sorting method that 1) required minimal user input, to remove bias from the sorting procedure, 2) allowed for estimating the quality of classification, to convincingly argue for the presence of multiple active neurons, and 3) uses

multiple parameters for comparison, particularly since the second GRN activity was very low (~17 spikes/s) and often was associated with the first GRN as a superposition (~10 superpositions/s; see chapter 3). Further, spike amplitude and width were often found to decrease over the course of a sensillum recording, which makes these parameters less efficient for sorting. The sorting method provided by references [133] and [134] allowed me to accurately sort and classify the burst responses.

Spikes from both tip and tungsten channels, obtained from the 0.1-1.1 s window after stimulus onset, were used for sorting. The first 0.1 s window was skipped due to the presence of the large deflection in potential associated with stimulus onset. The deflection in part represents an artifact associated when the glass capillary electrode touches the sensillum, and also carries information about the receptor potential [44].

PouzatSort required very little user input during the spike sorting process. The only user defined threshold was for choosing a horizontal threshold line for detecting spikes. After this, the only user input was for estimating the quality of the clusters for generating spike templates, and estimating the quality of classification. This required manual removal of outlying noisy spikes or clusters, if required.

PouzatSort uses entire segments of spike waveforms from both the tip and the tungsten recording electrodes as parameters for spike sorting. Apart from providing a larger set of parameters for comparisons, using both channels also resulted in a lower error percentage from classification, as compared to when individual channels were used. The high error percentage when only the tungsten channel was used for sorting was mostly due to the similarity between the Class 1 and Class 2 spike waveforms, which resulted in incorrect classification. This similarity between the Class 1 and Class 2 spike waveforms in the tungsten recording could be due to the tungsten electrode being within equal proximity from both GRNs. For the tip recording, superpositions were not efficiently detected. This is possibly due to the large width of the spikes, which makes it difficult to detect the separate peaks of a superpositon; the peaks fuse together to form one contiguous waveform. The large spike width could be due to the nature of the tip recording, which monitors return currents associated with action potentials that are passively

transmitted into the sensillum from a region near the cell body via the outer dendritic lymph [4]–[6].

The tip and tungsten recordings were often associated with a decrease in spike amplitude over the duration of the recording. This has been observed for sensillum recordings in other insects as well, and is suggested to be dependent on spike frequency and the intensity of the receptor potential [60]. To accommodate for the decrease in amplitude, PouzatSort removes a segment of the waveform around the peak of the spike before comparing spike waveforms.

Overall, PouzatSort proved to be a very powerful tool for sorting spikes using both the tip and tungsten recordings. Using this method, I was able to sort 1 s recordings made with 100 mM sucrose stimulation, with 5 out of 11 recordings yielding less than 10% errors. PouzatSort provides a convincing way of suggesting the presence of multiple active neurons as opposed to existing sorting methods available for sensillum recordings.

2.5.2 Burst detection

Burst spiking is generally a feature of higher order neurons which do not exhibit a strong adaptation in spiking rate over time [166]–[168]. For this reason, bursts in recordings from these neurons can be detected using static ISI thresholds (thresholds that do not change over time). This can be done either by setting user-defined ISI thresholds [167] or thresholds derived from the ISI data [166], [168].

However, two features of GRN activity prevented static ISI thresholds from being implemented in the sucrose recordings. First, the distribution of ISIs depended on the concentration of the stimulus; for low concentrations, spiking frequency was low and hence the ISIs were large. The distribution of these large ISIs at low concentrations overlaps with the distribution of inter-burst intervals associated with the higher concentration stimulations. This means that the same ISI threshold could not be used over different concentrations. Second, the ISIs increased over the course of stimulation as the GRNs adapted. A time-varying threshold was therefore designed to account for adaptation in GRN activity, and the threshold was derived from

the ISIs of each dataset to account for the change in concentration. To the best of my knowledge, a burst detection method for neurons exhibiting adaptation has not been described before.

Power and logarithmic equations are commonly used for fitting ISI data as a function of spike timestamps for neurons exhibiting adaptation [162], [163]. Both a 3-term logarithmic equation and 3 term power equations, using weights proportional to 1/ISI and robust least squares regression, were found to be best at fitting the 100 mM sucrose recordings. A threshold of two times these fits were efficient at detecting bursts for up to 5 s of stimulation, as well as 1 s recordings made and over increasing concentrations of sucrose.

2.5.3 Concluding Remarks

This chapter shows that methods for spike sorting that were developed for multi-channel extracellular recordings made from central brain regions can be used for sorting and classification of spikes from sensillum recordings measured using tip and tungsten electrodes. The efficiency for obtaining well classified recordings was less than 50%, with 5 of 11 recordings yielding less than 10% errors. However, it provides a more convincing way of suggesting the presence of multiple active neurons as opposed to existing sorting methods available for sensillum recordings, particularly due to its minimal user input and analyses to estimate quality of sorting. Further, it allows using multiple channels of recording, which improves spike sorting. It remains to be seen whether PouzatSort can be used to sort sensillum recordings which exhibit more than two active GRNs.

Finally, I show that a time-varying burst detection method using a three-parameter logarithmic curve can be used to detect burst positions for up to 5s from stimulus onset for 100mM sucrose recordings, and from 1s recordings obtained from increasing concentrations of sucrose. The simplicity of this method makes it usable for detecting bursts in any other neuron that exhibits a similar adaptation. Even if the adaptation rates are different, a suitable fit and threshold can be chosen depending on the dataset.

Chapter 3. Bee Gustatory Neurons Encode Sugar Concentration as a Coherent Temporal Pattern of Spiking

3.1 Abstract

The gustatory system encodes taste stimuli to drive appropriate feeding behaviors. In insects, individual first-order gustatory neurons are commonly observed to encode stimulus intensity by a brief increase in rate of spiking that adapts with prolonged stimulation. In this study, I report my findings that showcase the first evidence of a coherent, temporal pattern of spiking produced by the interaction of the gustatory receptor neurons (GRNs) of the mouthparts of bumble bees (*Bombus terrestris*) that encodes information about sugar concentration. Stimulation of gustatory sensilla with sucrose concentrations >10 mM elicited bursts of spikes riding on an oscillation in voltage of ~21 Hz. Each burst was defined by the activity of one sugar sensing neuron that was active within the burst until punctuated by a final 'end of burst' spike by a second neuron. The activity of these neurons adapted over time and resulted in a tonic, unstructured firing. Bursting bee GRNs exhibited a high rate of firing that persisted for longer durations than any other GRN reported thus far. Only concentrations that evoked threshold spiking activity from both GRNs were found to elicit the bee's feeding reflex. These data are the first to show that primary chemosensory neurons encode stimulus features such as concentration as a coherent temporal pattern of spiking, and suggests that it is driven by an interaction between two neurons.

3.2 Introduction

Primary chemosensory neurons in insects translate chemical information into action potentials that are assembled by the brain to form representations of complex, natural stimuli. Hair-like sensilla house the dendrites of 2-5 chemosensory neurons in a tightly packed space surrounded by lymph through which molecules pass prior to binding with receptors on the dendritic membranes [10], [20], [45], [66], [70], [71], [143]–[145]. Studies in several insects suggest that the olfactory receptor neurons (ORNs) within sensilla do not have independent rates of firing [74]–[76]. It was shown in *Drosophila* that when one ORN within a sensillum begins spiking in response to stimulation, the spiking activity of its neighboring ORN is inhibited. This form of lateral inhibition is thought to occur through an ephaptic interaction, whereby the electric

field associated with spiking activity of a neuron modifies the excitability of neighboring neurons [75]. By inhibiting its neighbor, an ORN affects downstream coding through its influence on the antennal lobe circuitry that encodes odour representations [53], [54]. However, there is little evidence to date that explores how an interaction between neurons of a sensillum could affect the information encoded by the rate of firing of the activated neuron.

Gustatory receptor neurons (GRNs) in insects encode taste category (e.g. sweet or bitter) in part through the spiking responses of GRNs [1], [7]–[11] that express receptors that bind to individual taste categories [9], [26], [31], [47], [48]. For example, in *Drosophila*, sugars like sucrose elicit spikes from a single type of GRN per sensillum that expresses several gustatory receptors (GRs) that are sensitive to sugars [48]. Like ORNs, sugar-sensing GRNs encode stimulus concentration as a sigmoidal increase in rate of firing in blowflies [61], [156], [169], fruit flies [57], [155], [170], moths [65], [90], mosquito [171], butterflies [66], [71], and honeybees [63]. In most insects where such recordings have been reported, GRNs produce a phasic burst of spiking during the first ~100-200 ms of stimulation, and the frequency decreases over time as the neurons adapt until it reaches tonic firing [56]–[59], [63], [172].

Lateral inhibition as seen in ORNs is not commonly observed in GRNs. A study in gustatory sensilla of grasshoppers show that they possess a GRN responsive to nicotine hydrogen tartarate, which was inhibited for a brief period of time (order of 0.01 s) by the occasional activity of a second GRN [81]. A similar observation was made in cockroach antennal sensilla when stimulated with sucrose [173]. Activated sugar-sensing GRNs can also be inhibited by the presence of some toxic compounds [70], [89], [90], but this form of inhibition arises from direct interaction of the ligand with the sugar-sensing neuron.

In this chapter, I recorded from the GRNs of the mouthparts of adult worker bumblebees to identify the thresholds for sugar detection that were necessary to elicit feeding. Sugars are particularly important for bees as they provide the major source of energy required for flight [106], [125], and they form a major component of the food bumble bees provide for their colony [105], [174]. Bumble bees in particular have been shown to acquire complex behaviors associated with a carbohydrate reward ([120]–[122]). Unexpectedly, I found that *B. terrestris* GRNs exhibited a novel, coherent temporal pattern of spiking characterized by bursts of rapid spiking activity formed from the interaction of two neurons. Production of bursting in these

neurons was a function of sugar concentration, depended on sugar identity, and correlated with the initiation of feeding. In contrast to other sensory neurons and other insect GRNs, bursting bee GRNs exhibited very low rates of adaptation in response to prolonged stimulation, indicating a novel role for bursting in sensory neurons that is likely to function to promote the continuation of feeding during fluid consumption.

3.3 Methods

3.3.1 Bumblebees

Experiments were performed on female (worker) *Bombus terrestris audax* (Koppert Biological Systems, NATURPOL, the Netherlands). Colonies were maintained at 24 ±1°C and 28 ±1% relative humidity with natural light conditions, and fed commercial pollen and sugar solution bee food.

3.3.2 Electrophysiological recordings

Bees were chill-immobilized and harnessed as described in reference [116]. Mouthpart nerves were then severed by making an incision at the base of the mouthparts, to prevent movement. The galea were then oriented with the help of wire pins on a wax base.

The tip electrode recording method, originally described by Hodgson *et al.* ([64]) was used to stimulate sensilla and record the responses of their GRNs, as described in Chapter 2. Briefly, a glass capillary electrode was filled with the stimulating solution and placed on the tip of a sensillum. A chlorinated silver wire served to connect the solution to a headstage which in turn was connected to a TastePROBE amplifier (TastePROBE, Syntech, Germany). The output of this amplifier was connected to an AC amplifier (AM-systems 1800) which was set to filter the signal between 10-10000 Hz and apply a gain of 100x. A minimum latency period of 3 minutes was allowed between stimulations from the same sensillum to avoid adaptation.

In some experiments, a sharpened tungsten electrode was used to monitor GRN activity simultaneously with the tip electrode. Tungsten electrodes were prepared by electrolytically sharpening a 0.05 mm outer diameter uninsulated tungsten wire by repeatedly dipping in a 250 mM KOH solution attached to a 3V AC power supply. The tungsten electrode was attached to a headstage (AM-systems 1800), and was pushed a few microns into the base of the sensillum using a motorized micro-manipulator (MPC-200, Sutter Instrument, USA).

3.3.3 Data acquisition, filtering and normalization

Signals were digitized (DT9803 Data Translation) and acquired using DbWave (version 4.2014.3.22). Acquired signals were imported into MATLAB (The Mathworks) for analysis. Using MATLAB, stimulus onset and offset were determined by the contact artifacts from the tip

electrode recording. Signals were filtered in the appropriate pass-band using a 2nd order Butterworth filter. Band-stop filters constructed using a 1 Hz window around 50, 100, 150 and 200Hz were then implemented to remove line noise frequencies. The filtered signal was then normalized to the estimate for noise in the filtered signal. This noise estimate was calculated as 1.48 * median absolute deviation (MAD) of the filtered signal. The MAD is a measure similar to the standard deviation (SD), but is not sensitive to the presence of outliers in the dataset. 1.48 is a constant that is used when the distribution is normal, as is the case for the distribution of noise frequencies.

3.3.4 Nerve recordings

To measure responses from the maxillary nerve, a 0.025 mm OD tungsten wire was used, with ~0.5 mm of the polyamide insulation removed from the tip. The wire was pushed into the base of an ablated galea, until it reached a position ~2 mm from the tip of the galea (near the maxillary palp), and was positioned as close to the maxillary nerve as possible. This wire was connected to a head stage (AM-systems 1800). Sensilla were stimulated using the tip recording technique. Data from the tungsten wire electrode and the tip electrodes were acquired, filtered and normalized as described for the sensillum recordings. For recordings where two neighboring A-type sensilla were stimulated with tip electrodes, whichever electrode made contact with its sensillum first was used to define the stimulus onset time.

3.3.5 Spike Sorting

Spike waveforms obtained from both the tip and tungsten electrodes were sorted using a semi-automated, model based spike sorting method developed by [133] and [134] that has been used for spike sorting gustatory recordings in *M.sexta* [103], [165], implemented in MATLAB. This method is described in detail in Chapter 2. Briefly, this method can be divided into two steps: clustering and classification. In the clustering step, spike waveforms are first detected from a 0.1-1.1 s window after stimulus onset. A series of thresholds are then used to 1) choose a window around the peak of the spike waveform to use for comparisons, 2) remove a segment around the amplitude peak of each spike waveform, and 3) remove noisy waveforms that lie outside a threshold standard deviation envelope around the waveforms. Noisy waveforms can arise due to artifacts in the recording, or from superposition features that arise when multiple

neurons fire action potentials very close together such that their waveforms add together. A principal component analysis (PCA) is then done on the segments of the spike waveforms that remain after these three steps of thresholding. In the 100 mM sucrose recordings obtained from the A-type sensilla, there was evidence for at least two separate active GRNs. My aim was therefore to detect the positions of these two GRNs within the recording trace. I therefore used the first 5 principal components to divide the dataset into two clusters.

The quality of clustering is estimated by 1) plotting the residuals of each cluster (average of differences between each spike waveform from the median waveform of the cluster). Recordings are only used if the residuals fall near a 95% confidence interval set around the noise estimate for the trace. 2) A Fisher's Linear Discriminant Analysis (LDA) between the two clusters using the 5 principal components obtained from the PCA. The Fisher's LDA projects data onto the axis that is best for separation of different clusters. If clusters are not well separated, the LDA reports a small 'distance' value between the two clusters. Recordings are used only if the Fisher's LDA yields a distance > 4. The median spike waveform of each cluster was used as the cluster template.

In the classification stage, each spike waveform in the recording is attributed to a cluster. First, superposition waveforms are detected. This is done by first calculating the Mahalanobis distance of each spike of a cluster from the median spike waveform of that cluster. Then, a threshold distance is derived from the channel noise as described in Chapter 2. Any waveform having a distance greater than this threshold is considered a superposition spike. Superposition spikes are then classified to superposition templates, while the remaining spikes are classified to the cluster templates, using a minimum Euclidean distance measure. To estimate the quality of classification, the percentage of Type-1 and Type-2 errors are obtained. These result from 1) false positives from refractory period violations, 2) false positives and false negatives due to overlap between both clusters, and 3) false negatives due to missed spikes from thresholding during detection. If the percentage of Type-1 and Type-2 errors fell beneath 10% of the dataset, the recording was considered to be well sorted. To sort spikes obtained from the 30 s tip recordings, I followed the same procedure but used spikes obtained between 1 and 30 s from stimulus onset.

3.3.6 Frequency analysis

To measure the frequency of oscillations, recordings were first bandpass filtered between 10-3000Hz. Then, Welch's averaged periodogram method was used to estimate the Power Spectral Density (PSD) of the recording trace, using a Hanning window of 6000 samples and a 300 sample overlap with a sampling rate of 30 kHz, for 0.1 Hz increments between 10-100 Hz. For tungsten recordings, the PSD was estimated for three time windows: 0.7 to -0.2 s before stimulus onset, 0.1 s to 0.6 s after stimulus onset and 0.2 s - 0.7 s after stimulus offset.

The power of the oscillatory components were measured from the 0.1 – 0.6 s window after stimulus onset from the tip recordings. Recordings were first band-pass filtered between 10-3000 Hz. Then, the signal was normalized to a noise estimate, calculated by first filtering the signal between 300 – 3000 Hz and obtaining the noise estimate as 1.48*MAD(filtered signal). Welch's averaged periodogram method was then used to obtain the peak frequency component in the 10-3000 Hz range.

3.3.7 End of Burst detection

A burst detection method was developed based on inter-spike intervals (ISIs) of a recording. Bursts were only detected from traces having a minimum of 4 spikes, otherwise the trace was considered to have no bursts. The inter-spike interval (ISI) for each spike was calculated as the duration following the spike until the next spike is found. ISIs less than 0.001 s were then removed. A logarithmic curve having equation y=a*log(b*x+c) was fit to the spike timestamps (x) vs ISI (y). The lower and upper limits of a,b and c were set as 0 and infinity, respectively. Weights proportional to 1/y were used (inverse of the ISI), and the fit was made using robust least-squares regression. A spike timestamp was considered as an end of burst spike if its ISI exceeded a value of 2 times the fit at that time point (see figure 2.8 for example).

3.3.8 Analyses of the spike and burst frequencies in function of the sugar concentrations

To evaluate the effect of the sugar concentrations on the spiking and bursting rates generated by the GRNs, a 3-parameters log-logistic model having equation

$$f(x) = b/(1+e^{a(log(x)-c)})$$

was fitted to the data with the *drm* command from the *R* (3.3.2) package drc [175]. *x* denotes the concentration, *f(x)* denotes the response (i.e spike frequency), parameter *a* the steepness of the dose-response curve,parameter *b* denotes the upper asymptote or limit of the response, and parameter *c* denotes the EC_{50} (i.e the concentration where 50% of the maximum response is reached). Differences between the *c* parameter (EC_{50}) were assessed with the *SI* command in *R* whereas differences between the *b* parameter (upper asymptote) were assessed using the *compParm* command in *R*. Credit for this method goes to Dr. Sebastien Kessler, post-doctoral researcher in Prof. Geraldine Wright's lab, who taught me how to implement this analysis.

3.3.9 Proboscis Extension Response

To measure behavioural responses in function of sugar concentrations, bumblebees were harnessed as described above and starved for 3 to 8 hours at room temperature in a dark environment. Mouthparts were stimulated with a droplet of tastant stimuli of varying concentrations. Behaviors were video recorded with a digital microscope (Dinolite), and MATLAB custom software was used to track the position of the mouthparts. This was done by defining a movement threshold as two times the maximum movement obtained from a control water stimulus. To test whether the probability of eliciting "twitching" or PER behaviors depends on concentration and sugars, separate logistic regressions were fitted to the data for each behavior.

3.4 Results

3.4.1 Mouthparts

The proboscis of bumblebees is formed by the maxillae and the labium. The labium is made of the glossa and the labial palps whereas each maxilla are composed of a galea and a small maxillary palp present at the base of the galea (figure 3.1 a). Scanning electron microscopy (SEM) shows that the galea contain two morphologically distinct contact chemosensilla present on the outer ridge: the longer (~20 um) A-type and shorter (<10 um) B-type (figure 3.1 b) sensilla. Transmission electron microscopy (TEM) cross sections at the middle of an A-type sensilla revealed the presence of an outer and an inner cavity within the cuticle of the sensillum. The inner cavity contains the dendrites of 4 GRNs (figure 3.1 c).

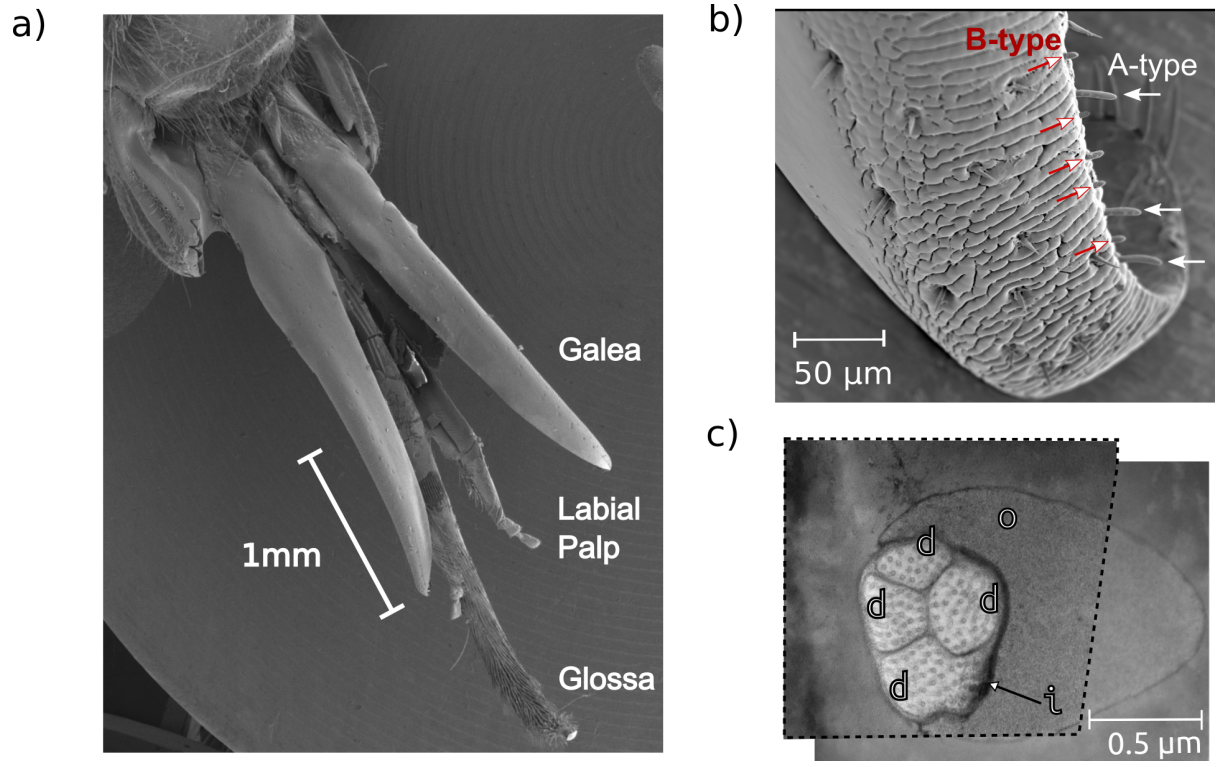

Figure 3.1 (legend on next page)

Figure 3.1: Distribution of sensilla on mouthparts of B. terrestris. a) *The galea, labial palps and glossa form the prominent mouthparts of the proboscis in B. terrestris.* ***b)*** *The galea possess the longer 'A-type' sensilla (white arrows) and the shorter 'B-type' sensilla (red arrows) that have a diameter of ~5 um.* ***c)*** *TEM cross sections of the 'A-type' sensilla show that they house the dendrites [d] of 4 GRNs. These dendrites are ~0.25 μm in diameter, and are tightly clustered within a inner cavity [i], which is encompassed by an outer cavity [o]. Figure shows two overlaid images, obtained at different magnifications.*

The activity of A-type GRNs was monitored using two electrodes placed at different positions along the length of the sensillum; a tip electrode [64] placed at the tip of the sensillum and a sharpened tungsten electrode punctured ~1 mm into the base of the sensillum (see methods). Using these techniques, it was found that 91% of the tested A-type sensilla did not possess a GRN responsive to distilled water (n=80 sensilla, 26 animals). My investigation was focused on the A-type sensilla that did not exhibit a water responsive GRN, and which were located distally on the galea. The responses of these sensilla were measured to sucrose stimulation.

3.4.2 Sucrose stimulation evokes a burst spiking response involving multiple GRNs

GRNs are found to encode the quality and category of sweet taste stimuli as a rate of spiking that adapts with prolonged stimulation [7], [31]. Unexpectedly, I found that stimulating the A-type sensilla with 100 mM sucrose instead evoked bursts of spikes and a low frequency oscillation (figure 3.2 a). This burst pattern was measured by both the tip and tungsten electrodes.

My first aim was to characterize the spiking component of this response. All values in this section are represented as mean ± standard deviation (SD) and were obtained from 1 s recordings from 5 separate animals, unless otherwise stated. From filtered recordings (pass-band 300-3000Hz), it was revealed that spikes from the tip recording have 1) a larger half-height width and 2) reach peak amplitude $0.2 \pm 0.1 \times 10^{-3}$ s later than spikes from the tungsten recording (figure 3.2 b). Visual inspection of filtered recordings from both recording electrodes shows the presence of spike waveforms having different shapes, as well as superpositions features that arise due to the summation of action potentials from separate neurons (figure 3.2 b top). The presence of

multiple spike waveforms and superpositions suggests the activity of multiple GRNs in the response to sucrose. By sorting spikes using a method that compares filtered spike waveforms obtained from both channels of recording [133], [134] ; see methods), two spike clusters were detected, termed as Class 1 and Class 2 (figure 3.2 c). The superposition features detected during spike sorting (10±4 superpositions per recording) were attributed to the activity of the Class 1 and Class 2 spikes (figure 3.2 d). Over recordings, the firing rates of the Class 1 and Class 2 spikes were 81±15 spikes/s and 17±7 spikes/s, respectively.

The spiking activity of these two spike classes formed the burst response to 100 mM sucrose (17±7 bursts per recording; see methods for burst detection). This burst pattern of firing could be characterized by the multi-modal distribution in the ISIs caused by firing of both spike classes (figure 3.2 e). The positions of the Class1 and Class2 spikes within the burst structure were well organized; more than 95% of bursts (83/87 bursts, n=5 recordings, 5 animals) were formed from the activity of one or more spikes of the Class 1 neuron followed by a single spike from the Class 2 neuron. Each burst of spikes was followed by an inter-burst interval of 29±7 $x10^{-3}$ s. The ISI of the last two spikes of the burst ranged between 0-0.01 s (figure 3.2 e inset), and there were a minimum of 2 spikes within each burst.

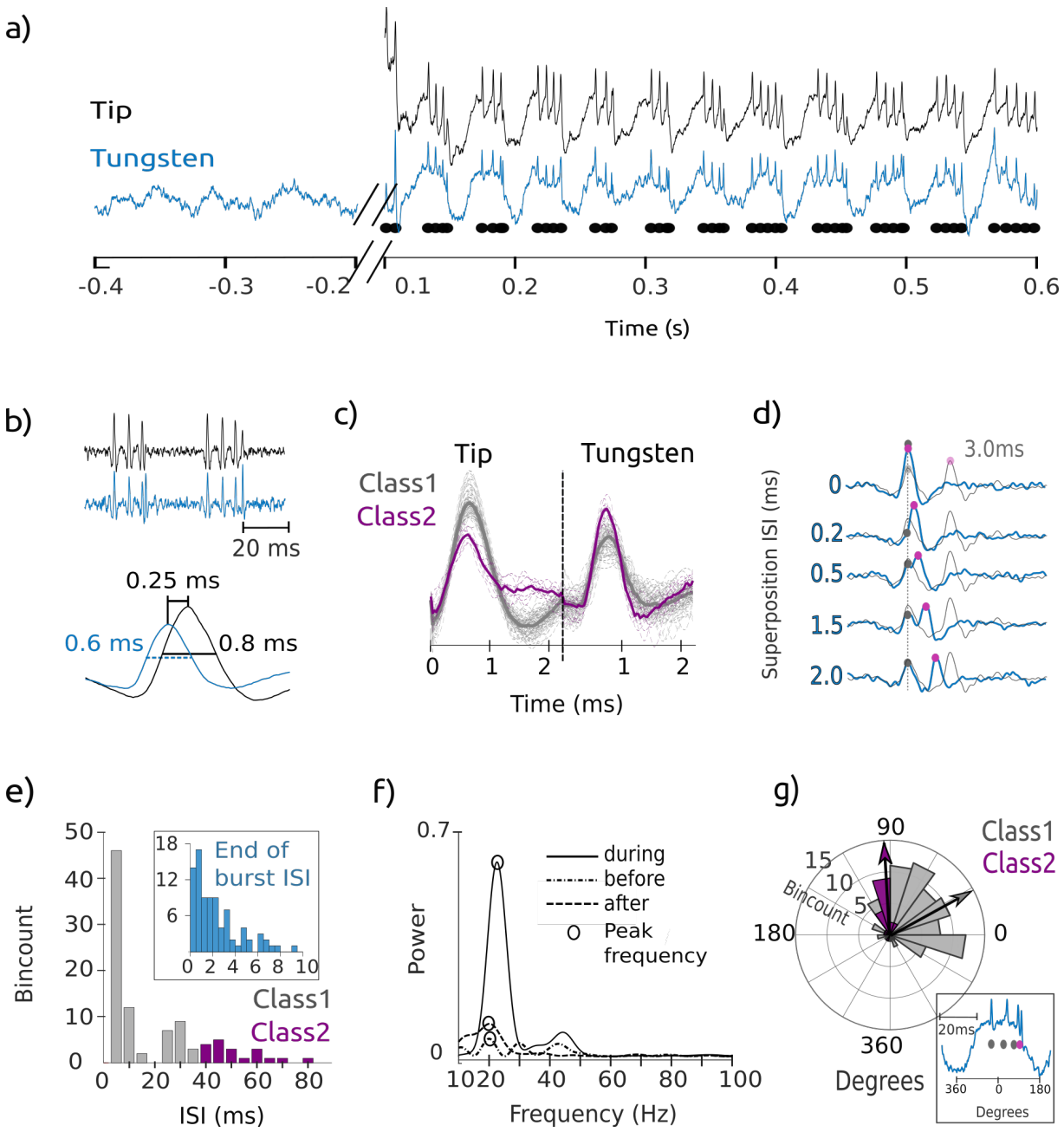

Figure 3.2 (legend on next page)

Figure 3.2: Coherent, multi-unit burst response from GRNs in an A-type sensillum to 100 mM sucrose stimulation a) *Tip and tungsten electrode recordings show spiking, bursting and low frequency oscillations are evoked during stimulation. Traces in a-d are normalized to the noise estimate for each channel.* ***b) Top****: Bandpass filtered (300-3000 Hz) recordings used for spike sorting.* ***Bottom****: Spikes propagate anti-dromically i.e from the tungsten electrode towards the tip electrode.* ***c)*** *Spikes from bandpass filtered recordings were sorted to reveal two clusters of spikes, termed as Class 1 and Class 2 spikes.* ***d)*** *Example detected superpositions (ISI< 2 ms) that were attributed to the firing of a Class 1 and Class 2 spike. A Class 1 and Class 2 spike separated by 3 ms (grey waveforms) are shown for comparison.* ***e)*** *The ISI histogram for Class 1 and Class 2 spikes has two visually distinct modes, indicating burst firing. Inset shows ISI histogram of last two spikes of each burst (end of burst ISI).* ***f)*** *Welch's power spectral density estimates from 10-100 Hz filtered tungsten recordings using 0.5 s durations before, during and after stimulation. The power of the peak frequency during stimulation was significantly greater than before and after stimulation.* ***g)*** *A rose plot derived from a Hilbert's transform on 10-100 Hz filtered tungsten traces using 1 s of recording shows that the Class 1 and Class 2 spikes fire at specific phases of the oscillatory component.* ***(inset)*** *a sample unfiltered tungsten recording trace showing the typical structure of Class 1 and Class 2 spike firing. All panels were obtained from the recording shown in* ***(a)***.

The spiking response to 100 mM sucrose was also associated with a low frequency oscillation in voltage. A power spectral density (PSD) estimate on the 10-100 Hz filtered tungsten recordings (see methods) revealed that the peak frequency of these oscillations ranged between 17-26 Hz (figure 3.2 f). A power estimate of these peak frequencies revealed that the power was significantly higher during stimulation as compared to the baselines ($p<0.001$, 1-way ANOVA, $F_{2,12}=8.4$; n=5 recordings, 5 animals; see methods), indicating that the oscillatory component is restricted to the stimulation period. Spikes were located at specific phases of this oscillatory component; Class 1 spikes fired around the peak with a mean at the 17±72° phase , and the Class 2 spike fired near the negative slope with a median at the 83±36° phase (figure 3.2 g).

The tungsten electrode recording also revealed that sucrose responsive GRN spiking activity was mostly restricted to the stimulation period (baseline firing=3±1 spikes/s, mean±STE; n=17 sensilla, 11 animals). The spiking frequency reached its peak within 0.01 s from stimulus onset and returned to baseline within 0.025 s from stimulus offset (figure 3.3). Further, bending the sensillum revealed that the A-type sensilla possess a mechanoreceptor neuron (figure 3.4). Bending the sensillum while stimulating with 100 mM sucrose showed that the mechanoreceptor neuron had a distinct spike waveform in comparison to the sucrose responsive GRNs, indicating that the mechanoreceptor is not involved in the burst response to sucrose (figure 3.4 b). The mechanoreceptor neuron dendrite appears to be located at the base of the A-type sensillum, as indicated by a TEM (figure 3.4 c).

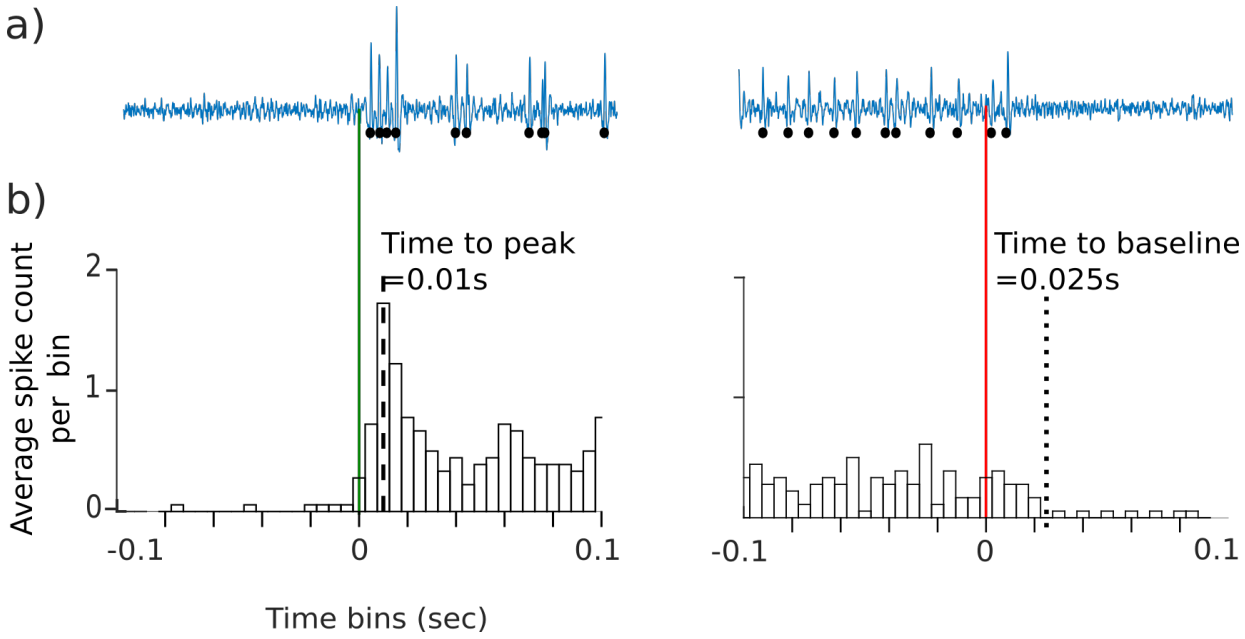

Figure 3.3: Spiking activity is restricted to stimulation period. a) *300-3000 Hz filtered tungsten recordings were used to monitor spiking activity (black dots) around the stimulus onset (green line) and offset (red line).* ***b)*** *A histogram of average spike count per 0.005 s bin (black bars; averaged over n=17 sensilla, 11 animals) shows that spiking response is restricted to stimulation period. Time to peak (dashed line) and time to baseline (dashed line) shows that the response is tightly bound to the stimulus onset and offset (baseline calculated as mean of the average spike count per 0.005 s bin calculated over the -1.1:-0.1s duration)*

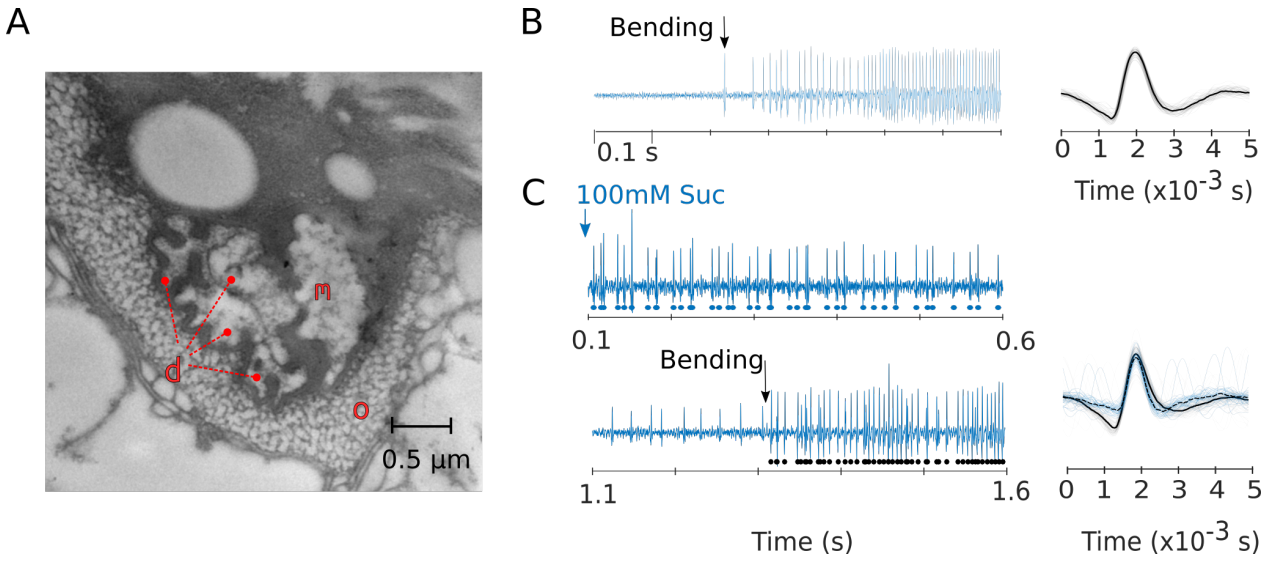

Figure 3.4. A-type sensilla possess a mechanoreceptor ***a)*** *A TEM image at the level of an A-type sensillum base shows the presence of four GRN dendrites [d] and what appears to be a larger mechanoreceptor dendrite (m), encompassed by the outer lymphatic cavity [l].* ***b)*** *Tungsten recording shows spikes of mechanoreceptor, activated by bending the sensillum.* ***c)*** *Bending the sensillum (onset shown by black arrow) during the sucrose stimulation (onset shown by blue arrow) shows that sucrose and mechanoreceptor spikes (blue and black dots/waveforms, respectively) have visually distinct waveforms, indicating that the mechanoreceptor neuron is distinct from the GRNs activated by sucrose.*

3.4.3 Bursting GRNs adapt over multiple time scales

A common feature of chemosensory neurons is that they adapt to prolonged stimulation. This adaptation can be observed as a decrease in the frequency of spiking i.e an increase in ISI over time. To measure the rate of adaptation of the Class 1 neuron, I fit a linear equation to its ISIs as a function of the spike timestamps over time. Surprisingly, the spiking activity of the Class 1 neuron did not exhibit a continuous adaptation. Instead, slopes of linear equation fit to Class 1 ISIs within bursts decreased, indicating acceleration in spiking over the course of the burst. However, this was only true for bursts having short duration (where the duration of a burst was defined as the time between its preceding Class 2 neuron spike and its terminal Class 2 neuron spike, i.e the Class 2 neuron ISI for that burst). For bursts having duration > 0.1 s, the

Class 1 neuron instead adapted over the course of the burst (figure 3.5 b). Over the course of the 1 s stimulation however, the Class 1 neuron spike frequency adapted (figure 3.5 ci). The short-duration bursts were more likely to occur early in the recording, and as the stimulation continued, the bursts became longer (figure 3.5 c). This was due to the adaptation in Class 2 firing rate over the duration of stimulation, which resulted in an increase in burst duration (figure 3.5 cii). The Class 1 neuron spiking frequency adapted by 0.002 ± 0.000 s (mean ± standard error of mean) over 1 s of stimulation and the Class 2 neuron spiking frequency adapted by 0.041 ± 0.005 s (figure 3.5 d; recordings had a minimum of 10 bursts / 1 s; n=23 recordings, 23 animals).

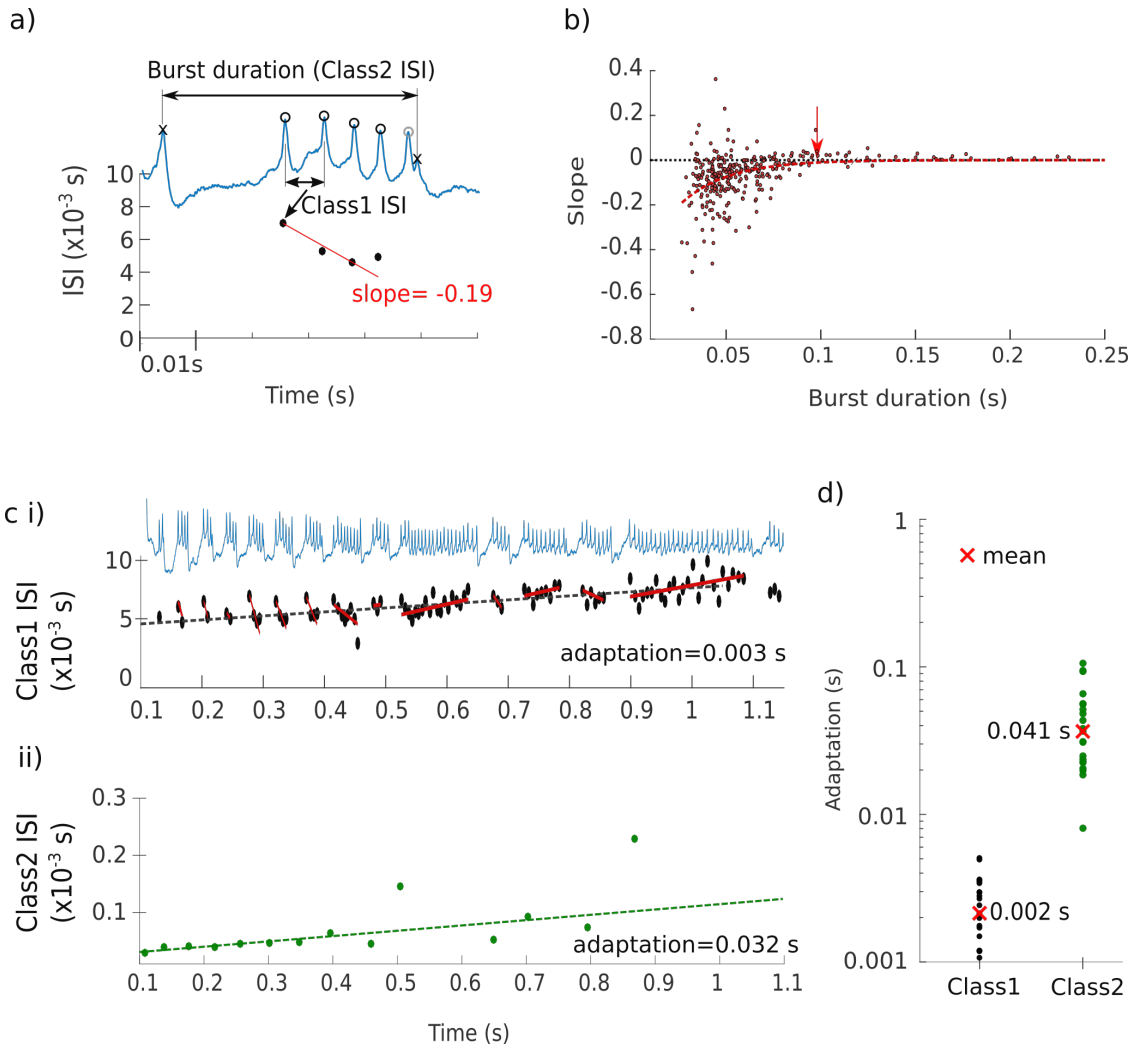

Figure 3.5 *(legend on next page)*

Figure 3.5: Adaptation depends on burst duration ***a)*** *Detected spikes in a segment of a recording, assuming Class 1 neuron spikes within bursts (open circles) and Class 2 neuron spikes at end of bursts (crosses). A linear equation (red line) was fit to the first N-1 Class 1 spikes per burst (open black circles).* ***b)*** *The slope of the linear fit was significantly dependent on burst duration, as shown from a non-linear model (y=a*exp(b*x); dashed red line; p<0.001) made to slopes obtained from bursts over several recordings (n=312 bursts, 11 recordings from 11 animals, using recordings with at least 3 bursts). Bursts with duration <~0.1 s had negative slopes, as indicated by the fit approaching a value of zero at this duration. This correlation is maintained for most bursts over a 1 s recording, as shown by linear fits for individual bursts (red lines) in a sample recording in* ***ci****.* ***c)*** *Linear fits (dashed lines) to the Class 1 ISIs (*ci*) and Class 2 ISIs (*cii*) show different rates of adaptation over 1 s. The slopes of these fits are shown for several recordings in* ***[d]****. Note that the y-axis in [d] is plotted on a logarithmic time scale.*

To see how long the burst structure was maintained, I stimulated the sensilla for 30 s with 100 mM sucrose. A sample tip electrode recording shows that the initial portion of the response is characterized by the structured burst firing of spikes, which changes over the course of stimulation as the GRNs adapt (figure 3.6 a). Sorting the spikes for the recording shown in *figure 3.6 a* revealed that the Class 1 and Class 2 neuron spikes are found at specific phases of the burst structure in the initial part of the recording, but fire more randomly as they adapt over the 30 s duration. A plot of the variance in ISI (per 0.3 s time bin) over time for several recordings suggests that the coherent burst structure persists for up to 4 s (figure 3.6 b).

To measure the time course of adaptation in spiking activity, the spike count (per 0.3 s bin) was plotted over the 30 s duration (figure 3.6 c). For recordings with high levels of bursting (>10 bursts in the first 1 s of stimulation) the spike rate increases up to ~1 s from stimulus onset and then rapidly decreases. At around 4 s, the rate of change in spiking slowed slightly for the remainder of the recording. This indicates that there are multiple time courses over which GRN spiking activity adapts. It was interesting to note that unlike for the high burst recordings, recordings with low levels of bursting (<10 bursts in the first 1 s) exhibited no initial increase in spiking rate from stimulus onset. Further, the GRNs in these recordings appeared to adapt faster; the spike count rapidly decreased up to 2 s after which the rate of change was nearly constant.

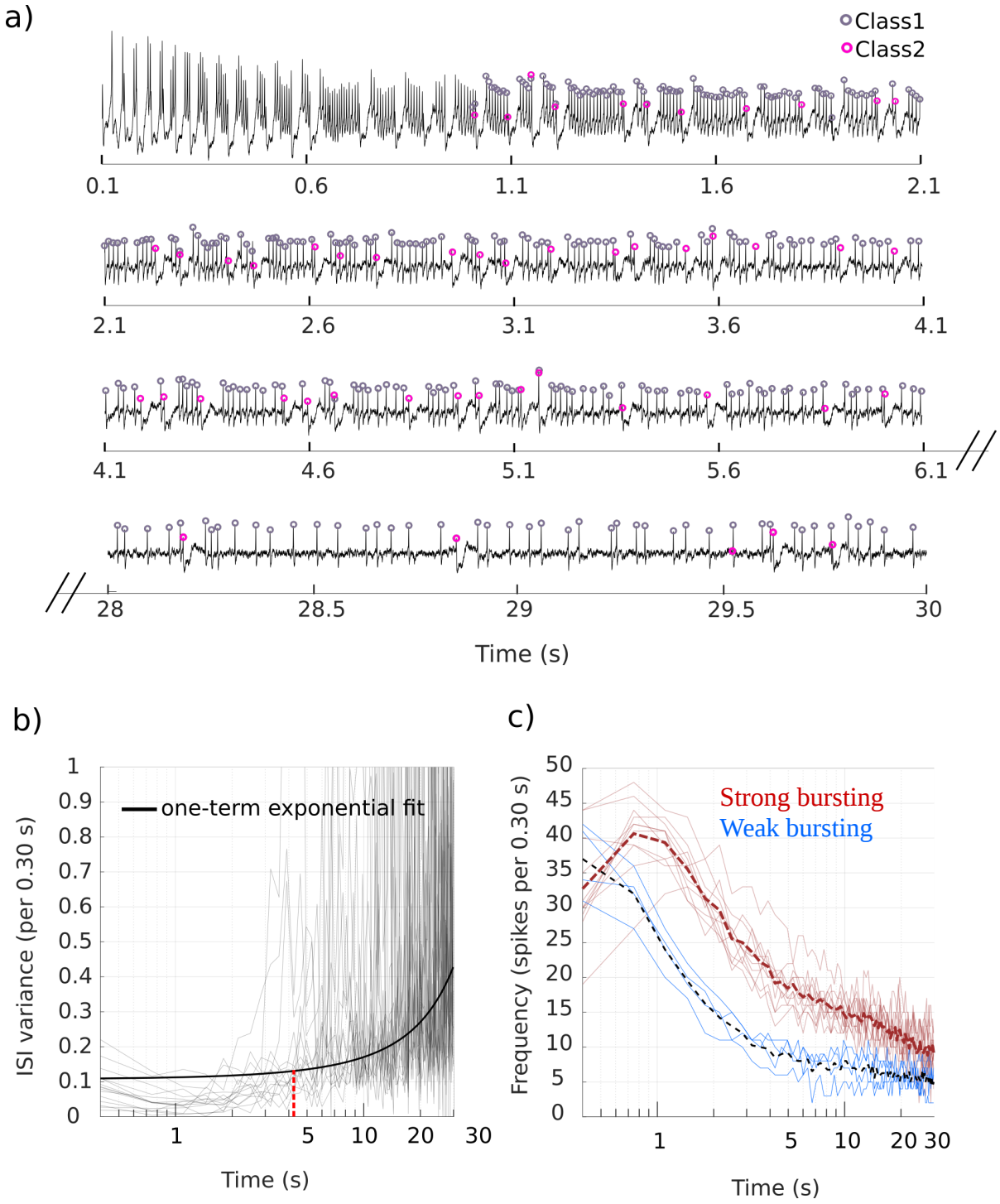

Figure 3.6 *(legend on next page)*

Figure 3.6 : Bursting is associated with low variance in ISI. ***a)*** *Segments of a 30 s stimulation with 100 mM sucrose obtained using the tip electrode recording method. The burst structure changes over the time course of stimulation as GRNs adapt.* ***b)*** *A plot of variance in ISI per 0.3 s time bin (using both Class 1 and Class 2 neuron spikes in the 0.1-30 s duration) for 15 recordings obtained from 15 animals. A one-term exponential fit made to these data reaches 5% of its maximum (red line) after 4 s of stimulation, suggesting that the burst structure persists for at least 4 s.* ***c)*** *Plotting the spike frequency (per 0.3 s time bin) shows that GRN spiking activity adapts over multiple time scales for recordings with high levels of bursting (recordings that had >10 bursts in the first 1s of stimulation; n=11 recordings; red traces). In comparison, low burst recordings (<10 bursts in first 1 s; n=4 recordings; blue traces) adapt much faster. Note that the x-axis in b and c are plotted on logarithmic time scale.*

Since the coherent burst structure persisted for up to 4 s, I monitored the adaptation of the Class 1 neuron spikes located within bursts (figure 3.5 a), for the 4 s duration. In contrast to the spike count which peaks 1 s after stimulus onset, the peak Class 1 neuron ISI is found at the stimulus onset (figure 3.7 a). The rate of adaptation in Class 1 neuron spiking appears to depend on the number of bursts in the recording, suggesting that bursting could provide a mechanism that allows for prolonged rapid Class 1 neuron spiking within the burst structure.

To put these recordings in the context of other research, I compared the adaptation of Class 1 neuron ISIs of *B. terrestris* to the adaptation of ISIs in 8 other insect species (figure 3.7 b). At stimulus onset, the Class 1 neuron ISI was near 0.005 s for *B. terrestris*, which is similar to the ISIs reported in fruit fly (*D. melanogaster, [57]*), tobacco hornworm larvae (*M. sexta, [90]*),blowflies (*P. regina, [176]*), the honeybee (*A. mellifera, [63]*), cabbage white butterfly caterpillar (*P. brassicae*, [56] and mosquitoes (*A. gambiae, [70]*; *A. aegypti*, [172]). Within 1 s of stimulus onset, the firing activity of sucrose GRNs in *Drosophila*, mosquito and *M. sexta* caterpillar almost stopped spiking, indicating that they have adapted completely. At 3 s after stimulus onset, recordings from *B. terrestris* have the shortest ISI, indicating that its GRNs exhibit the highest persistent spiking frequency for this duration among these insects. The GRNs of the butterfly, the honeybee, and the Mediterranean fruit fly (*C.capitata, [177]*) have a slow adaptation rate as well, but these species have a lower rate of spiking than *B.terrestris*.

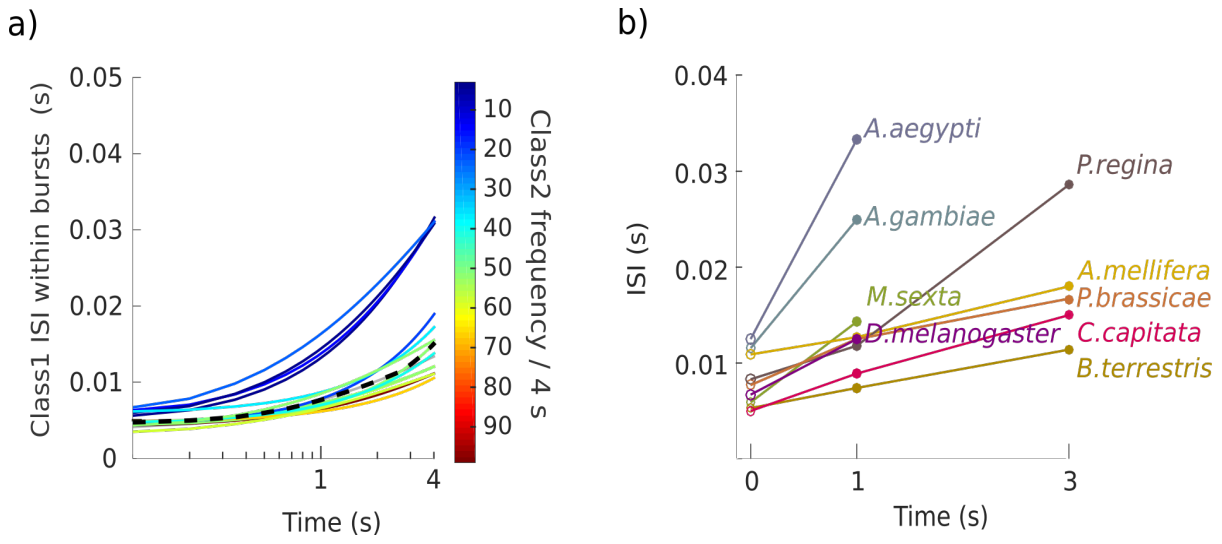

Figure 3.7: Class1 spiking in <u>B. terrestris</u> exhibits a low rate of adaptation in comparison to other insects. ***a)*** *The ISIs of Class 1 neuron spikes within bursts were monitored over a 4 s duration of stimulation by fitting a three-term logarithmic equation to its ISIs over time (same as for burst detection, see methods). Recordings with higher burst count (number of bursts indicated by color) are associated with a prolonged fast rate of spiking (i.e low rate of adaptation). Using the median of these fits (dashed black line) as a measure for the ISIs, B. terrestris was found to have the shortest ISI (highest firing rate) after 1 s from stimulus onset in comparison to other insects* ***(b)***.

3.4.4 Bursting response is generated within individual sensilla and is transmitted towards the sub-esophageal zone (SEZ)

The axons of galeal GRNs project via the maxillary nerve (MxN) and synapse within the sub-esophageal zone (SEZ) in the brain. To observe which features of the burst response are sent towards the SEZ, a galeal A-type sensillum was stimulated with a tip electrode while recording from the MxN at a position approximately 1 mm downstream from the sensillum (figure 3.8 a; see methods). Recordings revealed that spiking, bursting and the underlying oscillatory component were present in the nerve recording (figure 3.8 b), indicating that these features could persist up to the level of the SEZ to provide stimulus relevant information to post-synaptic neurons. In addition, the nerve recording revealed the presence of superposition features and

distinct spike waveforms characteristic of the Class 1 neuron spikes (within bursts) and Class 2 neuron spikes (at end of bursts).

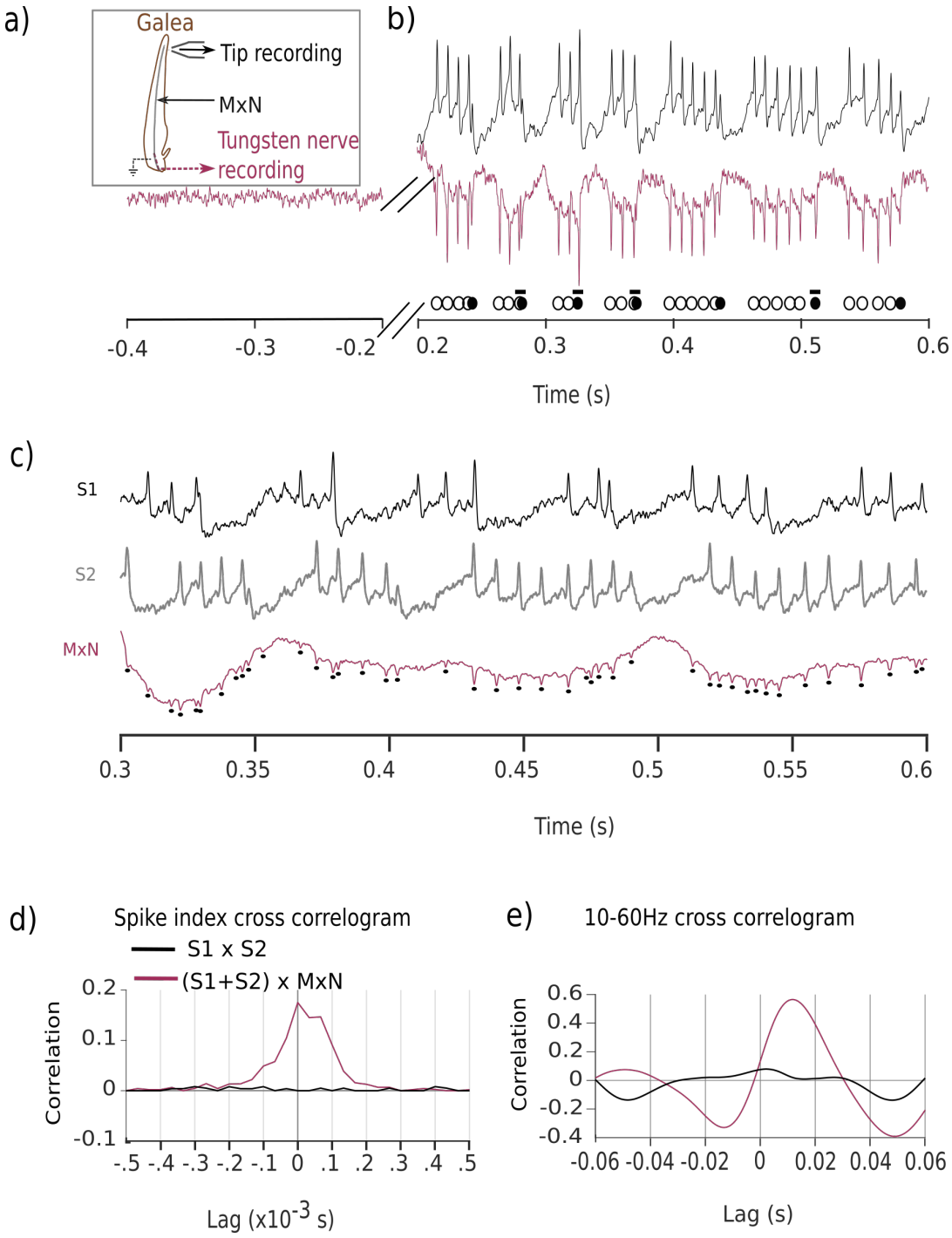

Figure 3.8 *(legend on next page)*

Figure 3.8: GRN activity is not coherent between sensilla. a) *Recording setup for monitoring MxN nerve activity using a tungsten wire electrode during stimulation of an A-type sensillum with a tip electrode.* ***b)*** *Both channels of recording reveal bursts of spikes (open circles), low frequency oscillations, superposition features (bars) and distinct shorter spike shapes (Class 2 neuron spikes) at end of burst positions (closed circles).* ***c)*** *Simultaneous recordings from two neighboring A-type sensilla (sensillum 1 (S1), top; sensillum 2 (S2), middle) and the MxN (bottom trace). The MxN recording shows spikes (dots) and oscillations summed across both sensilla.* ***d)*** *A spike time cross correlogram between the spike times from S1 and S2, obtained by shifting the spike time vector of S1 (a vector of zeros having length equal to the duration of the recording x sampling rate, with a value of 1 at each spike time) to the left and right (indicated by lag on the x-axis) of the spike time vector for S2 and calculating the correlation at each lag. This shows an absence of any correlation (black trace), which is clearly seen in comparison to the cross correlation between the cumulative spike times across both sensilla (S1+S2) and the MxN (blue trace).* ***e)*** *A cross correlogram between the 10-60 Hz filtered recordings from S1 and S2 shows an absence of correlation in low frequency components (black trace). Adding these low frequencies from both sensilla (S1+S2) however does show coherence with the MxN (blue trace). Cross correlograms in c) and d) are averages over 3 trials from the same sensillum.*

To test whether the burst response to sucrose was synchronized between sensilla, two galeal A-type sensilla were stimulated with separate tip electrodes while monitoring the activity from the MxN (figure 3.8 c). The nerve recording shows that spikes from both sensilla were transmitted towards the SEZ. Further, this transmission was independent of the silent period of the neighboring sensillum; spikes in one sensillum were present during the inhibitory period in the other sensillum. A spike time cross-correlogram between the two tip recordings shows the absence of any correlation in spike timing between the two sensilla during stimulation with 100 mM sucrose (figure 3.8 d, black trace). This is intuitively seen from the two sensillum recordings in figure 3.8 c, since the spike times in both sensilla do not appear to align. However, combining the spike times across both sensilla and taking a cross correlogram with the spike times in the MxN recording shows that the spikes are transmitted along the MxN, with a short lag (i.e time delay in transmission) lasting about 0.1 ms. Further, a cross-correlogram between the 10-60 Hz filtered tip recordings shows that the oscillatory components do not indicate coherence,

which suggests that their activity is not coupled (figure 3.8 e, black trace). This is intuitively apparent from the sensillum recordings as well, since the oscillatory components do not appear to be phase locked. Again, combining the low frequencies across both sensilla and obtaining the cross-correlogram with the low frequency components of the MxN recording reveals that the low frequency components are present in the MxN recording as well, showing that the MxN carries the oscillatory components of both sensilla. Taken together, these results show that the silent period of each sensillum does not affect spiking in neighboring sensilla, and each sensillum transmits both spiking and oscillatory components via the MxN.

3.4.5 Burst response encodes for concentration

GRNs encode concentration as a dose-dependent increase in the rate of firing of action potentials. To measure how the activity of both the Class 1 and Class 2 neurons varied over concentration, I stimulated A-type sensilla with increasing concentration of sucrose using a tip electrode. Both the Class 1 neuron (measured as number of spikes in 1 s of stimulation) and the Class 2 neuron (measured as number of bursts in 1 s of stimulation; figure 3.9 a) exhibited an increase in their spiking rate over concentration. The Class 1 neuron started firing at concentrations > 5 mM, whereas the Class 2 neuron fired at higher concentrations i.e > 25 mM. There was also a concentration dependent increase in the power of the underlying oscillatory component (figure 3.9 b; see methods). The peak oscillatory power revealed a significant effect of concentration on the activity of sucrose responsive GRNs (Kruskal-Wallis, $p<0.001$, n=11 sensilla, 7 animals; figure 3.9 c).

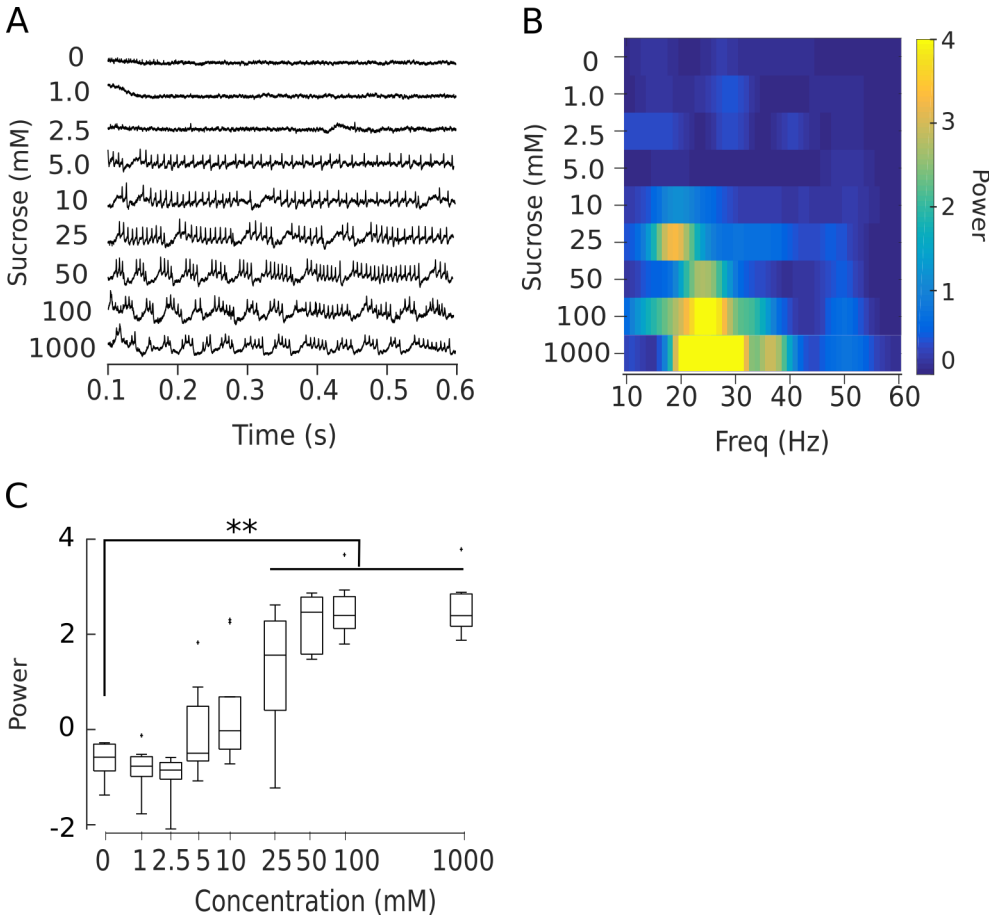

Figure 3.9: Spiking, bursting and oscillatory power are concentration dependent. ***a)*** *Tip recordings show that stimulating a sensillum with increasing concentrations of sucrose evokes a concentration dependent increase in spiking and bursting. The corresponding power spectral density estimates for each of these recordings are shown in* ***b****.* ***c)*** *The maximum power in the 10-60 Hz range increases as a function of concentration (N=11 sensilla, 7 animals).*

A similar trend can be seen from a sample recording from a B-type sensillum, which additionally possess a water responsive GRN (figure 3.10). The water-responsive GRN is silenced as the concentration of sucrose is increased; this is indicated by the presence of superposition waveforms i.e summation of action potentials from both neurons when they fall within a small time window (figure 3.10, arrows). This time window is defined by the absolute refractory period, which is the minimum time required for a neuron to fire two subsequent action potentials. These results indicate that the Class 1 neuron spiking and Class 2 neuron spiking activity is concentration dependent.

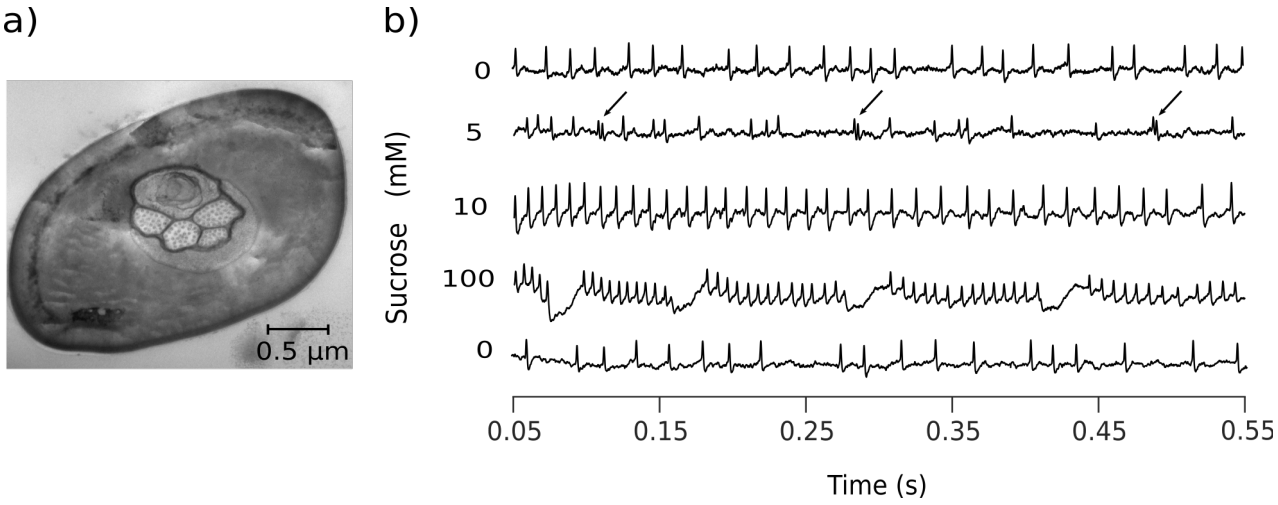

Figure 3.10: B-type sensillum exhibit burst response to sucrose. a) *A TEM shows that the B-type sensilla contain the dendrites of 5 GRNs.* ***b)*** *Tip recordings from a B-type sensillum stimulated from 0 mM - 100 mM, in that order. B-type sensilla possessed a water responsive GRN (top trace), whose activity was silenced with increasing concentration of sucrose; this is indicated by the presence of superposition waveforms (arrows) at 5 mM sucrose, which occur when two or more neurons fire action potentials within a small time window defined by the absolute refractory period for a neuron. From 10mM onwards the water GRN activity is inhibited and only the sucrose GRNs are activated. 100mM sucrose evoked 106 ± 9 spikes/s and 8±3 bursts/s (mean±SEM, n=11 sensilla, 7 animals). The bottom most 0 mM recording shows that the water-responsive GRN activity is recovered.*

In comparison to the galea, sensilla on the labial palps exhibited a far reduced rate of spiking and bursting over increasing concentrations of sucrose, with approximately 32 spikes/s and 3 bursts/s at the plateau of the dose response curves (figure 3.11). This shows that the burst spiking response is spatially distributed across the mouthpart sensilla.

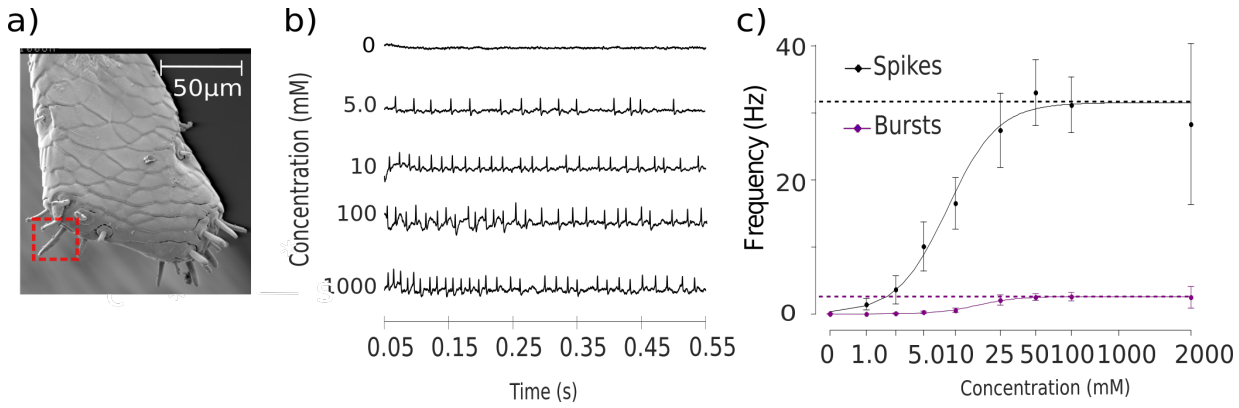

Figure 3.11: Sucrose responses from labial palp sensilla. ***a)*** *A TEM of the labial palps shows that, like the galea, the labial palps possess sensilla of two distinct lengths.* ***b)*** *Stimulating a longer sensillum (outlined red in* ***[a]****) with increasing concentrations of sucrose shows that it does not possess a water responsive GRN, and exhibits slow rate of firing and almost no bursting over concentration. This is reflected in a dose-response curve for spiking and bursting over concentration* ***(c)****. N=13 animals, 1-2 sensilla per animal).*

3.4.6 Proboscis extension is initiated at the threshold of GRN activity for different sugars

Apart from sucrose, nectar contains high concentrations of two other carbohydrates: fructose and glucose. To observe whether the burst response was common to sugars, I stimulated A-type sensilla with 100 mM fructose and glucose. While stimulation with fructose evoked a strong burst response similar to sucrose, stimulation with glucose evoked weak bursting at this concentration (figure 3.12 a).

To observe the concentration dependence for spiking and bursting for these three sugars, A-type sensilla were stimulated with increasing concentrations for sucrose, fructose and glucose. The spike frequency of both the Class 1 neuron (measured as total spike count in 1 s of stimulation) and the Class 2 neuron (measured as burst count in 1 s of stimulation) were modeled with a three-parameter log-logistic fit, made to each sugar (see methods for fitting for summary of the models; figure 3.12 b). The models for all three sugars reveal a concentration dependent increase in spiking activity for the Class 1 neuron (Table 3.1). A comparison between the models

for each sugar revealed a significant difference between their EC_{50} values (effective concentration at 50% of upper asymptote), which shows that the Class 1 GRN is most sensitive to lower concentrations of sucrose, followed by fructose and then glucose (Table 3.2). Further, the models revealed that the upper asymptote of Class 1 spiking frequency for each sugar were significantly different from each other, with fructose evoking the highest rate of spiking followed by sucrose and then glucose (Table 3.3). This indicates that the Class 1 neuron encodes sugar quality in part through its rate of spiking.

Applying the three term log-logistic model to the Class 2 neuron activity revealed a concentration dependent increase in spiking rate for sucrose and fructose (Table 3.4). The model for glucose did not give an accurate estimate for the onset of the Class 2 neuron activity to glucose stimulation nor the onset of the asymptote. However, it predicted that it was activated and reached its plateau at glucose concentrations above 100 mM. At the plateau for spiking, the models show that sucrose and fructose exhibit significantly higher Class 2 spiking rate as compared to glucose (Table 3.5). Further, the Class 2 GRN was more sensitive to lower concentrations of sucrose as compared to glucose, as indicated by a significantly smaller EC_{50} (Table 3.6).

Table 3.1: Summary of the three-parameter log-logistic model having equation $f(x)=b/(1+e^{a(\log(x)-c)})$, for the **Class 1** spiking frequency (Hz; estimated as number of spikes in 1 s of recording) in function of the increasing concentration. The parameter *a* refers to the steepness of the model, the parameter *b* refers to the upper asymptote, the parameter *c* refers to the effective concentration at 50% ($EC_{50,}$ the point at which the rate of firing reaches half of its maximum value). A model was fitted for each sugar tested (fructose, sucrose and glucose). The t-statistics and corresponding p-values are for testing the null hypotheses that the parameters are equal to 0. All three parameters for the curve for each sugar are significantly different from 0 (all $p<0.05$).

Sugar	*Parameter*	*Estimate*	*Std. error*	*t-value*	*p-value*
fructose	a (steepness)	-2.2	0.3	-6.7	0.00
	b (upper asymptote)	111.6	4.0	27.7	0.01
	c (EC_{50})	15.2	1.4	11.1	0.00
sucrose	a	-1.7	0.2	-7.1	0.00
	b	94.6	3.3	29.0	0.00
	c	7.1	0.7	9.8	0.00
glucose	a	-1.7	0.5	-3.3	0.00
	b	68.4	7.1	9.7	0.00
	c	67.8	13.7	5.0	0.00

Table 3.2: The parameter *c* (EC_{50}) of the log-logistic equation for the **Class 1** spiking rate are significantly different between all combinations of sugars.

Comparison	*t-value*	*p-value*
Fructose-glucose	-15.7	<0.001
Fructose-sucrose	3.9	<0.001
Glucose-sucrose	4.0	<0.001

Table 3.3: The parameter *b* (upper asymptote) of the log-logistic equation for the **Class 1** spiking rate are significantly different between all three sugars.

Comparison	*Difference*	*Std. error*	*t-value*	*p-value*
Fructose-glucose	43.2	8.1	5.3	0.0000
Fructose-sucrose	16.9	5.2	3.3	0.0013
Glucose-sucrose	-26.2	7.8	-3.4	0.0009

Table 3.4: Summary of the 3-parameters log-logistic model (same as used for the Class 1 spikes in table 3.1) for the **Class 2** neuron spiking frequency in function of the increasing concentration of fructose, sucrose and glucose. The parameter *a* for glucose was not significant, indicating that the model is not accurate at predicting the onset of the Class 2 neuron response to glucose stimulation as well as the onset of the asymptote.

Sugar	*Parameter*	*Estimate*	*Std. error*	*t-value*	*p-value*
fructose	a (steepness)	-3.3	1.7	-2.0	0.0498
	b (upper asymptote)	22.8	1.9	12.3	0.0000
	c (EC_{50})	25.2	3.4	7.5	0.0000
sucrose	a	-1.5	0.5	-3.1	0.0020
	b	17.9	2.0	8.9	0.0000
	c	16.6	5	3.3	0.0010
glucose	a	-4.9	10.7	-0.5	0.6454
	b	7.6	3.0	2.5	0.0123
	c	88.3	35.6	2.5	0.0140

Table 3.5: The *c* parameter (EC_{50}) of the log-logistic equation for the **Class 2** spiking rate are significantly different between sucrose and glucose

Comparison	*t-value*	*p-value*
Fructose-glucose	-5.8	0.08
Fructose-sucrose	1.0	0.15
Glucose-sucrose	1.6	< 0.05

Table 3.6: The *b* parameter (upper asymptote) of the log-logistic equation for the **Class 2** spiking rate are significantly different between fructose and sucrose in comparison to glucose.

Comparison	*Difference*	*Std.error*	*t-value*	*p-value*
Fructose-glucose	15.2	3.5	4.3	0.0000
Fructose-sucrose	4.9	2.7	1.8	0.0759
Glucose-sucrose	-10.3	3.6	-2.9	0.0047

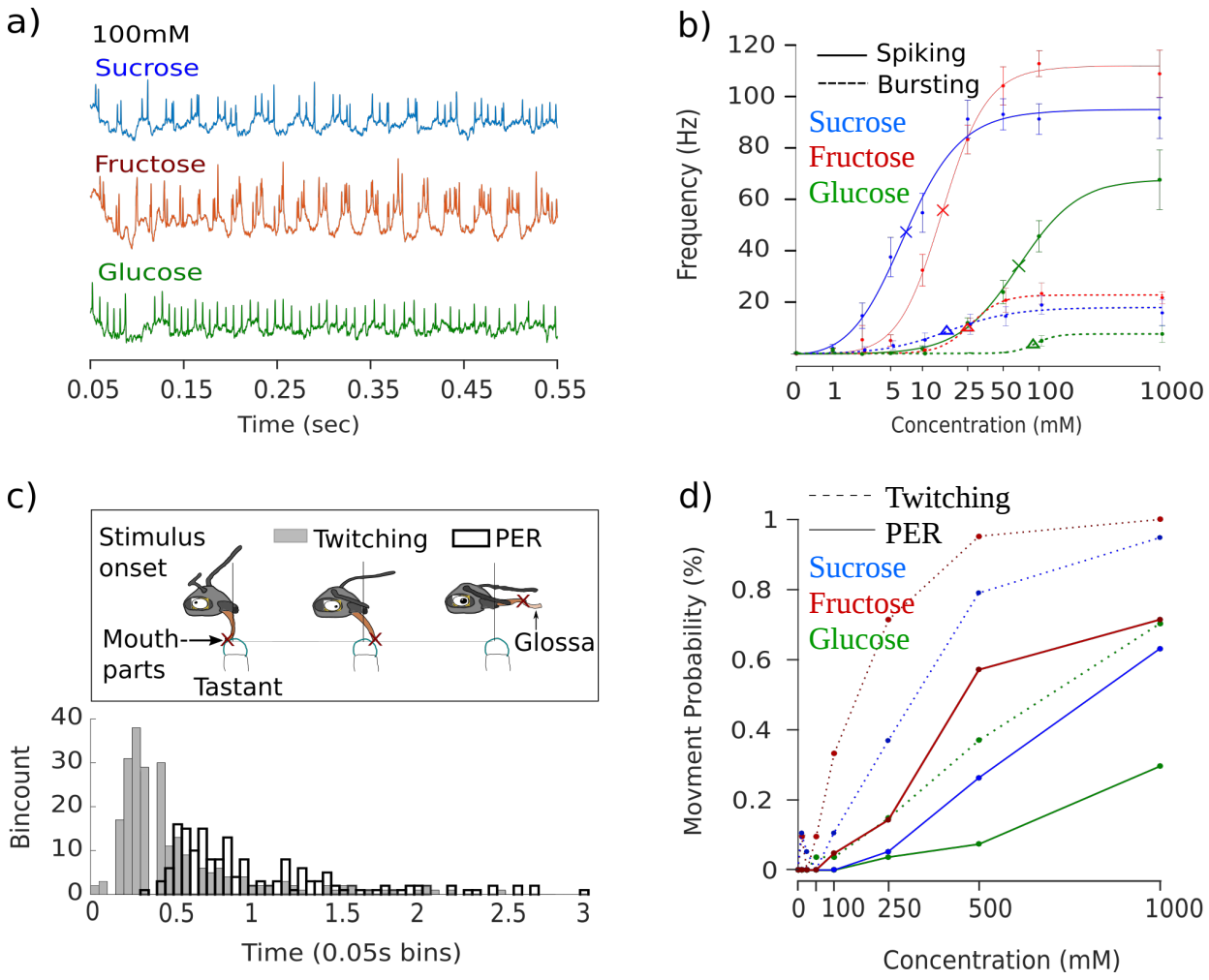

Figure 3.12: Feeding behaviors are evoked at threshold of GRN activity ***a)*** *Tungsten recordings from the same sensillum, in response to the three major sugar components in nectar. All three sugars evoke burst firing, but with different intensities.* ***b)*** *Three-parameter log-logistic equations were fit to the spiking (solid traces) and bursting (dashed traces) responses averaged over recordings, for all three sugars (see methods; n>10 animals per sugar). The crosses and triangles indicate the* EC_{50} *values for spiking and bursting, respectively* ***c) top****: cartoon showing 'twitching' and PER behaviors after stimulus onset.* ***Bottom)*** *Histograms of onset times for 'twitching' and PER (grey and black bars, respectively), compiled from trials using sucrose, fructose and glucose (N=233 trials for twitching, N=173 trials for PER) of varying concentrations (0,10,25,50,100,250,500,1000 mM)* ***d)*** *concentration dependence on the 'twitching' (dashed lines) and PER (solid lines) behaviors over concentration for the three sugars (N>19 animals tested for each sugar).*

The activity of GRNs are responsible for driving feeding related behaviors. Stimulating the mouthparts of *B. terrestris* with droplets of sugar solutions of varying concentrations evoked two distinct feeding responses that occurred within 1 s from stimulus onset (figure 3.12 c). The first behavior was described as a 'twitching' of the mouthparts, which was defined as a threshold movement of the mouthparts in response to the stimulus (see methods). The 'twitching' behavior was evoked near 0.25 s from stimulus onset. At certain high stimulus concentrations, 'twitching' would lead to to full proboscis extension and licking (proboscis extension response [PER]). PER was initiated after nearly 0.6 s from stimulus onset. These two behaviors show that GRN activity in the first 1 s of stimulation is responsible for driving proboscis extension.

The probability of producing 'twitching' or PER increased over concentration (twitching: GLM, $\chi_7^2 = 118$, $p < 0.001$; PER: GLM, $\chi_4^2 = 51.4$, $p < 0.001$) and depended on the sugar used to stimulate the mouthparts (twitching: GLM, $\chi_2^2 = 10.9$, $p = 0.004$; PER: GLM, $\chi_2^2 = 5.83$, $p = 0.054$; figure 3.12 b). Bees were found to exhibit the twitching behavior earliest for fructose at concentrations above 100 mM, followed by sucrose at concentrations greater than 250 mM and glucose above 500 mM. For all three sugars, these were the concentrations at which both the Class 1 and Class 2 neurons reached their threshold of spiking, as described in figure 3.13 d However, bees were only interesting in feeding at even higher concentrations than those that evoked twitching for all three sugars; they exhibited PER for fructose above 500 mM and for both sucrose and glucose this was closer to 1000 mM. In general, fructose and sucrose were the most likely to produce the two behaviors, and stimulation with fructose and sucrose elicited both responses at earlier concentrations than glucose (lsd, all $p < 0.050$).

To observe whether the burst response was common to bumble bees, I stimulated A-type galeal sensilla in *Bombus pascorum* (Scopoli) with 100 mM sucrose (figure 3.12). The recordings revealed the characteristic burst structure with two visually distinct spike waveforms. I extended the study to fructose and glucose as well, and found that while responses to all sugars exhibited bursting, there was an apparent difference in the magnitude of activity between sugars, with fructose and sucrose evoking higher spiking and bursting than glucose.

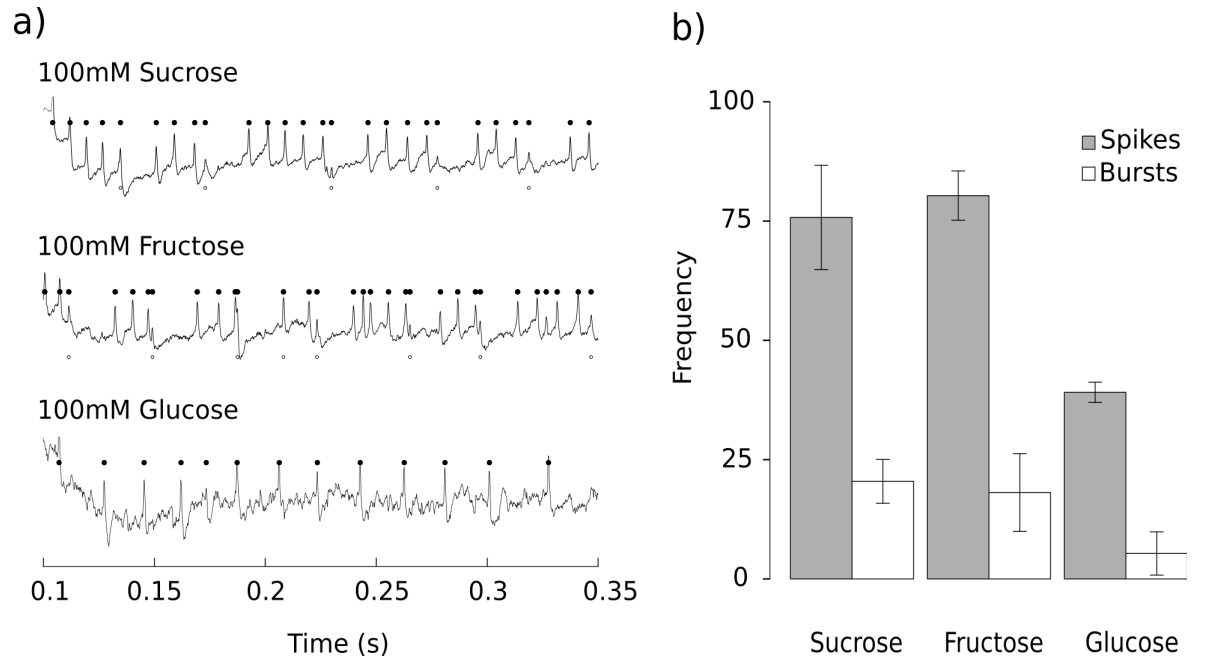

Figure 3.13: Bombus pascorum A-type sensilla exhibit burst spiking GRNs. a) *Tip recordings made from Bombus pascorum galeal A-type sensilla, to 100 mM sucrose, fructose and glucose. Fructose and sucrose exhibit strong bursting (end of burst positions indicated by open circles, spike positions by solid circles), whereas glucose exhibits few to no bursts.* ***b)*** *The mean frequency of spiking and bursting in the 0.05-1.05 s duration from stimulus onset were greater for fructose and sucrose as compared to glucose (Mean±SEM; n=1-3 sensilla per animal, 3 animals).*

3.5 Discussion

3.5.1 Characterizing the gustatory sensilla in B. terrestris

The distribution of gustatory sensilla on the galea of the bumble bee *Bombus terrestris* was similar to that described for the honey bee (*A. mellifera* [45], [109] and other species of bumble bees [110]. The longer A-type and shorter B-type galeal sensilla of *B. terrestris* are referred to in *A. mellifera* as the longer sensilla *chaetica* (~40 µm) and shorter *basiconica* (<10 µm) respectively [45].

In *B. terrestris*, the A-type sensilla possess 4 GRNs, as do the sensilla *chaetica* in *A. mellifera* [45]. This is similar to other insects whose sensilla possess between 2-5 GRNs as well [10], [20], [66], [70], [71], [144]. The dendrites of the *B. terrestris* sensilla are tightly packed within an inner lymphatic cavity, similar to that of butterflies [66], [71]. In comparison, there is a larger spacing between the dendrites in moth [20], *A. gambiae* Kessler et al. 2013), *Drosophila* [143], [144] and blowfly (*Phormia regina;* [20].

Using the tip and tungsten electrodes, I found that GRN activity is mostly restricted to the stimulation period. This suggests that these GRNs transmit information primarily via an increase in spiking activity. In comparison, olfactory receptor neurons (ORNs) encode stimulus information through inhibition in baseline activity as well as through spiking activity that outlasts the stimulation period [53]. While tungsten recordings in *Drosophila* [150] and cotton leafworm (*S.littoralis*; [149]) also suggest response types similar to ORNs, these studies did not test how repeatable the response structures were to determine their role in gustatory coding.

From the tip and tungsten recordings, I found that the GRN action potentials travel anti-dromically. Previous studies in other insect species' gustatory sensilla suggest that spikes are transmitted from an initiation site at the cell body up through the sensillum [4]–[6]. This could occur either by active propagation through the dendrite [6] or by passive transmission through the inner and outer lymphatic cavities of the sensillum [5], [60]. In the bumblebee, I measured anti-dromic conduction velocity of spikes within the A-type sensillum to be ~0.1 m / s (0.25 x

10^{-3} s between spike peaks with ~10 µm distance between tip and tungsten electrodes). This slow conduction suggests spikes are passively transmitted via the sensillum lymph, as suggested by [5].

3.5.2 Two GRNs are involved in the burst response

In most insects, only a single GRN within each sensillum responds to stimulation with sucrose, including blowfly [7], [61], [156], Drosophila [8], [25], [170], moth [65], [90], ants [178] and butterfly [66], [71]. In *B. terrestris*, there was strong evidence to suggest that the burst response to sugars involved the activity of at least two separate GRNs. First, spike sorting tip and tungsten recordings obtained from stimulating A-type sensilla with 100 mM sucrose revealed two well separated spike clusters (Class 1 and Class 2 spikes) that had distinct waveforms on both electrodes. Differences in spike shape could arise due to the relative proximity of the recording electrodes to each GRN soma, where the spikes are initiated [4]–[6], and resistance in the extracellular medium [135].

Second, sorting revealed the presence of superposition waveforms. In sensillum recordings, as in other extracellular records of neural activity, superposition features arise when multiple neurons fire within a small time window such that their action potentials summate. The time window is described by the absolute refractory period (ARP), which is the minimum time required for a neuron to fire an action potential following a previous action potential [89], [155], [156]. The ARP is due to the inactivation of the Na^+ channels that generate the rising phase of the action potential, which take time to reactivate again. Further, the K^+ channels that are responsible for the falling phase of the action potential exhibit delayed closing, such that the potential drops below membrane potential which makes it more difficult to fire a subsequent action potential.

On the other hand, superpositions can also arise from individual neurons that have multiple spike initiation zones (SIZs). If an action potential is initiated at both SIZs simultaneously, they can be monitored as a superposition feature by an extracellular electrode. Extracellular recordings made from GRNs in a cockroach gustatory sensilla [146] revealed superposition features that were due to spiking activity from an SIZ in the distal dendrite and

another SIZ ~250 µm away, near the GRN soma. However in this study, the superpositions always had the same distance between spike peaks, whereas for *B. terrestris* the peaks of superpositions were separated between 0-0.002 s. Further, the A-type sensilla are <20 µm long, which means that a spike initiated at the distal dendrite would propagate towards the soma (located some tens of microns below the sensillum base in most insects; [20], [179]) within the somatic ARP and prevent an additional spike from firing. It is therefore unlikely that the superposition features are due to action potentials generated at multiple SIZs within the GRN. Superposition features could also arise when a spike propagates along different dendritic branches of the same neuron [180], [181]. However, GRN dendrites of insects like bees are single fibers [20], [45]. Finally, visually distinct spike waveforms and superpositions were present in recordings at the level of the GRN axons from the MxN, which strongly suggests that at least two separate GRNs are active during sucrose stimulation.

The Class 1 neuron was active within bursts, and its activity was terminated by the single action potential of the Class 2 neuron at the end of bursts (figure 3.2). Each burst consisted of at least one GRN1 and GRN2 spike, and hence a minimum of 2 spikes defined each burst. This presents the first evidence from sensillum recordings where multiple GRNs are involved in a structured pattern of activity. While studies in other insects suggest that multiple GRNs within each sensillum can be activated by sucrose [18], [182] or that there are multiple GRNs within each sensillum that are responsive to different sugars [183], [184], the spiking response of the GRNs in these insects do not follow any apparent structure.

The absence of a water response from the A-type sensilla indicates the water sensitive GRN was not involved in the burst structure. Even for the B-type sensilla, which possess 5 GRNs of which one responds to water, the water responsive GRN is silenced by the activity of the sucrose GRNs. The burst response did not involve the mechanoreceptor neuron either, as the mechanoreceptor had a distinct spike waveform. In comparison to the galeal sensilla, sensilla on the labial palp responded to sucrose stimulation with mostly a single GRN and a reduced magnitude of spiking and bursting.

3.5.3 Possible mechanisms driving bursting in A-type sensilla

This study provides the first evidence for a persistent burst structure in first order neurons. Most existing descriptions of bursting are exhibited by higher-order neurons, and are driven either through intrinsic mechanisms [185]–[189] or via synaptic interaction between neurons [186]. It is unlikely that the GRN bursting in *B. terrestris* is driven by synaptic mechanisms, as the first synapse for GRNs is considered to be within the sub-esophageal zone (SEZ) in the insect brain [15]. Lemon and Turner [187] describe a neuron intrinsic mechanism that drives bursting, in pyramidal neurons of weakly electric fish. This mechanism involves a back-propagation of spikes from the soma into the dendrites, which generates a return current that contributes to a depolarization following the somatic spike. This depolarization builds up over the course of the burst until a final 'doublet spike' is fired, with the second spike of the doublet falling outside the somatic ARP. The 'doublet spike' inactivates Na^+ channels and generates an hyperpolarization which terminates the burst. However, it is unlikely that this mechanism of bursting in pyramidal neurons as described by [187] explains the burst structure observed in *B. terrestris* GRNs, for two main reasons. First, the pyramidal neurons never exhibited spikes within the ARP, whereas spike superpositions having action potential peaks within the ARP were common in the A-type sensilla of *B. terrestris*. Second, ISIs did not always decrease over the burst duration in *B. terrestris* as they did for pyramidal neurons; instead, ISIs increased over longer duration bursts.

Instead, it is likely that an interaction between both GRNs is driving the burst structure. This is indicated by 1) both GRNs firing at specific phases of the burst structure, and 2) the fact that the spike timing of the Class 1 neuron was dependent on Class 2 neuron spiking activity. There are at least two separate mechanisms which drive this burst structure: one which drives GRN spiking activity and another which drives inhibition between bursts. These are described in the following sections.

3.5.4 Mechanisms driving GRN spiking

The spike timing of both classes of GRNs was strongly correlated in the first 1 second of the recording. However, as the GRNs adapted during longer recordings, we found that the correlation in their activity disappeared as a result of their different adaptation rates. In fact, the

Class 2 neuron had ~20x higher adaptation rate than the Class 1 neuron. This suggests that each GRN is independently activated by the sugar ligand. When a compound is a good ligand for the receptor, it will bind with high efficiency at low concentrations. In our recordings, the Class 1 neruon was activated by lower concentrations of sugars than the Class 2 neuron. The response tuning curves towards sucrose, fructose, and glucose were very similar for both neurons, with the threshold for detection shifted towards higher concentrations for the Class 2 neuron.

Alternately, only the Class 1 neuron possesses the sucrose binding GR, and activity of the Class 1 neuron induces a Class 2 neuron spike through an excitatory lateral interaction. Such an lateral interaction should be non-synaptic, as the first region of synapse for GRNs is within the sub-esophageal zone (SEZ) [45], [92]. The close proximity of the dendrites within the A-type sensilla, along with the fact that insect neurons are non-myelinated [190], [191], could allow for two well known types of lateral interactions between these GRNs : 1) interaction via electrical synapses such as gap junctions, and 2) ephaptic interactions.

Gap junctions are protein channels that form connections between cell bodies, axons or dendrites of neighboring neurons, and allow flow of electric current, small metabolites and intracellular signaling molecules (for review see [192]). They can mediate the transmission of depolarizing and hyperpolarizing potentials between neurons, as shown for coupled interneurons in the vertebrate neocortex [84], [85]. The close proximity of the GRN dendrites within the A-type sensillum could allow for the presence of a gap junction between both classes of GRNs, and could therefore allow the Class 1 neuron spikes to drive depolarizations in the Class 2 neuron to eventually generate a spike. Only a few studies report evidence for gap junctions in insect chemosensory neurons. One detailed study of contact chemosensilla in the inner cavity of the cockroach hypopharynx identified gap-junction like articulations among its GRN dendrites (a.k.a inedite jonction intercellulaire, [87]. Similarly, Ma [66] reported connections like gap junctions among the ciliary connective tissues of the GRN dendrites of the maxillary sensillar styloconicum of larvae of the cabbage moth, *Pieris brassica*. These are the only studies I know of where gap-junction like connections have been reported among the dendrites of GRNs. Whether or not this is a general feature of GRNs in insects, therefore, remains uncertain.

In an ephaptic interaction, the electric field associated with the spiking activity of a neuron modifies the excitability of a neighboring neuron, depending on their electrical and anatomical proximity [76]–[78]. This could allow for an action potential to evoke a depolarization in an ephaptically coupled neuron that leads to the generation of a spike. Such a spike 'transmission' was shown to occur between axons in vertebrate [193] and squid [194], with delays in transmission varying between tens to hundreds of milliseconds.

3.5.5 Mechanisms driving inhibition between bursts

The periods between bursts are most likely held under an inhibition which prevents spiking from both GRNs. As the inhibition wears off, the Class 1 neuron spiking activity picks up again; this describes the decrease in ISI over the course of short duration bursts. The shape of the Class 2 neuron spike in unfiltered recordings (figure 3.6 a), along with the fact that its spikes are located at the negative phase of the underlying oscillation, suggests that the Class 2 neuron spike is associated with an after-hyperpolarization (AHP) that generates this inhibitory period.

A spike AHP refers to the phase following the peak of an action potential where the neurons membrane potential falls below the resting potential. This occurs due to the delayed closing of K^+ channels which are responsible for repolarizing the membrane, which functions to raise the threshold of generating subsequent action potentials for varying durations of time [195], [196]. For action potentials, the AHP is of short duration (~1 ms; [140]). However, an AHP can last longer if the activity of the K^+ channels are modified. For example, in hippocampal neurons of guinea pigs [197], mice [198] and rats [140], [199], bursts of action potentials lead to a Ca^{2+}-mediated increase in permeability to K^+ at the soma that results in an extended AHP. This AHP takes between 50-100 ms ('medium' AHP duration; [140]–[142]) or even up to 1 s ('slow' AHP duration) or 1 minute (sensory neurons in the CNS of leech, [200]) to repolarize.

AHPs have been shown to effect neural spiking activity. For example, inter-ictal spiking activity (durations of activity between epileptic neural events) is associated with AHPs that are suggested to play a key role in preventing epileptic discharge [201]. In the burst response in B. terrestris, the IBI lasts ~0.029 s which is near the time scale for a medium AHP. A hyperpolarization generated by the Class 2 neuron could effect the Class 1 neuron through a gap

junction. This is because gap junctions have been shown to efficiently transmit low frequencies such as hyperpolarizations [192]. The AHP can account for the observed low frequency oscillation in the tip and tungsten recordings. It could also account for the oscillations in the maxillary nerve recording, if the GRN axons possess the same ion channels that produce the AHPs. However as far as I know, AHPs have not yet been shown to be transmitted across the length of a neuron.

In the insect antennal lobe, oscillations observed in LFP recordings are generated by synchronous firing in a population of neurons within the antennal lobes [202], which is driven by the inhibitory GABAergic feedback provided by interneurons [94], [95]. It is unlikely that these oscillations in the A-type sensilla are driven by synchronous GRN activity, because there are only two active GRNs during the response and there are only 4 GRNs within each sensillum.

Inhibition in spike firing could also be mediated through ephaptic interactions between neurons. Inhibitory ephaptic interactions have been described for the Purkinje cells in mice [203], [204] and Mauthner cells in teleost fish [79], [205]. The spike initiation zones (SIZs) near the axon hillock of these neurons are surrounded by dendrites. The electric field associated with the dendritic activity influences the potential around the SIZ, which generates a hyperpolarization that inhibits spiking for a duration of the order of ~0.001 s [79]. While the sensillum environment could allow for an inhibitory ephaptic interaction between neurons [75], it is unlikely that this is the mechanism that drives the inhibitory period following the Class 2 neuron spikes since the inter-burst interval (~0.029 s) was approximately 10 times longer than the inhibitory periods described for the Purkinje and Mauthner cells.

In sensillum recordings, low range frequencies (<300 Hz) are assumed to be contributed by receptor potentials. Receptor potentials are a form of graded potentials (potentials established from passive diffusion of ions), and are associated with the transduction mechanisms that are initiated when a tastant molecule binds to a GR. However, receptor potentials for sensilla are typically described at the onset and offset of a stimulus [44], [147], [206], which does not describe the persistent oscillation exhibited in the sucrose response.

For some invertebrate first order sensory neurons [207], [208], graded potentials have been shown to be transmitted for distances up to 1cm. However, these neurons have high space constants (a measure that describes how far graded potentials can be passively transmitted through a neuron) due to their large diameters (~25 µm). In comparison, the axons of GRNs are very short (~3 µm; [112], [209], which suggests that the passive diffusion of ions would not reach the brain.

3.5.6 Possible functions of bursting

Burst firing has been observed in several vertebrate neurons, and have been documented to drive a variety of functions regarding processing of information. For example, thalamic relay neurons, which relay retinal information to the cortex, exhibit both tonic and burst firing modes, each of which effects the way the neurons respond to incoming input [210]. In weakly electric fish, bursting in the second order pyramidal neurons extract stimulus specific information [211]. Bursts have also been suggested to increase the reliability of synaptic transmission through facilitation [189], [212], [213], lead to synaptic potentiation [211], [214] and plasticity [188], as well as allow for selective communication between neurons [215].

In the insect antennal lobe (AL; brain region that receives axonal projections of ORNs) and the optic lobe (brain region for processing visual stimuli), temporally structured spiking activity is implicated in stimulus coding. For example, fly visual neurons encode for stimulus relevant information through short sequences of spikes [210] as well as over multiple longer time scales as the neurons adapt to the stimulus [216], [217]. In the AL, temporally structured spike trains and oscillations have been shown to drive synchrony between populations of neurons which aids in stimulus discrimination [53], [218]. The burst response of *B. terrestris* GRNs was temporally structured as well, with ISIs decreasing over short duration bursts and exhibiting multiple time scales of adaptation over a 30 s period of stimulation. Unlike for the AL, the structured spike firing and oscillations did not function to drive synchrony between neighboring sensilla. Whether the temporal structure could encode for information is cannot be deduced from the limited types of stimuli I used here.

The *B. terrestris* GRNs encoded concentration through a concentration dependent increase in the rate of spiking and bursting, as well as the power of the underlying oscillatory component. In insects, GRNs synapse onto neurons in the SEZ, which in turn coordinates the activity of motor neurons that generate proboscis extension and food ingestion [15]. While the activity of most insect GRNs is concentration dependent, there are only a few studies that reveal a direct correlation between GRN spiking intensity and motor activity that controls feeding behaviors [14], [15]. In this study, I found instead that feeding behaviors are initiated at concentrations that evoke threshold spiking from the Class 1 and Class 2 neurons. This suggests that the threshold activity of a population of GRNs drives behavior [103].

The burst structure to sucrose persisted for up to 4 s from stimulus onset. This falls within the time window (1-5 s) that bees spend accessing and ingesting nectar from individual flowers [219]. This short time window could be due to the low volume of nectar in flowers, which is typically less than 6 µl [219]. When bees encounter larger volumes of solution, their first bouts of feeding typically last for 1-5 s as well [220]. This suggests that the burst portion of the GRN response is important for driving natural feeding behaviors in bumble bees.

This study suggests a novel mechanism for burst firing in prolonging adaptation. Burst firing in *B. terrestris* was associated with GRN 1 spiking activity that continued to adapt even after 30 s of stimulation. This extended adaptation could be associated with the fact that *B. terrestris* can spend up to 60s feeding on a large source of food [220]. Further, bumble bees forage not only for satiety but to provide food for their colony, and have been shown to ingest up to 50 µl of food on a single feeding session [220]. This could predict that they need a strong driving form of gustatory input to maintain continuous feeding on a solution. Finally, *B. terrestris* exhibited the highest firing rate of the GRN1 activity in comparison to studies in other insect species, after just 3 s of stimulation. The burst structure could therefore provides bumble bees with a unique advantage when it comes to detecting sucrose.

3.6 Conclusion

From these studies, it can be seen that bumble bees like *B. terrestris* and *B. pascorum* present a unique model for studying how peripheral gustatory neurons encode for taste stimuli. The GRNs of galeal sensilla in bumble bees interact with each other to form a temporally structured representation for sugars like sucrose, glucose and fructose at the periphery. The data presented here are the first to show 1) that first order neurons can respond to stimulation with a persistent burst structure of spike firing with a coherent oscillatory component, 2) that bursting can be driven by two separate neurons firing at specific phases in the burst structure, and 3) a burst firing response that is concentration dependent.

The data suggest that bursting could allow for a persistent high rate of spike firing of the most responsive class of gustatory neuron in the response (Class 1 neuron). This would be the first time that bursting was reported as a mechanism for resisting spike frequency adaptation. Feeding behavior is correlated to the threshold of spiking and bursting, suggesting that a population of neurons are required to drive behavior.

Chapter 4. Recording Gustatory Neuron Activity From Central Locations in the Bumble Bee

4.1 Abstract

Studying how gustatory stimuli are encoded, distributed and integrated by gustatory neurons at the periphery and in the central nervous system is fundamental for understanding how feeding behaviors are controlled. In insects, the coding structure of peripheral gustatory neurons (gustatory receptor neurons, GRNs) has been well documented through microscopy, genetics, imaging and electrophysiology. In contrast, the way gustatory information is transformed over synapses and how neural ensembles at different levels of the brain represent quality and quantity of tastant information at any given time to drive behavior has not been thoroughly examined. In the previous chapters, I have established the bumble bee *B. terrestris* possesses GRNs within their galeal sensilla that exhibit a unique coding strategy. This was described by bursts of action potentials that appears to be driven by an interaction between neighboring GRNs of a sensillum. My next goal was to develop a method to observe how the coherent activity from these GRNs coordinates activity from downstream neurons in the bee's brain. Further, I wanted to access the GRNs individually using intracellular methods, in order to approach the mechanism that drives the interaction. In this chapter, I show how to approach these goals in an American species of bumble bee, *Bombus impatiens*. I present a dissection procedure for accessing the mouthpart nerves that carry the axons of GRNs, and the primary gustatory region (sub-esophageal zone, SEZ) at the level of the brain. I use techniques such as dye staining and intracellular and extracellular recording to monitor the activity of these neurons.

4.2 Introduction

All sensory circuits share similar fundamental features for processing stimuli : stimulus relevant information is initially encoded by peripheral neurons, this information is distributed and integrated within the central nervous system, and as a result motor output is coordinated to generate an appropriate behavior. In insects, the sense of taste, known as gustation, starts with the peripheral gustatory receptor neurons (GRNs). The structure of firing and coding characteristics used by GRNs have been well documented across a variety of insect species.

GRNs are organized in groups of 2-5 units, with their dendrites housed by hair-like sensilla that are distributed across the insect's body [10], [20], [45], [66], [70], [71], [143]–[145]. Each GRN within a sensillum is activated by tastants belonging to one of the four taste categories: bitter (or aversive compounds), sweet, water (or solutions with low osmolarities), and salt [9], [26], [31], [47], [48]. Once activated, the GRN generates a train of spikes, whose structure is characterized as a brief (~100ms) increase in spiking frequency that adapts with prolonged stimulation to tonic firing [56]–[59], [63], [172]. In this way, GRN spiking activity encodes taste category, and the rate of firing of action potentials encodes concentration [1], [7]–[11].

The axons of these GRNs project into the sub-esophageal zone (SEZ), which is the first region of gustatory processing in the insect brain. The SEZ has been characterized in detail in several insects with regards to the organization of its gustatory input. The SEZ receives GRN axonal projections from across the insect's body into specific zones, which reflect their organ of origin [9], [22], [96]. For example, studies in the bee have shown that the majority of the SEZ is divided into the labial, maxillary and mandibular neuromeres, that receive input from those respective mouthpart organs [22]. Studies in Drosophila have revealed that the axonal projections of the GRNs exhibit a certain level of functional organization as well : sweet and bitter GRNs synapse onto mostly non-overlapping (yet spatially distributed) subsets of post-synaptic neurons [31], [48], [73], [97], and their activity evokes attractive and aversive behaviors, respectively [47].

Studies in *Drosophila* are starting to reveal how gustatory input is integrated within the SEZ. For example, one study revealed the function of GABAergic interneurons in regulating the pre-synaptic output of sweet responsive GRNs, to act as a gain mechanism for detecting bitter compounds [92]. Other studies have revealed several interneurons that coordinate the activity of motor neurons involved in initiation, continuation and cessation of feeding [99]–[101]. On the other hand, there is also almost nothing known about the importance of the structure of the GRN spike trains in driving downstream activity. In the insect olfactory circuit, temporally structured spiking activity of the peripheral olfactory neurons [53], [54] has been shown to drive coherent and oscillatory activity from ensembles of downstream neurons [92]–[94], which aids in stimulus discrimination ([218]). In the insect visual circuit, stimulus relevant information is encoded by

statistics in spike timing [210], [216]. This indicates that the temporal structure of GRN activity could influence how information is coded and integrated in the SEZ.

Studies in blowfly show that the intensity of GRN spiking activity within the first 0.03 s of stimulation is enough to drive muscle activity [14]. Studies in the blowfly and *Drosophila* show that the interneurons retain information regarding the strength of the GRN input to drive a graded activity from the motor neurons [14], [15]. Recordings from moth GRNs suggest that tastant specific information is initially encoded by spatio-temporal patterns of GRN activity, and that this information is temporally transformed over synapses [103], similar to that observed in the olfactory circuit. The mechanisms driving this transformation of GRN input and their role in gustatory coding and integration within the SEZ is yet to be answered.

Bees provide a perfect model for studying strategies used by gustatory circuits. This is because their gustatory circuitry needs to be efficient for encoding tastants, which would enable them to find the most rewarding sources of nectar and pollen, as well as to build associations with location and floral cues to plan return visits [120], [121], [124]. In my previous work (Chapter 2), I show that bumble bee GRNs exhibit unique strategies for encoding sugars that are not observed in any other insect. These data showed that a subset of maxillary sensilla responded with bursts of spikes involving two GRNs when stimulated with sucrose (figure 3.2). Understanding how this burst structure contributes to driving behavior would require recordings to be made from individual populations of gustatory neurons at regions downstream to the sensilla.

In this chapter, I describe a dissection protocol that allows for accessing the gustatory regions of the bumble bee *B. impatiens*. This gives access to the MxN and the SEZ, so that populations of neurons can be monitored using extracellular electrodes and individual neurons can be monitored using intracellular electrodes. To obtain extracellular recordings, I use twisted tungsten wire electrodes. Each neuron will have a unique spike shape on each electrode, based on its proximity from the recording electrode and resistance of the extracellular medium [135], [138]. I then use a spike sorting method developed by [133] and [134] to monitor the activity of individual neural units in the recording. For intracellular recordings, I use a blind sharp electrode

recording technique, by which a sharp glass electrode is lowered into the region of interest until it punctures a neuron. Finally, I stain the nerves with dyes such as rhodamine to observe their projections into the gustatory regions. The advantages and limitations of these techniques for *B. impatiens* are then discussed.

4.3 Methods

4.3.1 Bees

Female *Bombus impatiens* (Koppert Biologial Systems, NATURPOL, Netherlands) were used for all physiological studies. Bees were first cold anesthetized and pushed through a cut pipette tube until only their heads stuck out. Using a wax melter, wax was applied to the body of the bee to keep it in place in the tube. To access the gustatory regions of the brain, the dissection can be made from either the dorsal side of the head or from the ventral side. The entire preparation takes approximately 45 minutes.

4.3.2 Dye staining

To stain nerves, a pressure ejection technique was used. A glass capillary electrode (Sutter Instruments) was first pulled to a tip diameter of 1 µm using a horizontal electrode puller (P87, Sutter Instruments). The electrode tip was then broken using fine forceps, so its diameter was just smaller than the diameter of the nerve of interest (~0.02 mm for the MxN). This capillary was attached to a suction electrode holder, and the tip of the electrode was positioned next to the open end of the severed nerve. A small amount of suction was applied so that the nerve entered into the tip of the capillary. Best results for staining are obtained when there is a tight seal formed by the nerve and the electrode tip, as it prevents any dye in the electrode from leaking out. The electrode is then filled with a 4% solution of rhodamine dye made in 100 mM LiCl, and is kept on the nerve for 3 hours to allow the dye to be taken up by the nerve. During this time, the brain should be covered with saline to prevent the preparation from drying up.

After 3 hours, the region of interest (brain if a back-filling was done or the mouthpart if a forward-filling was done) is excised and placed in a 1 ml tube filled with fixative in a phosphate buffer (4% paraformaldehyde in 200 mM Sorenson's PBS), and is kept in the fridge overnight. This is followed by a wash with an ethanol series (30%, 50%, 70%, 90%, 100%), allowing at least 15 minutes in each solution. At this point the sheath is removed. The tissue is then cleared with methyl salicylate and is sandwiched between a conical glass slide and a glass coverslip without applying too much pressure on the tissue. The sample can then be imaged with a confocal microscope.

4.3.3 Electrophysiology

The brain and nerves are coated with a thin sheath that has to be removed to allow for recording from the neurons using extracellular and intracellular electrodes. Further, the muscles have to be inhibited to prevent movement and to prevent spikes from the neuro-muscular junction from being picked up by extracellular recording electrodes. Muscle spikes can be identified by their large amplitude and width, and a strong low frequency component (Fig. 4.1). Their presence in the recording makes spike sorting difficult as they interfere with the spike shapes recorded from the MxN, even after filtering out the low frequency components. Recordings are only used if the muscle spikes are absent. To remove the sheath and inhibit muscle activity, the wax cup around the bees brain is filled with a solution of 0.5 µg collagenase/dispase (Roche Diagnostics) in 100 µl of saline. After two minutes, the brain is washed thoroughly with saline. Care must be taken not to use a high concentration of collagenase or keep the solution for too long as it can damage the neurons. At this point, the sheath can be teased apart using fine forceps. For the MxN, the sheath appears like a sleeve that can be pulled back to reveal the underlying axons that constitute the nerve.

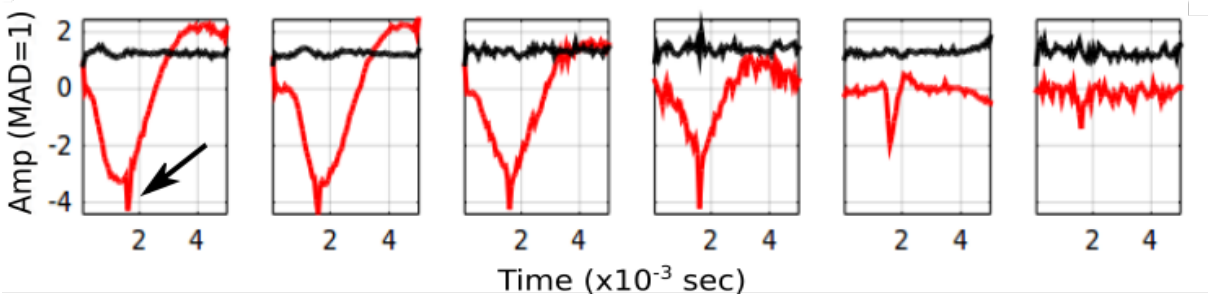

Figure 4.1. Muscle spikes contaminate the extracellular recording. *Example sorted spikes from an extracellular recording made from the MxN show the presence of spikes having multiple amplitudes and widths (red waveform represents mean waveform of each cluster, in black is the standard deviation [SD] of all waveforms in each cluster). Larger spikes are most probably from muscle activity originating from outside the MxN (first 4 waveforms), whereas smaller spikes are from activity of axons carried by the MxN (last two waveforms). The larger spikes drown out the smaller spikes, as can be seen in the first panel (arrow points to a smaller MxN spike that rides*

on top of the larger spike). Y-axis is amplitude (Amp) normalized to the MAD of the waveforms of the clusters.

For multichannel extracellular recordings, twisted wire electrodes were used. Three or four tungsten wires having outer diameter 0.013 mm (Sandvik- KANTHAL wire with polyamide coating) were fixed between two pieces of tape, and one end was suspended from a horizontal rod. The other end was loosely clipped to a rotor which revolves at a steady rate to twist the wires. When the process of twisting builds up certain tension, the bottom piece of tape is naturally released from the rotor. A heat gun is used to melt the coating around the wires, and then the wires are allowed to untwist until they come to a standstill. Carbide scissors (Biomed instruments, 4.5 inch straight sharp points, 25 mm blades) are then used to cut the wire at the twisted end at a 90 degree angle. The face of the exposed tips of the tungsten wires form a rhombus. The loose end of the wires are then fixed into separate channels of a 16 dip pin. A thin capillary electrode is then fed onto the twisted portion of the wires, and is held in place by a piece of wax to the 16 dip pin. Finally, another 16 dip pin is used to sandwich the glass electrode and tungsten wires to hold them in place, and is glued to the first pin.

The tip of the tungsten electrodes are then electroplated with gold. This is done by supplying a 3.3 Hz square pulse (VC 1002 Function Generator attached to a 360 WPI Stimulus Isolator which is powered by an A362 WPI battery charger) to an impedance meter, which is connected across two terminals: one terminal connecting to an individual tungsten wire and the other to a drop of gold solution. When the tungsten wire is dipped into the gold solution, the portion of the wire that is not covered by insulation is electroplated with gold. The square pulse is applied until a 100 kΩ impedance is achieved.

Intracellular recordings were made using a blind sharp electrode recording technique. Borosilicate glass capillaries (1.0mm outer diameter, Sutter Instruments) were pulled to an impedance of 90 MΩ using a horizontal puller (P87 Sutter Instrument Company). Electrodes were filled with a 0.2 M LiCl solution which acted as the electrolyte, and were attached via a chlorinated silver wire to a headstage (Axon Instruments, HS-2A, gain x 0.1) which was connected to an AxoClamp-2B amplifier (Axon Instruments). The electrode was fixed to a mechanical manipulator (Leica Leitz) and was positioned with its tip vertical to the region of

interest. It was then lowered until a neuron was impaled. Data were sampled at 20,000 Hz (custom LabVIEW software), amplified 3000 times, and post-acquisition filtered between 300 Hz to 7000 Hz.

4.3.4 Tastant delivery

After making a dorsal preparation, the MdN are severed to prevent movement of the mandibles. This allows for the mouthparts to be extended to allow for tastant delivery. The mouthparts are propped on a glass slide, and the glass slide is fixed with wax to the base of the tube that holds the bee. A tastant delivery system (Bioscience tools, PC-16 controller driven by Manostat Compulab 3) then pumps the tastant solution onto the mouthparts. This tastant system was set up to supply a 2 second flow of distilled water, followed by a 3 second flow of tastant solution, and finally a 3 second wash with distilled water. This was repeated for as many stimulations as required.

4.3.5 Spike sorting

The same technique was used as described in Chapter 2 for spike sorting the multi-channel tungsten recordings. The only difference here was that three or four channels of recording were used for the sorting procedure. Spike waveforms from all channels that exhibited prominent peaks of action potentials were used.

4.4 Results

4.4.1 Physiological preparation

The axons of GRNs project towards the sub-esophageal zone (SEZ) via the MxN, which in insects like the bumble bee can be accessed from either the dorsal or ventral sides of the head. For a ventral preparation, the head was tilted up and fixed in place by building a column of wax on either side of the head just under the eyes. To prevent the mandibles from closing on the mouthparts, incisions are then made a few millimeters into the cuticle below the mandibles to cut the muscles which control their movement.

The mouthparts are then pushed forwards along the elbow joint between the cardo and the base of the cardo, which exposes the membranous floor of the proboscis fossa (figure 4.2 a). The nerves from the SEZ leading towards the mouthparts are slack, which allow for the mouthparts to be moved forwards without damaging the nerves. The mouthparts are then kept in place by threading them through plastic tubing, and fixing the plastic tubing to the top of the head using wax. A wax dome is then built around the head capsule and is filled with a few drops of Manduca physiological saline [221]. Next, an incision is made in the proboscis fossa and the cardo are cut at the base on both sides. The thin layer of trachea that is underneath the fossa is then removed, which exposes part of the SEZ and the mouthpart nerves (figure 4.2 b).

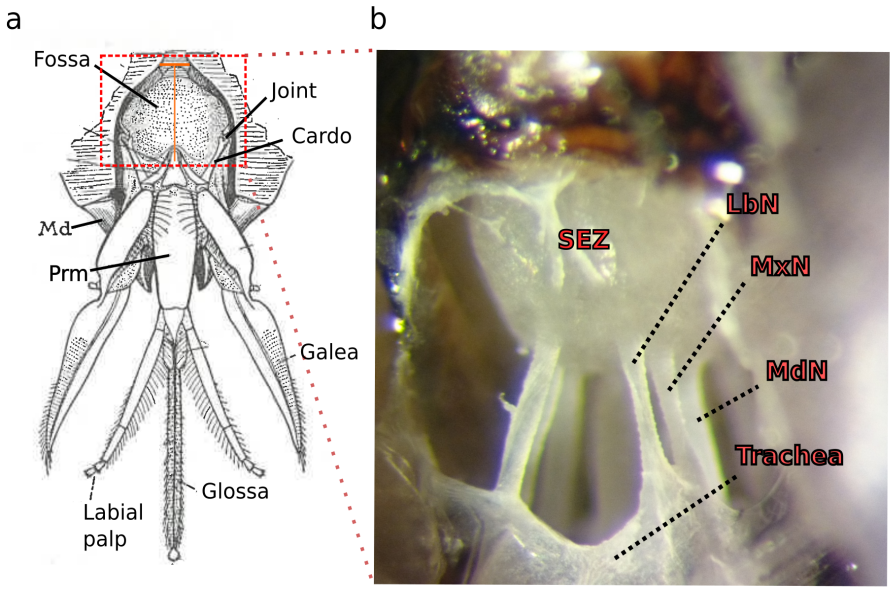

Figure. 4.2: Ventral dissection. a) *Ventral view of the bee head, anterior end facing the bottom of the page. Pushing the mouthparts forward exposes the proboscis fossa. Making an incision in the fossa exposes the sub-esophageal zone (SEZ) (**b)** Md, mandibles; Prm, prementum; LbN, labial nerve; MxN, maxillary nerve; MdN, mandibular nerve. Figure 4.1 a obtained from Snodgrass 1956*

While the ventral preparation provides a way to reach the nerves and SEZ with minimal dissection, it was associated with several complications. First, the animals show a high tendency of either dying (4 out of 7 preparations died), as indicated by the absence of spiking activity from extracellular recordings made from the SEZ and the absence of any physical movement from the bee. The remaining 3 bees did not exhibit any response to tastant stimulation. Second, it was difficult to de-sheath the nerve and SEZ due to the fact that the working area for using forceps is very small in a ventral preparation. Finally, it was difficult to get the esophagus to stop generating movement, even if a muscle-dissolving enzyme such as collagenase is used.

Approaching the SEZ from the dorsal side of the head overcomes these complications. The dorsal head capsule of *B. impatiens* measures approximately 2.5 x 3.0 x 3.5 mm (anterior-posterior x dorso-ventral x lateral ; see figure 1.2 a for orientation). To make a dorsal preparation, the head is fixed in place with drops of wax on the sides of the head. A wax dome is then built around the head to hold saline. The antennae are then gently threaded through plastic tubing to prevent any injury, and the tubing was fixed to the wax dome. The resulting setup is shown in figure 4.3 a.

Incisions are made in the head capsule as shown in figure 4.3 a, and the antennae are gently pulled to the sides, making sure not sever the antennal nerves. This serves to pull apart the antennal lobes by their antennal nerves, which allows better access to the SEZ. It additionally allows for measuring responses of SEZ neurons that receive input from antennal olfactory neurons. Next, the fat bodies and tracheae are removed, which exposes the esophagus (figure 4.3 b). An incision is made in the esophagus and it is gently pulled towards the back of the head capsule. Severing the esophagus prevents the pumping movement of the gut which leads to an

unstable preparation. Care has to be taken at this stage as it is easy to damage the mouthpart nerves, which lie just under the esophagus. Further, the forceps have to keep the esophagus pinched while making the incision, otherwise digestive fluids can flow into the brain which causes *immediate* damage to the neurons. Another pair of forceps should be used to tease apart the trachea connecting the ventral side of the esophagus to the nerves and the SEZ. A drop of wax is used to fix the esophagus to the wax dome. At this stage, the brain should be quite dry which makes it easy to observe the three pairs of mouthpart nerves (figure 4.2 c). The preparation can now be used to access the mouthpart nerves for staining, or can be readied for electrophysiological recording. The entire dorsal preparation takes approximately 45 minutes.

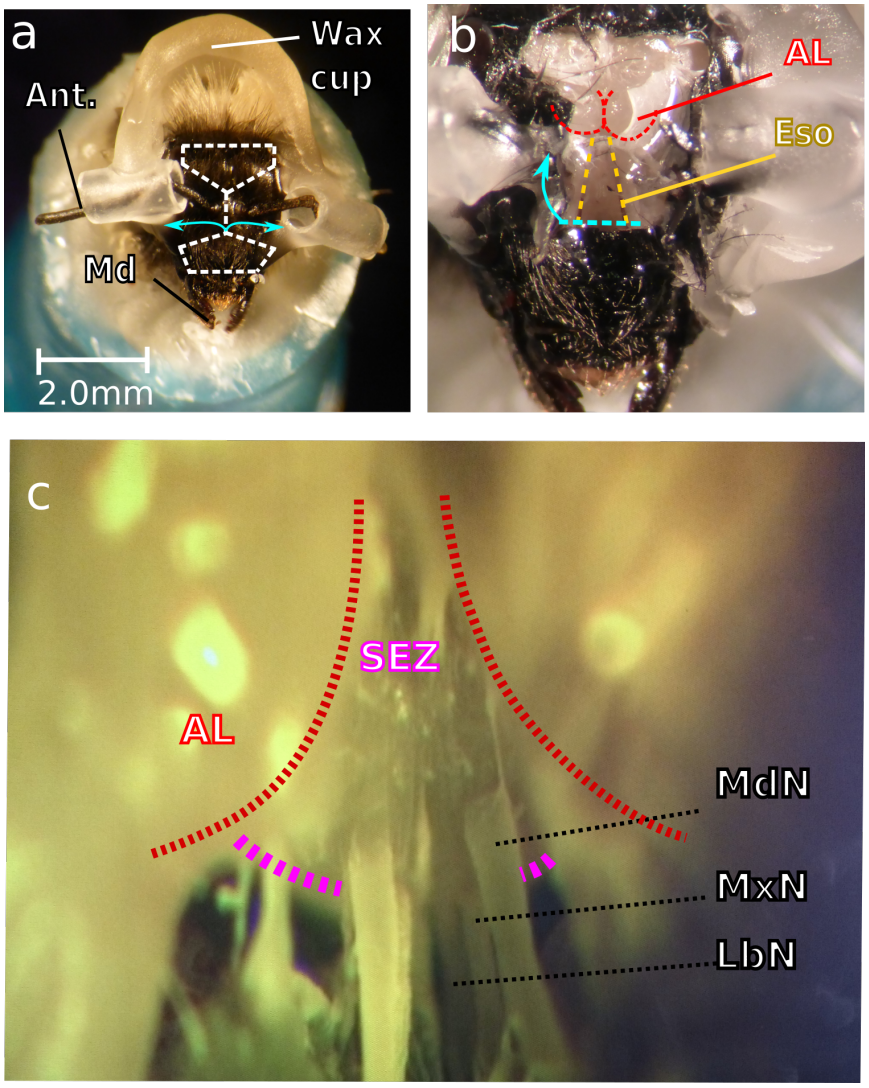

Figure 4.3 (legend on next page)

Figure 4.3 : Dorsal preparation. ***a)*** *The bee is held in a tube with the head sticking out. Antennae (Ant.) are threaded through silicone tubing and fixed to the wax dome built around the head. Incisions are made in the head capsule as indicated by dotted lines, which allow the cuticle at the base of the antennae to be pulled to the sides (arrows).* ***b)*** *View of the brain immediately after pulling apart the antennae. An incision (dashed blue line) is made in the esophagus (Eso, outlined by dashed yellow lines) and it is pulled towards the back of the head capsule (arrow).* ***c)*** *View of the dorsal dissection after moving the esophagus. SEZ: sub-esophageal zone (anterior surface outlined in orange), MdN: mandibular nerve, MxN: maxillary nerve, LbN: labial nerve, AL: antennal lobe (outlined in pink).*

4.4.2 Accessing the MxN

My next aim was to identify each of the three pairs of nerves extending from the SEZ. Each mouthpart nerve has a diameter of approximately 0.1mm, and are arranged dorso-ventrally in two rows (figure 4.2 b). I used a pressure injection technique that stains individual nerves with rhodamine (see methods) to observe their projection within the head capsule (figure 4.4 a). The most dorsal nerve was found to extend approximately 2 mm into the mandibles. This nerve branched at multiple positions into various muscle regions (figure 4.4 b). Severing the nerve revealed that these muscles controlled the movement of the mandibles, indicating that this was the mandibular nerve (MdN). Forward-staining the most ventral nerves revealed that they extend into the prementum, which indicate that these are the labial nerves (LbN). Finally, forward-staining the nerves between the MdN and LbN showed that they extend into the galea, indicating that this is the MxN. The MxN was found to branch at several positions before reaching the galea (figure 4.4 c), suggesting that it carries the axons of efferent motor neurons as well.

Next, I observed the projection of the stained MxN into the galea. To do this, I made use of the fact that the galea is made up of a dorsal and a ventral cuticular layers that can be teased apart to expose the MxN. A confocal image taken near the galeal tip after forward staining the MxN reveals a cell body located below and laterally displaced from the base of a B-type sensillum (figure 4.4 d). The position of this cell body suggests it belongs to a GRN, with its axon projecting towards the MxN. While this technique describes a feasible way to access GRNs

within the galea, it needs to be developed as it was difficult to obtain a preparation where the GRNs did not appear damaged.

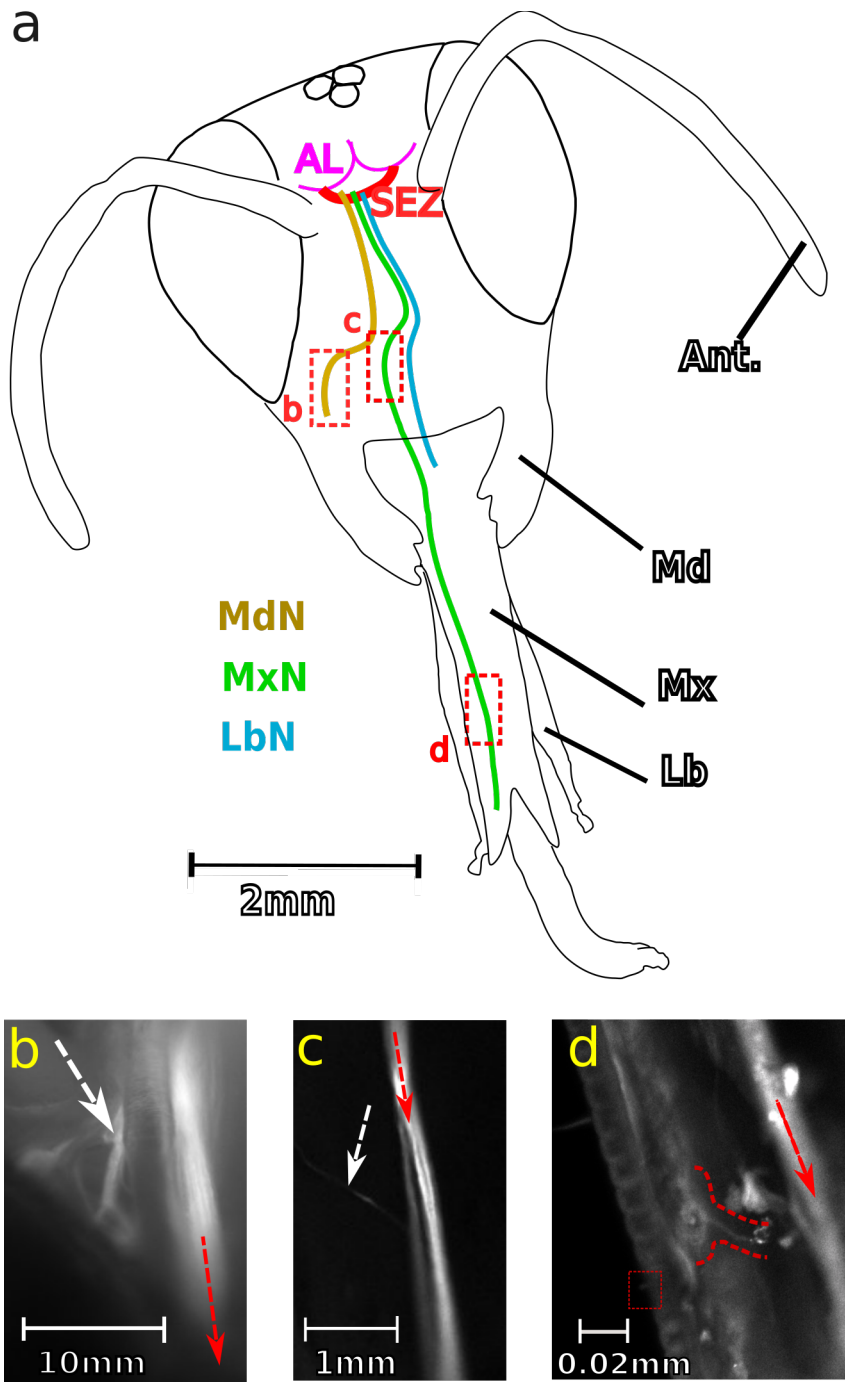

Figure 4.4 (legend on next page)

Figure 4.4. Organization of mouthpart nerves and SEZ in the bumble bee brain. a) Approximate paths followed by the various mouthpart nerves from the SEZ, shown on a drawing of the head of *B. terrestris*. Red boxes are approximate locations from where confocal images of forward-stained nerves in **b) c)** and **d)** were obtained. The MdN **(b)** and MxN **(c)** exhibit branching into muscle regions on their way to the mouthparts. White arrows point at branches, red arrows indicate main nerves and point in the direction of the mouthparts. **d)** Forward staining of the MxN within the galea shows what appears to be the cell body of a GRN with its axon projecting towards the MxN (indicated by red arrow). AL, Antennal Lobe; SEZ, Sub-esophageal ganglion; MdN, Mandibular nerve; MxN, Maxillary nerve; LbN, Labial nerve; Ant. , Antenna; Md, Mandible; Mx, Maxilla; Lb, Labia.

4.4.3 Electrophysiology from MxN

My next aim was to record from populations of GRNs by placing an extracellular electrode on the MxN. From histology, it was determined that the best way to access the MxN was from a dorsal dissection and at a position near its entry into the SEZ. At this position, the diameter of the MxN was ~0.02 mm. An extracellular electrode made of three or four twisted tungsten wires (each having outer diameter of 0.012 mm; see methods) was used to measure activity. Upon contact with the MxN, spiking activity was observed on each of the channels (figure 4.5 a). This activity could be monitored while stimulating the mouthparts with tastants.

The spikes from these recordings were sorted using a technique that compares waveforms across all channels, developed by Pouzat *et al*. [133] and Hill *et al*. [134]. Multiple spike waveforms could be observed, each of which had a unique shape on each recording channel (figure 4.5 b). Spikes from the MxN typically lasted under 0.002 s. In some recordings, the electrodes picked up large spikes having large amplitudes and widths up to 0.004 s (figure 4.7) which are most probably from muscles that were not inactivated by collagenase. Recordings with these large spikes were not used for analysis. Spikes within each cluster exhibit a noticeable variability (figure 4.5 c). This indicates that there is only a limited certainty for which the spikes for each cluster can be determined to belong to a single neuron. However, clusters were well separated from each other (figure 4.5 d, e), and estimating the percentage of errors during classification (see methods) reveals that a subset of the detected clusters have less than 5% errors

(clusters 1 and 2 in figure 4.5 a). This strongly suggests that each cluster consists of spikes that arise from the activity of different neurons.

These results show that extracellular recordings from the MxN using twisted tungsten electrodes can be used to measure the activity of GRNs, and sorting techniques can be used to separate the spiking activity from different GRNs with a high level of confidence. In this way, four out of seven recordings provided well separated spike clusters (n=7 animals). Using this technique, I observed neural responses that varied in intensity and duration. Some recordings revealed units that responded with an inhibition in spiking activity during stimulation, others exhibited excitation, and some units did not respond at all to stimulation (figure 4.4 f,g,h). I also found units whose response structures varied with 1M sucrose and 100mM NaCl (figure 4.4 h).

Figure 4.5 (figure on next page): Extracellular twisted tungsten wire recording from MxN. a) *Spikes are monitored by two out of three wires (channels 1 and 3).* ***b)*** *Spike waveforms were sorted to reveal three clusters (represented by each row), which had unique waveforms on on each tungsten wire (represented by each column). The Y-axis represents amplitude (Amp) normalized to the median absolute deviation of the waveforms of each cluster.* ***c)*** *Residuals for each cluster show that there is a lot of variability in spike shape within each cluster, suggesting possible contamination with multiple units.* ***d)*** *Projecting the first 3 largest principal components (PC) of each cluster shows that clusters are well separated from each other.* ***e)*** *A Fisher's Linear Discriminant Analysis between the spikes of each cluster (using the first five principal components of the waveforms of each cluster; see methods) reveals good separation (d>4) between all three clusters.* ***f)*** *Raster plots show the activity of spikes (each row represents an individual trial) .* ***b-f*** *represent spike sorting from the recording shown in* ***a****.* ***g)*** *A recording from another preparation shows a well separated cluster exhibiting an excitatory response to 1000 mM sucrose.* ***h)*** *A recording from yet another preparation shows a unit responding with an increase in spiking frequency to 1000 mM sucrose (top), and excitation followed by inhibition in spiking to 100mM NaCl (bottom). Shaded regions indicate duration of stimulus application.*

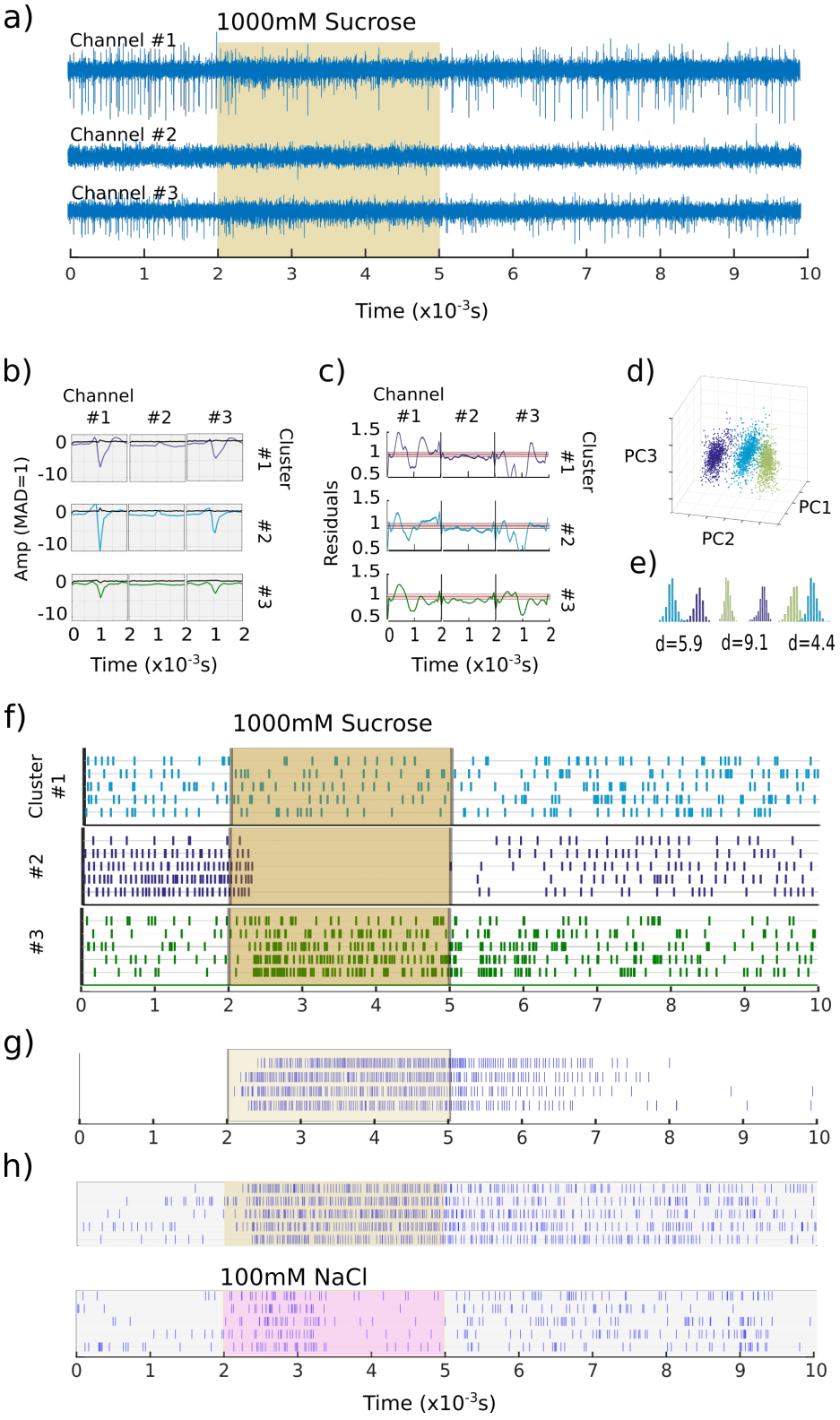

Figure 4.5 *(legend on previous page)*

To monitor the activity of individual neurons within the MxN, a sharp electrode recording technique was used (see methods). A sample recording shows that action potentials can be monitored from individual axons while stimulating the mouthparts with a tastant solution (figure 4.6). The rising and falling phases of the spikes lasted approximately 0.002 s, and were followed by a short after-hyperpolarization (~0.003 s). The efficiency of obtaining an intracellular recording was very low, with only 2 out of 8 preparations yielding recordings. Further, recordings were only stable for a short duration of time, as indicated by the decrease in spike amplitude within the first one minute of recording.

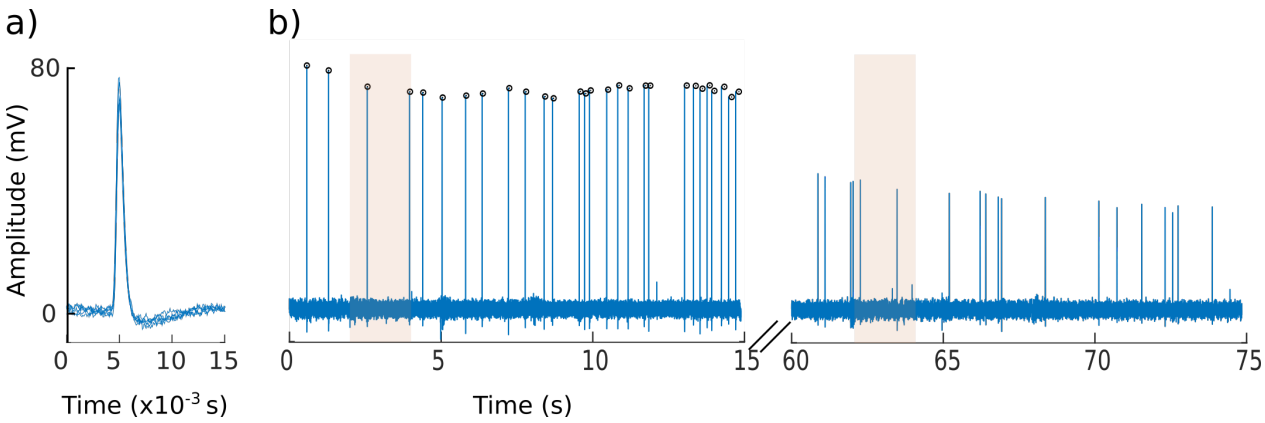

Figure 4.6: Intracellular recording from MxN a) *Stimulation with 1000 mM sucrose evoked spikes in a sample intracellular recording made using the sharp electrode technique. Spikes lasted approximately 0.002 s.* ***b)*** *Spikes initially had large amplitudes, but they gradually decreased over the course of the recording.*

4.4.4 Recording from the SEZ

To monitor how the gustatory input from the GRNs transforms over synapses, recordings have to be made from the post-synaptic neurons within the SEZ. The SEZ in *B. impatiens* measures approximately 0.7 x 0.45 x 0.4 mm (anterior-posterior x dorso-ventral x lateral; figure 4.7 a). To locate where galeal GRNs project in the SEZ, I first back-filled the MxN with dextran-rhodamine (see methods). Confocal images show branching near the anterior surface, near the site of entry of the MxN. The axons of GRNs project bilaterally, and are observed to branch dorsally and ventrally. The branches are seen to extend to the posterior end of the SEZ, and appear to terminate in the bulbous region that extends into the ventral nerve chord.

Targeting extracellular twisted wire electrodes at the regions where the MxN projects into the SEZ revealed that neural activity could be monitored in response to tastant stimulation (figure 4.7 b). Spike sorting allowed for monitoring individual units. Extracellular recordings were efficiently obtainable from the SEZ, with 7 of 10 preparations yielding responses. The high efficiency is probably due to the ease of removing the surrounding sheath after softening it with collagenase, and since any muscle activity disappears when the electrode makes contact with the neurons of the SEZ.

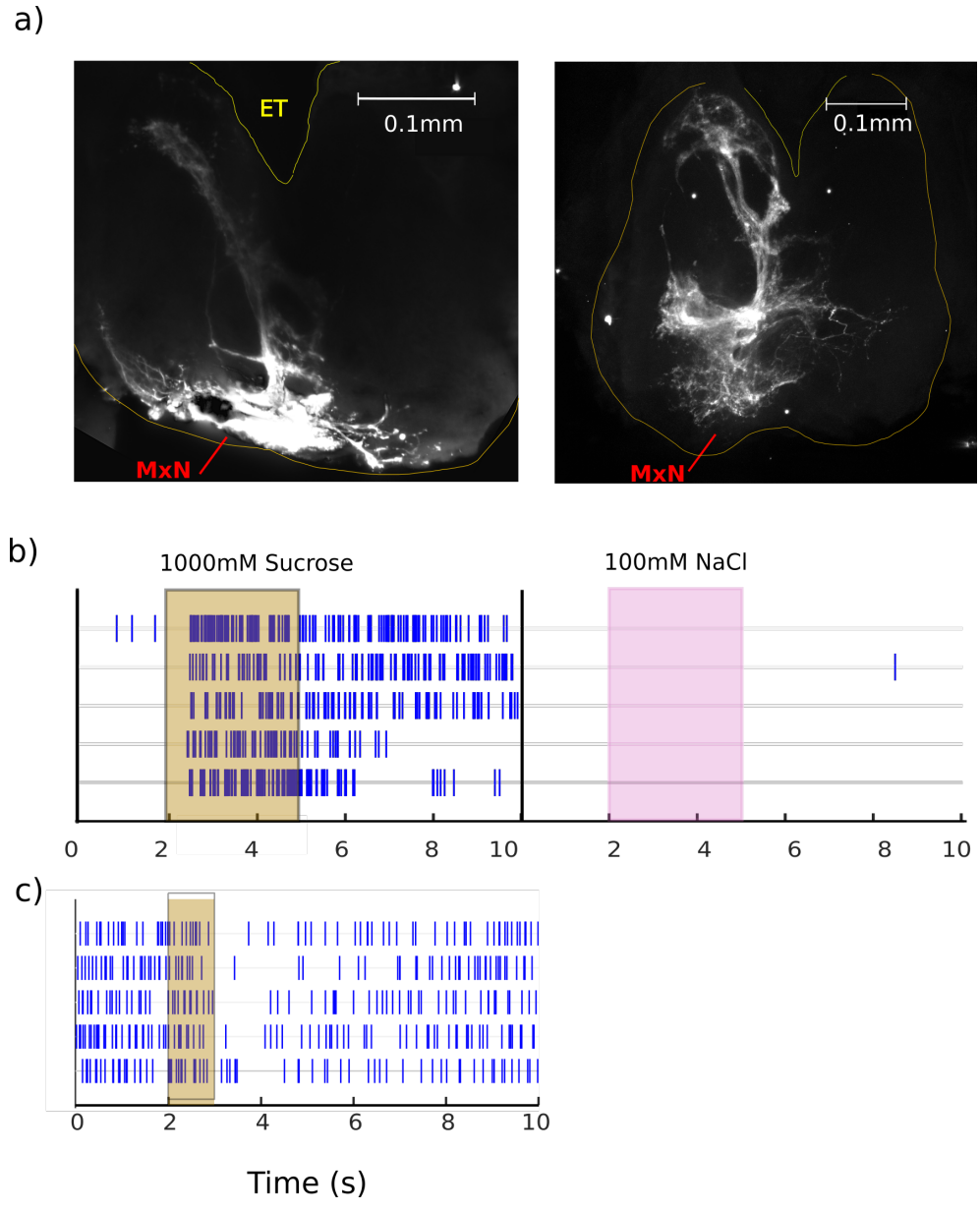

Figure 4.7 *(legend on next page)*

Figure 4.7 *.* ***Projections of MxN in SEZ and extracellular recordings from SEZ.*** ***a)*** *Back-filling the MxN with rhodamine for two separate brains shows axonal projections near the ventral region (left) and bilaterally through the SEZ (right), with a prominent region of synapse within the posterior bulbous region that extends into the ventral nerve chord. Site of entry of MxN is indicated by red arrow.* ***b)*** *The best isolated cluster from an extracellular recording shows an excitatory response to 1000 mM sucrose, but no response to 100 mM NaCl.* ***c)*** *A recording from a different animal shows a unit that exhibits a rebound inhibition to 1000 mM sucrose. Shaded regions depict duration of stimulus application, each row of the raster represents a trial. ET: Esophageal tract, region through which esophagus passes dorsal to the SEZ.*

It was also possible to obtain intracellular recordings from the SEZ with high efficiency, with 8/15 bees yielding stable recordings. Sample intracellular recordings made from the SEZ of *B. impatiens* reveal a variety of spike shapes and response characteristics to tastant stimuli (figure 4.8). Spike widths from different neurons varied from 0.5 ms to 2 ms. Measuring spiking responses to sucrose and NaCl from these neurons suggest that some neurons are tuned to respond to NaCl and not sucrose while others respond to both tastants to different degrees. Intracellular recordings from the SEZ were stable, which allowed for recordings to be made for up to 5 minutes, and allowed for multiple stimulations with different tastants.

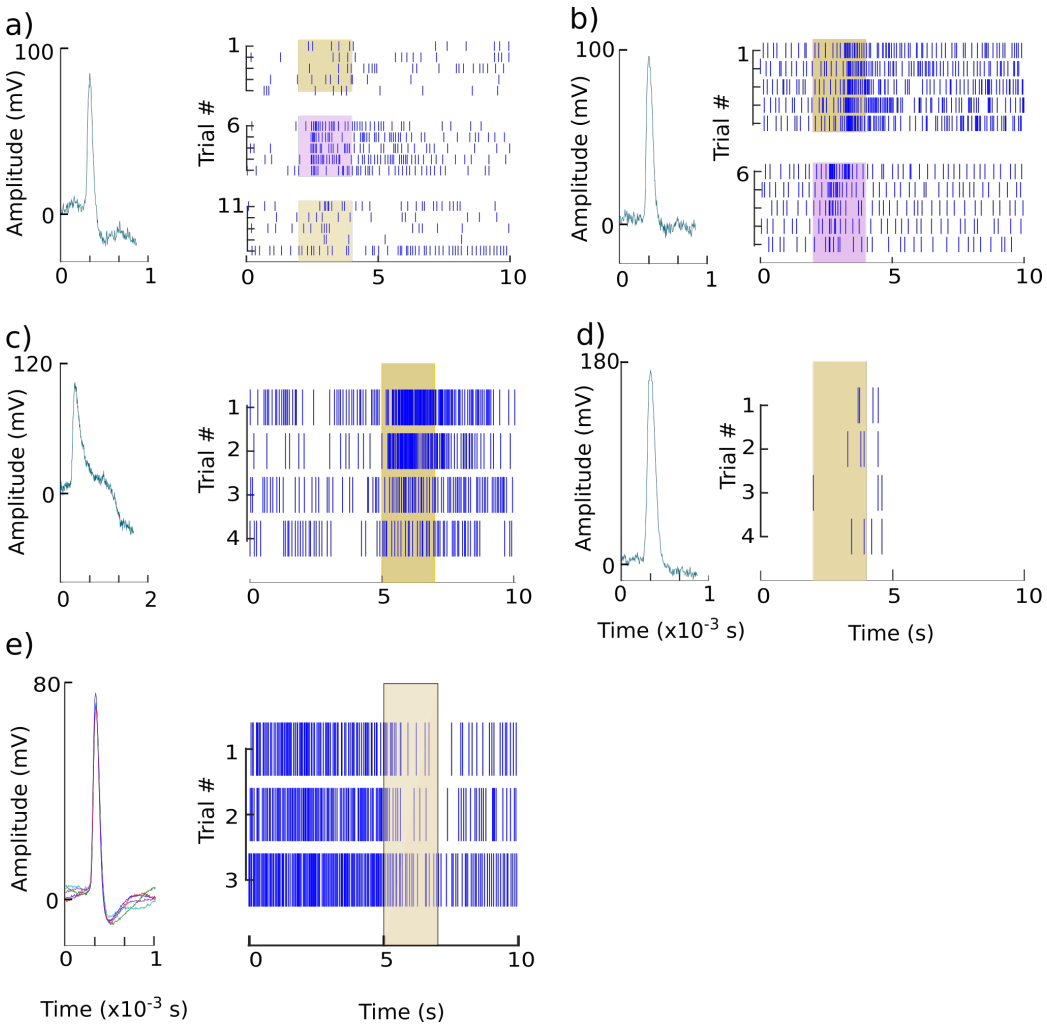

Figure 4.8 : Intracellular recordings from SOG. *Recordings showcase the diversity in response structures of different neurons.* ***a)*** *A neuron selectively responsive to 100 mM NaCl (shaded pink region indicates period of 100 mM NaCl stimulation, whereas shaded yellow region indicates 100 mM sucrose stimulation).* ***b)*** *A neuron responding to both 1000 mM sucrose and 100 mM NaCl* ***c)*** *A sucrose responsive neuron whose spike waveform has a large depolarizing after-potential.* ***d)*** *A neuron that responds with only a few spikes.* ***e)*** *A neuron that is inhibited during sucrose stimulation.*

4.5 Discussion

In this chapter, I showed for the first time in bees that it is possible to monitor neural spiking activity using extracellular recording methods from the MxN and SEZ. Combined with spike sorting methods, the activity of individual units could be monitored from both of these regions. Further, I was able to stain the MxN to observe its branching pattern within the SEZ, as well as obtain obtain intracellular recordings from the SEZ.

The dissection procedure for reaching the gustatory regions of *B. impatiens* was quite tricky for several reasons. First, the head capsule of *B. impatiens* is small, similar to that of a honey bee (1.0 x 3 x 3.3 mm; anteroposterior x dorsoventral x lateral [22], see figure 1.1 for orientation). Second, the SEZ had to be accessed from the dorsal side of the head capsule. This required manipulation of the antennal nerves and esophagus, and it was difficult not to damage the mouthpart nerves in the process of the preparation. While it would be easier to access the SEZ from the ventral side of the head capsule as it lies just underneath the mouthparts, ventral preparations in *B. impatiens* often resulted in either 1) the bee dying or 2) no measurable activity from the SEZ when recording with extracellular electrodes. This could be due to the strain put on the mouthpart nerves and the ventral nerve chords while making the preparation, which required the mouthparts to be pushed forwards and the head tilted upwards. However, ventral preparations were used for recordings in moth [103] and honey bees [117], which means that it could work for bumble bees with a modified preparation method.

The structure of the SEZ in *B. impatiens* was similar to that described by Rehder [22] for the honey bee; the SEZ was fused to the rest of the brain and it gave rise to the mandibular, maxillary and labial nerves. While the significance of a fusion between the different brain regions is still not understood, it could offer an advantage for sensory integration if different sensory regions are clustered close together. Back-filling the MxN revealed that GRN axons are widely distributed in the brain. However, there were two particular regions of dense staining near the posterior and the anteroventral regions, similar to that described in the honey bee [22] and moth (*M. sexta*) [179].

Using 3-4 twisted tungsten wire electrodes, I was able to obtain extracellular recordings from the MxN. Sorting spikes using waveforms from each of these electrodes, I found it was possible to obtain well separated clusters that allowed for monitoring individual neurons with decent efficiency (4/7 recordings yielded well separated spike clusters). Sorted recordings revealed responses characterized by inhibition and excitation from baseline spiking activity, and revealed neurons responsive to both sucrose and NaCl with different response structures. These types of response structures were observed from MxN recordings made from the moth as well [103].

It was interesting to see inhibitory responses as well evidence of neurons responding to both sweet and salty stimuli, as these types of responses were not observed from sensillum recordings in *B. terrestris*. This could suggest that there are sensilla on the maxillary mouthparts of bumble bees that exhibit baseline activity and broadly tuned GRNs that I have not yet recorded from, as were found for *Drosophila* [150] and *S. littoralis* [149]. However, it should be noted that the MxN in *B. impatiens* was found to carry efferent motor axons as well, as observed for honey bees [22]. It is therefore not certain whether the recordings were from afferent GRN input or efferent motor neuron activity. This problem can be addressed by using multiple electrodes positioned at different locations along the MxN, which would allow for obtaining the direction of propagation of the action potentials. In moths, the MxN carries only afferent GRN axons [222], which is why there was no issue in interpreting those extracellular recordings [103].

One of the drawbacks of the MxN extracellular recordings was that the spikes within each detected cluster often exhibited a high variability. This could in part be due to the small width of the MxN (~0.02 mm), which allowed only three or four tungsten wires (each having an outer diameter of 0.013 mm) to fit on the nerve. Of these wires, only two generally picked up spiking features. One possible fix for this is to increase the surface area of contact between the wires and the nerve, by cutting the wires at a 45 degree angle [137], instead of a 90 degree angle as was done for these experiments. I should also try using tetrodes with wires arranged in a linear array [151]. A suction electrode could also work as an alternative, by which the nerve is cut and the exposed end is suctioned into a glass capillary electrode. This would allow for recording responses of subsets of maxillary sensilla. Suction electrodes have been used to monitor the

activity of antennal nerves while stimulating olfactory receptor neurons (ORNs) in *Drosophila* [223].

Obtaining sharp electrode intracellular recordings from the MxN was very difficult. Recordings were unstable, lasting only up to 1.5 minutes from impaling the neuron. This could be due to an unstable preparation, or due to the fact that *B. impatiens* GRNs have very thin axons (~2 µm). However, sharp electrodes have been used to obtain recordings from axons in the MxN in moths [103], antennal lobe of locust [224], and from the SEZ in honey bee [117] which have similar axon widths [48], [112], [209]. This suggests that recordings can be made from *B. impatiens* as well, given a more stable preparation. I could try making the preparation more stable by applying a light upward force on the MxN using a hook electrode.

In comparison to the MxN, extracellular recordings were much easier to obtain from the SEZ. Spike sorting produced well separated clusters and revealed units that responded with excitatory, inhibitory and stimulus-specific responses. This method can therefore be used to study how the temporal structure of GRN input transforms across synapses. It was also much easier to obtain sharp electrode recordings from neurons within the SEZ. Recordings were stable for up to 7 minutes from stimulus onset, which allowed for multiple stimulations with different tastants. Future experiments should be aimed towards staining neurons within the SEZ with dyes like dextran. This will allow for determining whether the neuron under observation is a first order neuron, depending on whether the axon projects into the MxN.

One of the goals of these experiments was to standardize a method that would allow me to record from the SEZ in *B. terrestris* to study the GRN burst response exhibited to sucrose. Given that the head capsule is much larger for *B. terrestris* (1.5 x 3.5 x 3.6 mm; anteroposterior x dorsoventral x lateral) in comparison to *B. impatiens*, accessing the SEZ for intracellular and extracellular recording should be easier. Further, I found that *B. terrestris* was in comparison a more robust species of bumble bee, which would allow for the recording preparation to last much longer without the animal dying.

Overall, the efficiency of obtaining extracellular recordings from the MxN and SEZ, and intracellular recordings from the SEZ in *B.impatiens* suggests that these methods can be used in *B. terrestris*. Future experiments should be aimed towards obtaining intracellular recordings from the MxN, as these will be required to understand the burst spiking response. Extracellular recordings from the SEZ would reveal whether the burst structure and oscillation functions to drive coherent activity from neural ensembles, as they do within the insect antennal lobe (which receives axons of ORNs) [218], [225]. These methods will allow me to explore the novel mechanisms utilized by bumble bees for encoding gustatory stimuli.

Chapter 5. General Discussion

The decision of when to feed is a problem faced by all animals. At first glance, this gustatory problem is quite complex even for an insect like a bee. The nectar it feeds on contains hundreds of tastant chemicals including carbohydrates, salts, vitamins, proteins and fats, each of which it has to be able to detect in a food source since absence of these lead to different diseases [55]. Further, certain food sources can be laced with toxins that the bee has to avoid. However, decades of research in insects have revealed an efficient organization and coding strategy exhibited by the insect peripheral gustatory neurons (gustatory receptor neurons, GRNs) that allows for dealing with this complexity. This strategy involves 1) GRNs tuned to respond to individual tastant categories (e.g sweet, bitter), which form the concept of a 'labeled line' model for gustatory coding [1], [7]–[11], and 2) encoding concentration through the rate of firing of action potentials (spikes) [46], [60]. For example in *Drosophila*, each hair-like sensillum possesses one sweet gustatory receptor neuron (GRN) that responds to compounds like sugars with a concentration dependent change in the firing rate of spikes [57], [155]. The spike train is characterized as a brief increase in spiking frequency that adapts with prolonged stimulation to reach a tonic firing [7], [60]. This coding strategy is found to be quite similar for animals ranging from insects to vertebrates (for review see [2]).

My initial interest was to characterize the responses of GRNs from mouthpart sensilla in the bumble bee *B. terrestris* to different tastants. Unexpectedly, I found that GRNs within galeal sensilla exhibited a unique response structure when stimulated with sucrose. This structure was characterized by bursts of spiking activity that was coherent with a low frequency oscillation in voltage. The rate of spiking and bursting, as well as the power of the oscillatory component, were concentration dependent. There were two GRNs participating in the burst response, and there was evidence that they interact with each other to generate the burst structure. Further, the burst structure was exhibited in response to two other sugars, glucose and fructose. This shows that the coding strategy used by the GRNs of *B. terrestris* for detecting these sugars deviates from the typical 'labeled line' coding used by most insect GRNs as described above. The goal of my thesis was to 1) describe and characterize this burst structure to sucrose, 2) suggest a possible mechanism which drives the burst structure, 3) suggest potential functions for stimulus coding

and behavior, and 4) to discuss the implications of bursting in the field of peripheral gustatory coding.

5.1 Coding by the bumble bee GRNs

The burst response to sugars was exhibited by the two types of sensilla present on the galeal mouthparts of *B. terrestris*. At least two of the 4 GRNs in the A-type sensilla (5 GRNs in the B-type sensilla) were active in the burst structure, with each burst comprising of at least one Class 1 neuron spike within bursts and a Class 2 neuron spike at the end of bursts. The GRNs within these sensilla exhibited little to no baseline activity (~3 spikes / s) and their response to sucrose was largely restricted to the stimulation period. This burst response did not involve the water responsive GRN nor the mechanoreceptor also present in the sensilla.

These data provide the first evidence that multiple GRNs within the same sensillum can respond to sucrose stimulation with a structured firing of spikes. While studies in other insects suggest that multiple GRNs within each sensillum can be activated by sucrose [18], [182] or that there are multiple GRNs within each sensillum that are responsive to different sugars [183], [184], the spiking responses do not follow any apparent structure as they do in *B. terrestris*.

The fact that the Class 1 and Class 2 neurons were phase locked to specific positions within the burst structure suggests that both GRNs exhibit a degree of interaction which drives bursting. There are two mechanisms that are involved in the burst response, one which drives GRN spiking activity and another which drives inhibition between bursts. One possible mechanism that drives spiking is that both GRNs possess sugar binding GRs such that each GRN fires with its own rate of spiking. Alternately, it is possible that only the Class 1 neuron possesses the sugar binding GR, and the activity of Class 1 neuron in turn activates Class 2 neuron through a lateral interaction. There are two well known types of lateral interactions; those mediated by electrical synapses such as gap junctions, and ephaptic interactions.

Gap junctions are channels between neurons that allow the flow of electric current (for review see [82]. The close proximity of the GRN dendrites within the galeal sensilla could allow the presence of gap junctions between these neurons. While gap junctions are commonly

observed in the insect nervous system [226], only a few inconclusive reports have suggested they exist between GRNs [66], [87]. In an ephaptic interaction, the electric field associated with the activity of a neuron (such as a spike) modifies the excitability of a neighboring neuron (e.g. causes a depolarizing or hyperpolarizing potential), depending on their electrical and anatomical proximity (for review see [76]–[78]). The sensillum environment provides an electrically isolated environment that could allow for ephaptic interactions [75].

The period of silence between bursts could be mediated by an inhibitory lateral interaction. This could start with a spike after-hyperpolarization (AHP) that appears to follow each Class 2 neuron spike (as indicated by its shape and since the Class 2 neuron spikes are located on the falling phase of the underlying oscillation). AHPs decrease the excitability of a neuron for durations that can last up to 0.1 s [140]–[142], [197]–[199], which is the same time frame as the inter-burst interval (~0.029 s). Gap junctions have been shown to efficiently transmit low frequencies, which makes it possible that an AHP in the Class 2 neuron spike could inhibit the Class 1 neuron spiking via a gap junction.

The burst response to sugars therefore most likely involves a combination of independent responses via GRs and interactions via gap junctions and ephaptic coupling. These data are the first to suggest that a non-synaptic lateral interaction between neurons can drive bursting. Most other studies describe bursting either for individual neurons that are driven by intrinsic mechanisms [185]–[189], or that involve synaptic input that coordinates bursting [186].

White *et al*. [81] described a similar inhibitory lateral interaction in the tarsal gustatory sensilla in grasshopper. A GRN activated by nicotine hydrogen tartarate was inhibited by the occasional activity of a second GRN, for a duration of the same time scale as the inter-burst interval. Together with findings in *B. terrestris*, these studies suggest that GRNs of a sensillum can represent taste across fibers.

Overall, the GRNs within galeal sensilla in bumble bees appear to encode taste stimuli through temporally structured responses that involves interactions between neighboring GRNs within each sensillum. These features are shared by olfactory receptor neurons as well; ORNs

encode stimulus relevant information through temporally structured trains of spikes, and neighboring ORNs interact through lateral interactions [75]. This gives rise to an 'across-fiber' model of coding, which means that a single chemical stimulus is represented by a population of neurons within each sensillum.

5.2 Function of bursting

Temporally structured spiking and oscillations are commonly observed within the insect antennal lobe (AL, region within the brain that receives ORN axons). In the AL, one of their main functions is to drive synchrony between populations of downstream neurons [225] which aids in stimulus discrimination [218]. The bursting and oscillations exhibited by the GRNs in the A-type sensilla of *B. terrestris* did not function to drive coherence between sensilla. Their function downstream within the SEZ remains to be elucidated.

The *B. terrestris* GRNs encoded concentration through a concentration dependent increase in the rate of spiking and bursting, as well as the power of the underlying oscillatory component. While the spiking activity of most insect GRNs is concentration-dependent, it is still not clear whether this concentration dependent spiking activity is directly correlated to behavior; only a few studies in blowfly and *Drosophila* reveal such a correlation [14], [15]. In this study, I found instead that feeding behaviors are initiated at the threshold of spiking and bursting activity from the GRNs. This suggests that the threshold activity of a population of GRNs is responsible for driving behavior [103].

Bees have been observed to spend between 1-5 s accessing and ingesting nectar from individual flowers [219]. Given that the burst structure persisted for up to 4 s from stimulus onset, this could indicate that the bursting component of the GRN response is important for driving natural feeding behaviors in bumble bees. The activity of the Class 1 neuron (which fired within bursts) exhibited a very low rate of adaptation in comparison to other insect species, and continuously adapted over a 30 s duration of stimulation. The adaptation of the Class 1 neuron spiking activity appeared to be dependent on the intensity of bursting, which indicates that bursting could function to prolong adaptation of the Class 1 neuron. This could play a role in

driving the continuation of feeding, as bees have been observed to spend long durations of time (up to 60 s) consuming large quantities of food (up to 50 µl) on a single feeding session [220].

5.3 Studying gustatory coding at the level of the brain in bumble bees

In order to understand the mechanisms that drive this bursting activity from GRNs, it is essential to obtain intracellular recordings from individual GRNs. In Chapter 4, I show that it is possible to obtain intracellular sharp electrode recordings from the maxillary nerve (MxN) which carries the GRN axons towards the SEZ. One drawback of these recordings was that I could not monitor activity for long periods of time. However, sharp electrode recordings have been obtained from the axons in the MxN in moths [103] and the antennal lobe of locust [224], which have similar axon widths as bumble bees (~2 µm) [48], [112], [209]. This suggests that the intracellular recordings from the bumble bee MxN could be improved given a mechanically more stable preparation.

Studies in the *Drosophila* olfactory circuit revealed that the structure and organization of the ORN input within the antennal lobe is important for driving synchronous and temporally structured activity from post-synaptic neurons [53]. This activity in turn drives oscillations in LFP that aids in stimulus discrimination [218], [225]. In comparison, the importance of the temporal structure and organization of the GRN input to the SEZ is still unknown. The presence of spiking, bursting and oscillatory components in the GRN response make bumble bees an interesting system to study coding within the SEZ.

Studies in *Drosophila* have revealed GRN input is organized within the SEZ; sweet and bitter GRNs synapse onto a largely non-overlapping subset of post-synaptic neurons. However, these post-synaptic neurons are widely distributed throughout the SEZ. Therefore, extracellular recording techniques will have to be used to monitor how the structure of the GRN input is transformed and represented across synapses and populations of neurons. On the other hand, intracellular recordings can reveal which features of the GRN burst response is transmitted across synapses. In Chapter 4, I showed that both intracellular and extracellular recordings can be efficiently obtained from the SEZ in bumble bees. These studies have also been done in moth, where it was shown that GRN input is dynamically transformed across synapses [103].

5.4 New tools for spike sorting and burst detection from sensillum recordings

In order to accurately characterize the burst response, I needed to sort the spikes from the sensillum recordings. This required a method that 1) required minimal user input, to remove bias from the sorting procedure, 2) allowed for estimating the quality of classification, to convincingly argue for the presence of multiple active neurons, and 3) uses multiple parameters for comparison, particularly since the second GRN activity was very low and often was associated with the first GRN as a superposition. These three features were not provided by the existing spike sorting techniques available for sensillum recordings, such as DbWave [154] and AutoSpike (Syntech). These programs have many stages that require user-input, since they use visual estimates for clustering spikes and require visual detection of superpositions. In addition, they do not allow for estimating the quality of sorting. Finally, they use a reduced number of parameters for the sorting procedure; spikes are obtained from single channels of recording, and comparisons are made between a few user-selected parameters such as spike amplitude or width.

In Chapter 2, I showed that the spike sorting methods developed by Pouzat *et al*. [133] and Hill *et al*. [134], which I refer to as PouzatSort, cover for the limitations mentioned above and could be used to sort spikes from sensillum recordings. PouzatSort compares entire spike waveforms obtained from both recording electrodes for the sorting procedure. This increases the number of parameters available for sorting and reduces the errors from classification. PouzatSort only required user-input at two stages : the first was to choose a horizontal threshold line to detect spikes, and the second was to merge, split and 'clean' (i.e. remove noisy waveforms from) clusters after sorting. Superpositions on the other hand were automatically detected. After classification, PouzatSort allows for estimating the quality of the sorting procedure by estimating the errors arising from refractory period violations, overlap between clusters and missed spikes from thresholding. If cumulative errors fall under 10% of the dataset, the sensillum recording was considered to be well sorted.

It remains to be seen whether PouzatSort can be used to sort sensillum recordings which exhibit more than two active GRNs. In Chapter 2, I showed that this method could also be used to sort spikes from 30 s recordings made only using the tip electrode. However, the efficiency sorting using the 30 s tip recordings was very low (3/15 yielded <10% errors). Overall, while the

efficiency of PouzatSort was low (5/11 tip-tungsten channel recordings yielded <10% errors), it allowed for an accurate sorting and classification of spikes with minimal user interface.

In order to understand the mechanisms driving bursting, I needed to observe the position of each GRN spike within a burst. Existing burst detection methods are developed for higher-order neurons that do not exhibit strong adaptation over time. Hence, static ISI thresholds are often used to detect bursts [166]–[168]. The GRN activity on the other hand exhibited a strong adaptation over the course of stimulation. I therefore developed a time-varying burst detection method, which involved fitting a three-parameter logarithmic equation to the ISI data over time, and using a threshold of 2 times this fit to detect inter-burst intervals. This method was useful for detecting burst positions for up to 5 s from stimulus onset, and for varying concentrations of sugars. The simplicity of this method makes it usable for detecting bursts in any other neuron that exhibits a similar adaptation. Even if the adaptation rates are different, a suitable fit and threshold can be chosen depending on the dataset.

5.5 Conclusion

For most insects, GRNs encode stimuli via labeled lines and respond with a brief increase in spiking activity that quickly adapts. Bumble bee GRNs on the other hand exhibit bursts of spiking activity that is driven by interactions between two neighboring GRNs, which allows for extended periods of rapid spike firing. Given that carbohydrates are one of the most important components of a bee's diet, it is not surprising that the bumble bee GRNs exhibit a unique coding strategy for detecting them. While this coding strategy could be important for driving natural foraging behaviors and continuation of feeding, this is yet to be conclusively determined. This study sets the scene for exploring a novel form of sensory coding. Future work should be aimed at obtaining recordings from individual and populations of neurons within the SEZ to reveal how the burst response coordinates downstream activity to drive behavior.

Bibliography

[1] D. A. Yarmolinsky, C. S. Zuker, and N. J. P. Ryba, “Common Sense about Taste: From Mammals to Insects,” *Cell*, vol. 139, no. 2, pp. 234–244, 2009.

[2] E. R. Liman, Y. V. Zhang, and C. Montell, “Peripheral coding of taste,” *Neuron*, vol. 81, no. 5, pp. 984–1000, 2014.

[3] R. M. Joseph and J. R. Carlson, “Drosophila Chemoreceptors: A Molecular Interface Between the Chemical World and the Brain,” *Trends Genet.*, vol. 31, no. 12, pp. 683–695, 2015.

[4] H. Tateda and H. Morita, “Initiation of Spike Potentials in Contact Chemosensory Hairs of Insects I. The Generation Site of the Recorded Spike Potentials,” *J. Cell. Comp. Physiol.*, no. 54, pp. 171–176, 1959.

[5] R. Riley, “Transmission of receptor potential in dipteran chemoreceptors,” 1967.

[6] M. L. Wolbarsht and F. E. Hanson, “Electrical Activity in the Chemoreceptors of the Blowfly. III. Dendritic Action Potentials.,” *J. Gen. Physiol.*, vol. 48, pp. 673–683, 1965.

[7] V. Dethier, “The Hungry Fly,” *Psychology Today*, vol. 1, no. 2. pp. 64–72, 1967.

[8] M. Hiroi, N. Meunier, F. Marion-Poll, and T. Tanimura, “Two antagonistic gustatory receptor neurons responding to sweet-salty and bitter taste in Drosophila,” *J. Neurobiol.*, vol. 61, no. 3, pp. 333–342, 2004.

[9] K. Isono and H. Morita, “Molecular and cellular designs of insect taste receptor system.,” *Front. Cell. Neurosci.*, vol. 4, no. June, p. 20, 2010.

[10] N. Meunier, F. Marion-Poll, J. P. Rospars, and T. Tanimura, “Peripheral coding of bitter taste in Drosophila,” *J. Neurobiol.*, vol. 56, no. 2, pp. 139–152, 2003.

[11] G. S. Pollack and R. Balakrishnan, “Taste sensilla of flies: Function, central neuronal projections, and development,” *Microsc. Res. Tech.*, vol. 39, no. 6, pp. 532–546, 1997.

[12] T. Maeda, S. Tamotsu, M. Iwasaki, T. Nisimura, M. Shimohigashi, M. K. Hojo, and M. Ozaki, “Neuronal projections and putative interaction of multimodal inputs in the subesophageal ganglion in the blowfly, Phormia regina,” *Chem. Senses*, vol. 39, no. 5, pp. 391–401, 2014.

[13] S. R. Shanbhag and R. Naresh Singh, “Functional implications of the projections of neurons from individual labellar sensillum of Drosophila melanogaster as revealed by

neuronal-marker horseradish peroxidase," *Cell Tissue Res.*, vol. 267, no. 2, pp. 273–282, 1992.

[14] P. A. Getting, "The sensory control of motor output in fly proboscis extension," *Z. Vgl. Physiol.*, vol. 74, no. 1, pp. 103–120, 1971.

[15] M. D. Gordon and K. Scott, "Motor Control in a Drosophila Taste Circuit," *Neuron*, vol. 61, no. 3, pp. 373–384, 2009.

[16] S. J. Simpson, "Regulation of a Meal: Chewing Insects," in *Regulatory Mechanisms in Insect Feeding*, R. F. Chapman and G. de Boer, Eds. Boston, MA: Springer US, 1995, pp. 137–156.

[17] H. K. Inagaki, K. M. Panse, and D. J. Anderson, "Independent, reciprocal neuromodulatory control of sweet and bitter taste sensitivity during starvation in Drosophila," *Neuron*, vol. 84, no. 4, pp. 806–820, 2014.

[18] G. A. Wright, J. A. Mustard, N. K. Simcock, A. A. R. Ross-Taylor, L. D. McNicholas, A. Popescu, and F. Marion-Poll, "Parallel reinforcement pathways for conditioned food aversions in the honeybee," *Curr. Biol.*, vol. 20, no. 24, pp. 2234–2240, 2010.

[19] C. F. Moss and V. G. Dethier, "Central nervous system regulation of finicky feeding by the blowfly.," *Behavioral Neuroscience*, vol. 97, no. 4. American Psychological Association, US, pp. 541–548, 1983.

[20] B. K. Mitchell, H. Itagaki, and M. P. Rivet, "Peripheral and central structures involved in insect gustation," *Microsc. Res. Tech.*, vol. 47, no. 6, pp. 401–415, 1999.

[21] R. Snodgrass, *The Anatomy of the Honey Bee*, vol. 85, no. 2145. 1956.

[22] V. Rehder, "A neuroanatomical map of the SOG and prothoracic ganglia of the honey bee," *R. Soc. B*, vol. 235, pp. 179–202, 1988.

[23] I. Sinakevitch, M. Niwa, and N. J. Strausfeld, "Octopamine-like immunoreactivity in the honey bee and cockroach: Comparable organization in the brain and subesophageal ganglion," *J. Comp. Neurol.*, vol. 488, no. 3, pp. 233–254, 2005.

[24] J. S. Altman and J. Kien, "Suboesophageal neurons involved in head movements and feeding in locusts," *Proc.Roy.Soc.London B*, vol. 205, pp. 209–227, 1979.

[25] Z. Wisotsky, A. Medina, E. Freeman, and A. Dahanukar, "Evolutionary differences in food preference rely on Gr64e, a receptor for glycerol.," *Nat. Neurosci.*, vol. 14, no. 12, pp. 1534–1541, 2011.

[26] K. Ueno, M. Ohta, H. Morita, Y. Mikuni, S. Nakajima, K. Yamamoto, and K. Isono, “Trehalose sensitivity in Drosophila correlates with mutations in and expression of the gustatory receptor gene Gr5a,” *Curr. Biol.*, vol. 11, no. 18, pp. 1451–1455, 2001.

[27] E. G. Freeman and A. Dahanukar, “Molecular neurobiology of Drosophila taste.,” *Curr. Opin. Neurobiol.*, vol. 34, pp. 140–148, 2015.

[28] K. Sato, K. Tanaka, and K. Touhara, “Sugar-regulated cation channel formed by an insect gustatory receptor.,” *Proc. Natl. Acad. Sci. U. S. A.*, vol. 108, no. 28, pp. 11680–11685, 2011.

[29] K. Sato, M. Pellegrino, T. Nakagawa, T. Nakagawa, L. B. Vosshall, and K. Touhara, “Insect olfactory receptors are heteromeric ligand-gated ion channels.,” *Nature*, vol. 452, no. 7190, pp. 1002–1006, 2008.

[30] D. Wicher, R. Schafer, R. Bauernfeind, M. C. Stensmyr, R. Heller, S. H. Heinemann, and B. S. Hansson, “Drosophila odorant receptors are both ligand-gated and cyclic-nucleotide-activated cation channels,” *Nature*, vol. 452, no. 7190, pp. 1007–U10, 2008.

[31] A. Dahanukar, Y. T. Lei, J. Y. Kwon, and J. R. Carlson, “Two Gr Genes Underlie Sugar Reception in Drosophila,” *Neuron*, vol. 56, no. 3, pp. 503–516, 2007.

[32] Y. Jiao, S. J. Moon, X. Wang, Q. Ren, and C. Montell, “Gr64f Is Required in Combination with Other Gustatory Receptors for Sugar Detection in Drosophila,” *Curr. Biol.*, vol. 18, no. 22, pp. 1797–1801, 2008.

[33] T. Miyamoto, J. Slone, X. Song, and H. Amrein, “A fructose receptor functions as a nutrient sensor in the drosophila brain,” *Cell*, vol. 151, no. 5, pp. 1113–1125, 2012.

[34] L. A. Weiss, A. Dahanukar, J. Y. Kwon, D. Banerjee, and J. R. Carlson, “The molecular and cellular basis of bitter taste in Drosophila,” *Neuron*, vol. 69, no. 2, pp. 258–272, 2011.

[35] S. H. Kim, Y. Lee, B. Akitake, O. M. Woodward, W. B. Guggino, and C. Montell, “Drosophila TRPA1 channel mediates chemical avoidance in gustatory receptor neurons.,” *Proc. Natl. Acad. Sci. U. S. A.*, vol. 107, no. 18, pp. 8440–5, 2010.

[36] Y. V. Zhang, R. . Raghuwanshi, W. L. Shen, and C. Montell, “Food-Experience Induced Taste Desensitization Modulated by the Drosophila TRPL Channel,” vol. 16, no. 10, pp. 1468–1476, 2013.

[37] C. Montell, “Drosophila TRP channels,” *Pflugers Arch. Eur. J. Physiol.*, vol. 451, no. 1, pp. 19–28, 2005.

[38] Y. V Zhang, J. Ni, and C. Montell, “The molecular basis for attractive salt-taste coding in Drosophila.,” *Science*, vol. 340, no. 6138, pp. 1334–8, 2013.

[39] T. W. Koh, Z. He, S. Gorur-Shandilya, K. Menuz, N. K. Larter, S. Stewart, and J. R. Carlson, “The Drosophila IR20a Clade of Ionotropic Receptors Are Candidate Taste and Pheromone Receptors,” *Neuron*, vol. 83, no. 4, pp. 850–865, 2014.

[40] P. Cameron, M. Hiroi, J. Ngai, and K. Scott, “The molecular basis for water taste in Drosophila,” *Nature*, vol. 465, no. 7294, pp. 91–95, 2010.

[41] H. Ishimoto, K. Takahashi, R. Ueda, and T. Tanimura, “G-protein gamma subunit 1 is required for sugar reception in Drosophila.,” *EMBO J.*, vol. 24, no. 18, pp. 3259–3265, 2005.

[42] P. Kain, F. Badsha, S. M. Hussain, A. Nair, G. Hasan, and V. Rodrigues, “Mutants in phospholipid signaling attenuate the behavioral response of adult Drosophila to trehalose,” *Chem. Senses*, vol. 35, no. 8, pp. 663–673, 2010.

[43] E. S. Hodgson, J. Y. Lettvin, and K. D. Roeder, “Physiology of a Primary Chemoreceptor Unit,” *Science (80-.).*, vol. 122, pp. 417–418, 1954.

[44] H. Morita and S. Yamashita, “Generator Potential of Insect Chemoreceptor,” *Science (80-.).*, vol. 130, no. 3380, p. 922, 1959.

[45] A. T. Whitehead and J. R. Larsen, “Ultrastructure of the contact chemoreceptors of Apis mellifera L. (Hymenoptera : Apidae),” *Int. J. Insect Morphol. Embryol.*, vol. 5, no. 4–5, pp. 301–315, 1976.

[46] H. Tateda and H. Morita, “Initiation of spike potentials in contact chemosensory hairs of insects. I. The generation site of the recorded spike potentials,” *J. Cell. Comp. Physiol.*, vol. 54, no. 2, pp. 171–176, Oct. 1959.

[47] S. Marella, W. Fischler, P. Kong, S. Asgarian, E. Rueckert, and K. Scott, “Imaging taste responses in the fly brain reveals a functional map of taste category and behavior,” *Neuron*, vol. 49, no. 2, pp. 285–295, 2006.

[48] N. Thorne, C. Chromey, S. Bray, and H. Amrein, “Taste Perception and Coding in Drosophila,” *Curr. Biol.*, vol. 14, no. 2, pp. 1065–1079, 2004.

[49] S. Fujii, A. Yavuz, J. Slone, C. Jagge, X. Song, and H. Amrein, “Drosophila sugar receptors in sweet taste perception, olfaction, and internal nutrient sensing,” *Curr. Biol.*, vol. 25, no. 5, pp. 621–627, 2015.

[50] J. T. Knudsen, L. Tollsten, and L. G. Bergstrom, “Floral scents-a checklist of volatile compounds isolated by head-space techniques,” *Phytochemistry*, vol. 33, no. 2, pp. 253–280, 1993.

[51] G. Laurent, “Olfactory network dynamics and the coding of multidimensional signals.,” *Nat. Rev. Neurosci.*, vol. 3, no. 11, pp. 884–895, 2002.

[52] M. de Bruyne, P. J. Clyne, and J. R. Carlson, “Odor coding in a model olfactory organ: the Drosophila maxillary palp.,” *J. Neurosci.*, vol. 19, no. 11, pp. 4520–32, 1999.

[53] B. Raman, J. Joseph, J. Tang, and M. Stopfer, “Temporally Diverse Firing Patterns in Olfactory Receptor Neurons Underlie Spatiotemporal Neural Codes for Odors,” *J. Neurosci.*, vol. 30, no. 6, pp. 1994–2006, 2010.

[54] C.-Y. Su, C. Martelli, T. Emonet, and J. R. Carlson, “Temporal coding of odor mixtures in an olfactory receptor neuron,” *Proc. Natl. Acad. Sci.*, vol. 108, no. 12, pp. 5075–5080, 2011.

[55] S. W. Nicolson, M. Nepi, and E. Pacini, “Nectaries and Nectar | Springer.” 2007.

[56] L. M. Schoonhoven and J. J. A. Van Loon, “An inventory of taste in caterpillars: Each species its own key,” *Acta Zool. Acad. Sci. Hungaricae*, vol. 48, no. SUPPL. 1, pp. 215–263, 2002.

[57] S. Charlu, Z. Wisotsky, A. Medina, and A. Dahanukar, “Acid sensing by sweet and bitter taste neurons in Drosophila melanogaster,” *Nat. Commun.*, vol. 18, no. 9, pp. 1199–1216, 2013.

[58] J. W. Jung, K. W. Park, Y. J. Ahn, and H. W. Kwon, “Functional characterization of sugar receptors in the western honeybee, Apis mellifera,” *J. Asia. Pac. Entomol.*, vol. 18, no. 1, pp. 19–26, 2015.

[59] J. I. Glendinning and T. T. Hills, “Electrophysiological evidence for two transduction pathways within a bitter-sensitive taste receptor.,” *J. Neurophysiol.*, vol. 78, no. 2, pp. 734–45, 1997.

[60] N. Fujishiro, H. Kijima, and H. Morita, “Impulse frequency and action potential amplitude in labellar chemosensory neurones of Drosophila melanogaster,” *J. Insect Physiol.*, vol. 30, no. 4, pp. 317–325, 1984.

[61] T. Amakawa, “Effects of age and blood sugar levels on the proboscis extension of the blow fly Phormia regina,” *J. Insect Physiol.*, vol. 47, no. 2, pp. 195–203, 2001.

[62] P. J. Albert, “Electrophysiological responses to sucrose from a gustatory sensillum on the larval maxillary palp of the spruce budworm, Choristoneura fumiferana (Clem.) (Lepidoptera: Tortricidae),” *J. Insect Physiol.*, vol. 49, no. 8, pp. 733–738, 2003.

[63] A. T. Whitehead and J. R. Larsen, “Electrophysiological responses of galeal contact chemoreceptors of Apis mellifera to selected sugars and electrolytes,” *J. Insect Physiol.*, vol. 22, no. 12, pp. 1609–1616, 1976.

[64] E. S. Hodgson, “Electrophysiological studies of arthropod chemoreception. III. Chemoreceptors of terrestrial and fresh-water arthropods,” *Biol. Bull.*, vol. 115, no. 1, pp. 114–125, 1958.

[65] K. Jørgensen, T. J. Almaas, F. Marion-poll, and H. Mustaparta, “Electrophysiological characterization of responses from gustatory receptor neurons of sensilla chaetica in the moth Heliothis virescens,” *Chem. Senses*, vol. 32, no. 9, pp. 863–879, 2007.

[66] W.-C. Ma, “Dynamics of feeding responses in Pieris brassicae Linn. as a function of chemosensory input: a behavioural, ultrastructural and electrophysiological study.,” *Meded Landbouwhogesch. Wageningen*, vol. 72–11, p. 162, 1972.

[67] M. De Bruyne, K. Foster, and J. R. Carlson, “Odor coding in the Drosophila antenna,” *Neuron*, vol. 30, no. 2, pp. 537–552, 2001.

[68] E. A. Hallem, A. Dahanukar, and J. R. Carlson, “Insect Odor and Taste Receptors,” *Annu. Rev. Entomol.*, vol. 51, no. 1, pp. 113–135, 2006.

[69] V. G. Dethier, “The physiology and histology of the contact chemoreceptors of the blowfly,” *Q. Rev. Biol.*, vol. 30, no. 4, pp. 348–371, 1955.

[70] S. Kessler, M. Vlimant, and P. M. Guerin, “The sugar meal of the African malaria mosquito Anopheles gambiae and how deterrent compounds interfere with it: a behavioural and neurophysiological study.,” *J. Exp. Biol.*, vol. 216, pp. 1292–306, 2013.

[71] T. A. Inoue, K. Asaoka, K. Seta, D. Imaeda, and M. Ozaki, “Sugar receptor response of the food-canal taste sensilla in a nectar-feeding swallowtail butterfly, Papilio xuthus,” *Naturwissenschaften*, vol. 96, no. 3, pp. 355–363, 2009.

[72] S. C. Kessler, E. J. Tiedeken, K. L. Simcock, S. Derveau, J. Mitchell, S. Softley, J. C. Stout, and G. a. Wright, “Bees prefer foods containing neonicotinoid pesticides,” *Nature*, vol. 521, pp. 74–76, 2015.

[73] D. T. Harris, B. R. Kallman, B. C. Mullaney, and K. Scott, “Representations of Taste Modality in the Drosophila Brain,” *Neuron*, vol. 86, no. 6, pp. 1449–1460, 2015.

[74] T. C. Baker and H. Y. Fadamiro, “Moth uses fine tuning for odour resolution,” *Nature*, vol. 393, no. June, p. 530, 1998.

[75] C.-Y. Su, K. Menuz, J. Reisert, and J. R. Carlson, “Non-synaptic inhibition between grouped neurons in an olfactory circuit.,” *Nature*, vol. 492, no. 7427, pp. 66–71, 2012.

[76] A. Vermeulen and J. P. Rospars, “Why are insect olfactory receptor neurons grouped into sensilla? The teachings of a model investigating the effects of the electrical interaction

between neurons on the transepithelial potential and the neuronal transmembrane potential," *Eur. Biophys. J.*, vol. 33, no. 7, pp. 633–643, 2004.

[77] W. Van der Goes van Naters, "Inhibition among olfactory receptor neurons.," *Front. Hum. Neurosci.*, vol. 7, no. October, p. 690, 2013.

[78] J. G. R. Jefferys, "Nonsynaptic Modulation of Neuronal-Activity in the Brain - Electric Currents and Extracellular Ions," *Physiol. Rev.*, vol. 75, no. 4, pp. 689–723, 1995.

[79] S. a Weiss, T. Preuss, and D. S. Faber, "A role of electrical inhibition in sensorimotor integration.," *Proc. Natl. Acad. Sci. U. S. A.*, vol. 105, no. 46, pp. 18047–52, 2008.

[80] A. Arvanitaki, "Effects Evoked in an Axon by the Activity of a Contiguous One," *J. Neurophysiol.*, vol. 5, no. 2, pp. 89–108, 1942.

[81] P. R. White, R. F. Chapman, and A. Ascolichristensen, "Interactions between two neurons in contact chemosensilla of the grasshopper, Schistocerca americana," *J. Comp. Physiol. A-Sensory Neural Behav. Physiol.*, vol. 167, no. 3, pp. 431–436, 1990.

[82] M. V. L. Bennett, "Gap Junctions and Electrical Synapses," *Encycl. Neurosci.*, vol. 366, no. November 1996, pp. 529–548, 2010.

[83] M. Beierlein, J. R. Gibson, and B. W. Connors, "A network of electrically coupled interneurons drives synchronized inhibition in neocortex," *Nat. Neurosci.*, vol. 3, no. 9, pp. 904–10, 2000.

[84] M. Blatow, A. Rozov, I. Katona, S. G. Hormuzdi, A. H. Meyer, M. A. Whittington, A. Caputi, and H. Monyer, "A novel network of multipolar bursting interneurons generates theta frequency oscillations in neocortex," *Neuron*, vol. 38, no. 5, pp. 805–817, 2003.

[85] M. Galarreta and S. Hestrin, "A network of fast-spiking cells in the neocortex connected by electrical synapses.," *Nature*, vol. 402, no. 6757, pp. 72–5, 1999.

[86] a Draguhn, R. D. Traub, D. Schmitz, and J. G. Jefferys, "Electrical coupling underlies high-frequency oscillations in the hippocampus in vitro.," *Nature*, vol. 394, no. 6689, pp. 189–192, 1998.

[87] M. Moulins, "Les sensilles de I'organe hypopharyngien de Blabera craniifer Burm. (Insecta, Dictyoptera)," *J. Ultrastruct. Res.*, vol. 2, pp. 121–138, 1968.

[88] Y. Jeong, J. Shim, S. Oh, H. Yoon, C. Kim, S. Moon, and C. Montell, "An odorant-binding protein required for suppression of sweet taste by bitter chemicals," *Neuron*, vol. 79, no. 4, pp. 725–737, 2013.

[89] A. S. French, M.-J. Sellier, M. Ali Agha, A. A. Moutaz, A. Guigue, M.-A. Chabaud, P. D. Reeb, A. Mitra, Y. Grau, L. Soustelle, and F. Marion-Poll, “Dual mechanism for bitter avoidance in Drosophila.,” *J. Neurosci.*, vol. 35, no. 9, pp. 3990–4004, 2015.

[90] N. Cocco and J. I. Glendinning, “Not all sugars are created equal: some mask aversive tastes better than others in an herbivorous insect,” *J. Exp. Biol.*, vol. 215, no. 8, pp. 1412–1421, 2012.

[91] Q. Gao, B. Yuan, and A. Chess, “Convergent projections of Drosophila olfactory neurons to specific glomeruli in the antennal lobe.,” *Nat. Neurosci.*, vol. 3, no. 8, pp. 780–785, 2000.

[92] B. Chu, V. Chui, K. Mann, and M. D. Gordon, “Presynaptic gain control drives sweet and bitter taste integration in Drosophila,” *Curr. Biol.*, vol. 24, no. 17, pp. 1978–1984, 2014.

[93] K. I. Nagel and R. I. Wilson, “Mechanisms Underlying Population Response Dynamics in Inhibitory Interneurons of the Drosophila Antennal Lobe.,” *J. Neurosci.*, vol. 36, no. 15, pp. 4325–38, 2016.

[94] N. K. Tanaka, K. Ito, and M. Stopfer, “Odor-Evoked Neural Oscillations in Drosophila Are Mediated by Widely Branching Interneurons,” *J. Neurosci.*, vol. 29, no. 26, pp. 8595–8603, 2009.

[95] G. Laurent and M. Naraghi, “Odorant-induced oscillations in the mushroom bodies of the locust.,” *J. Neurosci.*, vol. 14, no. May, pp. 2993–3004, 1994.

[96] S. Yetman and G. S. Pollack, “Central projections of labellar taste hairs in the blowfly, Phormia regina Meigen,” *Cell Tissue Res.*, vol. 245, no. April, pp. 555–561, 1986.

[97] Z. Wang, A. Singhvi, P. Kong, and K. Scott, “Taste representations in the Drosophila brain,” *Cell*, vol. 117, no. 7, pp. 981–991, 2004.

[98] A. Manzo, M. Silies, D. M. Gohl, and K. Scott, “Motor neurons controlling fluid ingestion in Drosophila,” *Proc. Natl. Acad. Sci.*, vol. 109, no. 16, pp. 6307–6312, 2012.

[99] A. H. Pool, P. Kvello, K. Mann, S. K. Cheung, M. D. Gordon, L. Wang, and K. Scott, “Four GABAergic interneurons impose feeding restraint in Drosophila,” *Neuron*, vol. 83, no. 1, pp. 164–177, 2014.

[100] N. Yapici, R. Cohn, C. Schusterreiter, V. Ruta, and L. B. Vosshall, “A Taste Circuit that Regulates Ingestion by Integrating Food and Hunger Signals,” *Cell*, vol. 165, no. 3, pp. 715–729, 2016.

[101] T. F. Flood, S. Iguchi, M. Gorczyca, B. White, K. Ito, and M. Yoshihara, “A single pair of interneurons commands the Drosophila feeding motor program,” *Nature*, vol. 499, no. 7456, pp. 83–87, 2013.

[102] S. Lin, D. Owald, V. Chandra, C. Talbot, W. Huetteroth, and S. Waddell, “Neural correlates of water reward in thirsty Drosophila,” *Nat. Neurosci.*, vol. 17, no. 11, pp. 1536–1542, 2014.

[103] S. Reiter, C. Campillo Rodriguez, K. Sun, and M. Stopfer, “Spatiotemporal Coding of Individual Chemicals by the Gustatory System,” *J. Neurosci.*, vol. 35, no. 35, pp. 12309–12321, 2015.

[104] K. Von Frisch, “The dance language and orientation of bees.,” *Heredity (Edinb).*, vol. 90, no. 3, p. 212, 1967.

[105] M. Haydak, “Honey Bee Nutrition,” *Annu. Rev. Entomol.*, no. 6907, 1970.

[106] A. Arslan, L. N. Standifer, and H. Don, “Carbohydrates in honey bee Apis mellifera hemolymph,” *Comp. Biochem. Physiol. B Comp. Biochem.*, vol. 84, no. 3, pp. 363–368, 1986.

[107] G. R. Wykes, “The Preferences of Honeybees for Solutions of Various Sugars Which Occur in Nectar,” *J. Exp. Biol.*, vol. 29, no. 4, p. 511, 1952.

[108] V. Mommaerts, F. Wäckers, and G. Smagghe, “Assessment of gustatory responses to different sugars in harnessed and free-moving bumblebee workers (Bombus terrestris),” *Chem. Senses*, vol. 38, no. 5, pp. 399–407, 2013.

[109] H. W. Krenn, J. D. Plant, and N. U. Szucsich, “Mouthparts of flower-visiting insects,” *Arthropod Struct. Dev.*, vol. 34, no. 1, pp. 1–40, 2005.

[110] L. D. Harder, “Measurement and estimation of functional proboscis length in bumblebees (Hymenoptera: Apidae),” *Can. J. Zool.*, vol. 60, no. 5, pp. 1073–1079, 1982.

[111] S. S. Haupt, “Antennal sucrose perception in the honey bee (Apis mellifera L.): Behaviour and electrophysiology,” *J. Comp. Physiol. A Neuroethol. Sensory, Neural, Behav. Physiol.*, vol. 190, no. 9, pp. 735–745, 2004.

[112] M. F. Brill, M. Reuter, W. Rössler, and M. F. Strube-Bloss, “Simultaneous long-term recordings at two neuronal processing stages in behaving honeybees.,” *J. Vis. Exp.*, no. 89, p. 2014, 2014.

[113] B. M. Sadd, S. M. Barribeau, G. Bloch, and E. Al., “The genomes of two key bumblebee species with primitive eusocial organization,” *Genome Biol.*, vol. 16, no. 1, p. 76, 2015.

[114] H. M. Robertson, C. G. Warr, and J. R. Carlson, “Molecular evolution of the insect chemoreceptor gene superfamily in Drosophila melanogaster.,” *Proc. Natl. Acad. Sci. U. S. A.*, vol. 100 Suppl , pp. 14537–14542, 2003.

[115] H. M. Robertson and K. W. Wanner, “The chemoreceptor superfamily in the honey bee, Apis mellifera: Expansion of the odorant, but not gustatory, receptor family,” *Genome Res.*, vol. 16, no. 11, pp. 1395–1403, 2006.

[116] M. E. Bitterman, R. Menzel, A. Fietz, and S. Schäfer, “Classical conditioning of proboscis extension in honeybees (Apis mellifera).,” *J. Comp. Psychol.*, vol. 97, no. 2, pp. 107–119, 1983.

[117] M. Hammer, “An identified neuron mediates the unconditioned stimulus in associative olfactory learning in honeybees.” 1993.

[118] R. Menzel, “The honeybee as a model for understanding the basis of cognition,” *Nat. Rev. Neurosci.*, vol. 13, no. 11, pp. 758–768, 2012.

[119] M. Giurfa, “Behavioral and neural analysis of associative learning in the honeybee: A taste from the magic well,” *J. Comp. Physiol. A Neuroethol. Sensory, Neural, Behav. Physiol.*, vol. 193, no. 8, pp. 801–824, 2007.

[120] S. Alem, C. J. Perry, X. Zhu, O. J. Loukola, T. Ingraham, E. Søvik, and L. Chittka, “Associative Mechanisms Allow for Social Learning and Cultural Transmission of String Pulling in an Insect,” *PLOS Biol.*, pp. 1–28, 2016.

[121] B. D. Worden and D. R. Papaj, “Flower choice copying in bumblebees.,” *Biol. Lett.*, vol. 1, no. 4, pp. 504–507, 2005.

[122] O. J. Loukola and L. Chittka, “Bumblebees show cognitive flexibility by improving on an observed complex behavior,” vol. 836, no. February, pp. 833–836, 2017.

[123] D. Laloi, B. Roger, M. Blight Margaret, J. Wadhams Lester, and H. Pham Delegue Minh, “Individual learning ability and complex odor recognition in the honey bee, Apis mellifera L,” *J. Insect Behav. [print] Sept., 1999;*, vol. 12, no. 5, pp. 585–597., 1999.

[124] A. Dornhaus and L. Chittka, “Information flow and regulation of foraging activity in bumble bees (Bombus spp.),” *Apidologie*, vol. 37, pp. 275–292, 2006.

[125] B. Heinrich, “The Physiology of Exercise in the Bumblebee: Bumblebees are limited in their superb athletic performance by extremes of air temperature, but by regulating their body temperature they achieve considerable control,” *Sigma Xi*, vol. 65, no. 4, pp. 455–465, 2014.

[126] J. L. Osborne, A. P. Martin, N. L. Carreck, J. L. Swain, M. E. Knight, D. Goulson, R. J. Hale, and R. A. Sanderson, “Bumblebee flight distances in relation to the forage landscape,” *J. Anim. Ecol.*, vol. 77, no. 2, pp. 406–415, 2008.

[127] W. Stephan and F. A. M. Robin, “Foraging distance in Bombus terrestris L. (Hymenoptera: Apidae),” *Apidologie*, vol. 39, pp. 419–427, 2008.

[128] J. Cnaani, J. D. Thomson, and D. R. Papaj, “Flower choice and learning in foraging bumblebees: Effects of variation in nectar volume and concentration,” *Ethology*, vol. 112, no. 3, pp. 278–285, 2006.

[129] C. I. Bargmann, “Comparative chemosensation from receptors to ecology.,” *Nature*, vol. 444, no. 7117, pp. 295–301, 2006.

[130] B. Lindemann, “Receptors and transduction in taste.,” *Nature*, vol. 413, no. 6852, pp. 219–225, 2001.

[131] R. Dando and S. D. Roper, “Cell-to-cell communication in intact taste buds through ATP signalling from pannexin 1 gap junction hemichannels.,” *J. Physiol.*, vol. 587, no. Pt 24, pp. 5899–906, 2009.

[132] S. M. Royer and J. C. Kinnamon, “Ultrastructure of mouse foliate taste buds: synaptic and nonsynaptic interactions between taste cells and nerve fibers,” *J. Comp. Neurol.*, vol. 270, no. 1, pp. 11–24,58–59, 1988.

[133] C. Pouzat, O. Mazor, and G. Laurent, “Using noise signature to optimize spike-sorting and to assess neuronal classification quality,” *J. Neurosci. Methods*, vol. 122, no. 1, pp. 43–57, 2002.

[134] D. N. Hill, S. B. Mehta, and D. Kleinfeld, “Quality metrics to accompany spike sorting of extracellular signals.,” *J. Neurosci.*, vol. 31, no. 24, pp. 8699–8705, 2011.

[135] G. Buzsáki, C. a. Anastassiou, and C. Koch, “The origin of extracellular fields and currents — EEG, ECoG, LFP and spikes,” *Nat. Rev. Neurosci.*, vol. 13, no. 6, pp. 407–420, 2012.

[136] H. G. Rey, C. Pedreira, and R. Quian Quiroga, “Past, present and future of spike sorting techniques,” *Brain Res. Bull.*, vol. 119, pp. 106–117, 2015.

[137] M. S. Fee, P. P. Mitra, and D. Kleinfeld, “Variability of extracellular spike waveforms of cortical neurons.,” *J. Neurophysiol.*, vol. 76, no. 6, pp. 3823–33, 1996.

[138] R. Quian Quiroga, “What is the real shape of extracellular spikes?,” *J. Neurosci. Methods*, vol. 177, no. 1, pp. 194–198, 2009.

[139] C. a Anastassiou, R. Perin, H. Markram, and C. Koch, “Ephaptic coupling of cortical neurons.,” *Nat. Neurosci.*, vol. 14, no. 2, pp. 217–223, 2011.

[140] J. F. Storm, “An after-hyperpolarization of medium duration in rat hippocampal pyramidal cells.,” *J. Physiol.*, vol. 409, pp. 171–90, 1989.

[141] N. Gu, K. Vervaeke, H. Hu, and J. F. Storm, “Kv7/KCNQ/M and HCN/h, but not KCa2/SK channels, contribute to the somatic medium after-hyperpolarization and excitability control in CA1 hippocampal pyramidal cells.,” *J. Physiol.*, vol. 566, no. Pt 3, pp. 689–715, 2005.

[142] M. Ito and T. Oshima, “Temporal Summation of After-Hyperpolarization following a Motoneurone Spike,” *Nature*, vol. 195, no. 4844, pp. 910–911, 1962.

[143] R. Falk, N. Bleiser Avivi, and J. Atidia, “Labellar taste organs of Drosophila melanogaster,” *J. Morphol.*, vol. 150, no. 2, pp. 327–341, 1976.

[144] R. N. Nayak, S. V., Singh, “Sensilla on the tarsal segment and mouthparts of adult Drosophila melanogaster Meigen (Diptera: Drosophilidae),” *Int. J. Insect Morphol. Embryol.*, vol. 12, no. 5/6, pp. 273–291, 1983.

[145] B. T. Felt and J. S. Vande Berg, “Ultrastructure of the blowfly chemoreceptor sensillum (Phormia regina),” *J. Morphol.*, vol. 150, no. 3, pp. 763–783, 1976.

[146] E. Hansen-Delkeskamp and K. Hansen, “Responses and spike generation in the largest antennal taste hairs of Periplaneta brunnea Burm.,” *J. Insect Physiol.*, vol. 41, no. 9, pp. 773–781, 1995.

[147] J. J. de Kramer, “The electrical circuitry of an olfactory sensillum in Antheraea polyphemus.,” *J. Neurosci.*, vol. 5, no. 9, pp. 2484–2493, 1985.

[148] P. L. Newland, “Avoidance reflexes mediated by contact chemoreceptors on the legs of locusts,” *J. Comp. Physiol. - A Sensory, Neural, Behav. Physiol.*, vol. 183, no. 3, pp. 313–324, 1998.

[149] K. R. Szulewski, “Base recordings from caterpillar taste sensilla reveal new insights into taste coding mechanisms,” *Masters Thesis*, no. May, 2010.

[150] T. Tanimura, M. Hiroi, T. Inoshita, and F. Marion-Poll, “Neurophysiology of gustatory receptor neurones in Drosophila.,” *SEB Exp. Biol. Ser.*, vol. 63, pp. 59–76, Jan. 2009.

[151] C. Gold, D. A. Henze, C. Koch, and G. Buzsáki, “On the Origin of the Extracellular Action Potential Waveform : A Modeling Study On the Origin of the Extracellular Action Potential Waveform : A Modeling Study,” *J Neurophysiol*, vol. 95, pp. 3113–3128, 2006.

[152] M. S. Fee, P. P. Mitra, and D. Kleinfeld, “Automatic sorting of multiple unit neuronal signals in the presence of anisotropic and non-Gaussian variability,” *J. Neurosci. Methods*, vol. 69, no. 2, pp. 175–188, 1996.

[153] R. Q. Quiroga, Z. Nadasdy, and Y. Ben-Shaul, “Unsupervised spike detection and sorting with wavelets and superparamagnetic clustering.,” *Neural Comput.*, vol. 16, no. 8, pp. 1661–1687, 2004.

[154] F. Marion-Poll and T. R. Tobin, “Software filter for detecting spikes superimposed on a fluctuating baseline,” *J. Neurosci. Methods*, vol. 37, no. 1, pp. 1–6, 1991.

[155] M. Hiroi, F. Marion-Poll, and T. Tanimura, “Differentiated response to sugars among labellar chemosensilla in Drosophila.,” *Zoolog. Sci.*, vol. 19, no. 9, pp. 1009–1018, 2002.

[156] A. Liscia, C. Masala, R. Crnjar, G. Sollai, and P. Solari, “Saccharin stimulates the ‘deterrent’ cell in the blowfly: Behavioral and electrophysiological evidence,” *Physiol. Behav.*, vol. 80, no. 5, pp. 637–646, 2004.

[157] E. . Glaser and W. . Marks, “On-line separation of interleaved neuronal pulse sequences,” pp. 137–156, 1968.

[158] W. Press, S. Teukolsky, W. Vetterling, and B. Flannery, “Numerical recipes in C: the art of scientific computing, 1992,” *Cité en*, vol. 1, pp. 1–1018, 1992.

[159] M. S. Lewicki, “Network : Computation in Neural Systems A review of methods for spike sorting : the detection and classification of neural action potentials classification of neural action potentials,” vol. 6536, no. November, 2016.

[160] M. Sahani, “Latent Variable Models for Neural Data Analysis Maneesh Sahani,” *Electr. Eng.*, vol. 1999, 1999.

[161] M. Blatt, S. Wiseman, and E. Domany, “Superparamagnetic Clustering of Data,” *Phys. Rev. Lett.*, vol. 76, pp. 3251–3254, 1996.

[162] Z. Xu, J. R. Payne, and M. E. Nelson, “Logarithmic time course of sensory adaptation in electrosensory afferent nerve fibers in a weakly electric fish.,” *J. Neurophysiol.*, vol. 76, no. 3, pp. 2020–2032, 1996.

[163] J. Thorson and M. Biederman-Thorson, “Distributed relaxation processes in sensory adaptation.,” *Science*, vol. 183, no. 4121, pp. 161–72, 1974.

[164] C. a Shumway, “Multiple electrosensory maps in the medulla of weakly electric gymnotiform fish. I. Physiological differences.,” *J. Neurosci.*, vol. 9, no. 12, pp. 4388–99, 1989.

[165] Z. N. Aldworth and M. A. Stopfer, “Trade-off between information format and capacity in the olfactory system.,” *J. Neurosci.*, vol. 35, no. 4, pp. 1521–9, 2015.

[166] L. Chen, Y. Deng, W. Luo, Z. Wang, and S. Zeng, “Detection of bursts in neuronal spike trains by the mean inter-spike interval method,” *Prog. Nat. Sci.*, vol. 19, no. 2, pp. 229–235, 2009.

[167] M. Chiappalone, A. Novellino, I. Vajda, A. Vato, S. Martinoia, and J. van Pelt, “Burst detection algorithms for the analysis of spatio-temporal patterns in cortical networks of neurons,” *Neurocomputing*, vol. 65–66, no. SPEC. ISS., pp. 653–662, 2005.

[168] Y. Kaneoke and J. L. Vitek, “Burst and oscillation as disparate neuronal properties,” *J. Neurosci. Methods*, vol. 68, no. 2, pp. 211–223, 1996.

[169] E. Omand and V. G. Dethier, “An Electrophysiological Analysis of the Action of Carbohydrates on the Sugar Receptor of the Blowfly,” *Eur. Biophys. J.*, pp. 136–143, 1968.

[170] H. Wieczorek and G. Wolff, “The labellar sugar receptor of Drosophila,” *J. Comp. Physiol. A*, vol. 164, no. 6, pp. 825–834, 1989.

[171] S. Kessler, M. Vlimant, and P. M. Guerin, “Sugar-sensitive neurone responses and sugar feeding preferences influence lifespan and biting behaviours of the Afrotropical malaria mosquito, Anopheles gambiae,” *J. Comp. Physiol. A Neuroethol. Sensory, Neural, Behav. Physiol.*, vol. 201, no. 3, pp. 317–329, 2015.

[172] H. Kwon, M. Ali Agha, R. C. Smith, R. J. Nachman, F. Marion-Poll, and P. V. Pietrantonio, “Leucokinin mimetic elicits aversive behavior in mosquito *Aedes aegypti* (L.) and inhibits the sugar taste neuron,” *Proc. Natl. Acad. Sci.*, p. 201520404, 2016.

[173] E. Hansen-Delkeskamp, “Development of specific responses in antennal taste hairs after ecdysis. An electrophysiological investigation of the coackroach, Periplaneta brunnea,” *J. Insect Physiol.*, vol. 44, no. 7–8, pp. 659–666, 1998.

[174] R. Brodschneider and K. Crailsheim, “Nutrition and health in honey bees,” *Apidologie*, vol. 41, no. 3, pp. 278–294, 2010.

[175] C. Ritz and J. Strebig, “Analysis of Dose Response Curves.” 2015.

[176] M. Ozaki and T. Amakawa, “Adaptation-promoting effect of IP3, Ca2+, and phorbol ester on the sugar taste receptor cell of the blowfly, Phormia regina,” *J Gen Physiol*, vol. 100, no. 5, pp. 867–879, 1992.

[177] S. Gothilf, R. Galun, and M. Bar-Zeev, “Taste reception in the Mediterranean fruit fly: Electrophysiological and behavioural studies,” *J. Insect Physiol.*, vol. 17, no. 7, pp. 1371–1384, 1971.

[178] a Wada, Y. Isobe, S. Yamaguchi, R. Yamaoka, and M. Ozaki, “Taste-enhancing effects of glycine on the sweetness of glucose: a gustatory aspect of symbiosis between the ant,

Camponotus japonicus, and the larvae of the lycaenid butterfly, Niphanda fusca.," *Chem. Senses*, vol. 26, no. 8, pp. 983–992, 2001.

[179] T. Miyazaki and K. Ito, "Neural architecture of the primary gustatory center of Drosophila melanogaster visualized with GAL4 and LexA enhancer-trap systems," *J. Comp. Neurol.*, vol. 518, no. 20, pp. 4147–4181, 2010.

[180] S. Antic, J. P. Wuskell, L. Loew, and D. Zecevic, "Functional profile of the giant metacerebral neuron of Helix aspersa: temporal and spatial dynamics of electrical activity in situ.," *J. Physiol.*, vol. 527 Pt 1, pp. 55–69, 2000.

[181] D. Zecević, "Multiple spike-initiation zones in single neurons revealed by voltage-sensitive dyes.," *Nature*, vol. 381, no. 6580. pp. 322–325, 1996.

[182] H. Wieczorek and R. Köppl, "Effect of sugars on the labellar water receptor of the fly," *J. Comp. Physiol. □ A*, vol. 126, no. 2, pp. 131–136, 1978.

[183] J. I. Glendinning, A. Jerud, and A. T. Reinherz, "The hungry caterpillar: an analysis of how carbohydrates stimulate feeding in Manduca sexta.," *J. Exp. Biol.*, vol. 210, no. Pt 17, pp. 3054–3067, 2007.

[184] A. Wada-Katsumata, J. Silverman, and C. Schal, "Changes in taste neurons support the emergence of an adaptive behavior in cockroaches.," *Science*, vol. 340, no. 6135, pp. 972–5, 2013.

[185] N. L. Golding, H. Y. Jung, T. Mickus, and N. Spruston, "Dendritic calcium spike initiation and repolarization are controlled by distinct potassium channel subtypes in CA1 pyramidal neurons.," *J. Neurosci.*, vol. 19, no. 20, pp. 8789–98, 1999.

[186] M. E. Larkum, J. J. Zhu, and B. Sakmann, "A new cellular mechanism for coupling inputs arriving at different cortical layers.," *Nature*, vol. 398, no. 6725, pp. 338–341, 1999.

[187] N. Lemon and R. W. Turner, "Conditional spike backpropagation generates burst discharge in a sensory neuron.," *J. Neurophysiol.*, vol. 84, no. 3, pp. 1519–1530, 2000.

[188] J. E. Lisman, "Bursts as a unit of neural information: Making unreliable synapses reliable," *Trends Neurosci.*, vol. 20, no. 1, pp. 38–43, 1997.

[189] S. Murray Sherman, "Tonic and burst firing: Dual modes of thalamocortical relay," *Trends Neurosci.*, vol. 24, no. 2, pp. 122–126, 2001.

[190] M. R. Freeman and J. Doherty, "Glial cell biology in Drosophila and vertebrates," *Trends in Neurosciences*, vol. 29, no. 2. pp. 82–90, 2006.

[191] B. I. Roots, "The phylogeny of invertebrates and the evolution of myelin.," *Neuron Glia Biol.*, vol. 4, no. 2, pp. 101–109, 2008.

[192] M. Galarreta and S. Hestrin, “Electrical synapses between GABA-releasing interneurons.,” *Nat. Rev. Neurosci.*, vol. 2, no. 6, pp. 425–433, 2001.

[193] M. Rasminsky, “Ephaptic transmission between single nerve fibres in the spinal nerve roots of dystrophic mice.,” *J. Physiol.*, vol. 305, pp. 151–69, 1980.

[194] F. Ramón and J. W. Moore, “Ephaptic transmission in squid giant axons.,” *Am. J. Physiol.*, vol. 234, no. 5, pp. C162–C169, 1978.

[195] J. M. Power, C. Bocklisch, P. Curby, and P. Sah, “Location and function of the slow afterhyperpolarization channels in the basolateral amygdala.,” *J. Neurosci.*, vol. 31, no. 2, pp. 526–537, 2011.

[196] H. P. Larsson, “What determines the kinetics of the slow afterhyperpolarization (sAHP) in neurons?,” *Biophys. J.*, vol. 104, no. 2, pp. 281–283, 2013.

[197] J. R. Hotson and D. a Prince, “A calcium-activated hyperpolarization follows repetitive firing in hippocampal neurons.,” *J. Neurophysiol.*, vol. 43, no. 2, pp. 409–419, 1980.

[198] C. T. Bond, “Small Conductance Ca2+-Activated K+ Channel Knock-Out Mice Reveal the Identity of Calcium-Dependent Afterhyperpolarization Currents,” *J. Neurosci.*, vol. 24, no. 23, pp. 5301–5306, 2004.

[199] N. Savić, P. Pedarzani, and M. Sciancalepore, “Medium afterhyperpolarization and firing pattern modulation in interneurons of stratum radiatum in the CA3 hippocampal region.,” *J. Neurophysiol.*, vol. 85, no. 5, pp. 1986–1997, 2001.

[200] J. K. Jansen and J. G. Nicholls, “Conductance changes, an electrogenic pump and the hyperpolarization of leech neurones following impulses.,” *J. Physiol.*, vol. 229, no. 3, pp. 635–55, 1973.

[201] B. E. Alger and R. A. Nicoll, “Epileptiform burst afterhyperpolarization: calcium-dependent potassium potential in hippocampal CA1 pyramidal cells,” *Science (80-.).*, vol. 210, no. 4474, pp. 1122–1124, 1980.

[202] B. Leitch, B. Leitch, G. Laurent, and G. Laurent, “GABAergic Synapses in the Antenna1 Lobe and Mushroom Body of the Locust Olfactory System,” *J. Comp. Neurol.*, vol. 514, no. 372, pp. 487–514, 1996.

[203] A. Blot and B. Barbour, “Ultra-rapid axon-axon ephaptic inhibition of cerebellar Purkinje cells by the pinceau.,” *Nat. Neurosci.*, vol. 17, no. 2, pp. 289–95, 2014.

[204] H. Korn and H. Axelrad, “Electrical inhibition of Purkinje cells in the cerebellum of the rat.,” *Proc. Natl. Acad. Sci. U. S. A.*, vol. 77, no. 10, pp. 6244–7, 1980.

[205] E. J. Furshpan, "'Electrical Transmission' At an Excitatory Synapse in a Vertebrate Brain.," *Science*, vol. 144, no. 3620, pp. 878–80, 1964.

[206] K. Kaissling, "Chemo-Electrical Transduction in Insect Olfactory Receptors," *Annu. Rev. Neurosci.*, vol. 9, no. 1, pp. 121–145, 1986.

[207] V. M. Pasztor and B. M. H. Bush, "Impulse-Coded and Analog Signaling in Single Mechanoreceptor Neurons," no. October, 1981.

[208] B. Y. A. J. Hudspeth and A. N. N. E. Stuart, "Morphology and Responses to Light of the Somata, Axons, and Terminal Regions of Individual Photoreceptors of the Giant Barnacle," pp. 1–23, 1977.

[209] K. S. Kent and L. M. Griffin, "Sensory organs of the thoracic legs of the moth Manduca sexta," *Cell Tissue Res.*, vol. 259, no. 2, pp. 209–223, 1990.

[210] W. Bialek and R. R. Van Steveninck, "Real-time performance of a movement-sensitive neuron in the blowfly visual system: coding and information transfer in short spike sequences," *Proc. R. Soc. London*, vol. B-234, pp. 379–414, 1988.

[211] A.-M. M. Oswald, "Parallel Processing of Sensory Input by Bursts and Isolated Spikes," *J. Neurosci.*, vol. 24, no. 18, pp. 4351–4362, 2004.

[212] J. Keat, P. Reinagel, R. C. Reid, and M. Meister, "Predicting Every Spike: A Model for the Responses of Visual Neurons," *Neuron*, vol. 30, pp. 803–817, 2001.

[213] S. Martinez-Conde, S. L. Macknik, and D. H. Hubel, "The function of bursts of spikes during visual fixation in the awake primate lateral geniculate nucleus and primary visual cortex.," *Proc. Natl. Acad. Sci. U. S. A.*, vol. 99, no. 21, pp. 13920–5, 2002.

[214] R. Krahe and F. Gabbiani, "Burst firing in sensory systems.," *Natrevnsci*, vol. 5, no. 1, pp. 13–23, 2004.

[215] F. G. Pike, R. M. Meredith, A. W. A. Olding, and O. Paulsen, "Postsynaptic bursting is essential for 'Hebbian' induction of associative long-term potentiation at excitatory synapses in rat hippocampus," *J. Physiol.*, vol. 518, no. 2, pp. 571–576, 1999.

[216] A. L. Fairhall, G. D. Lewen, W. Bialek, and R. R. de Ruyter Van Steveninck, "Efficiency and ambiguity in an adaptive neural code.," *Nature*, vol. 412, no. 6849, pp. 787–92, 2001.

[217] M. Juusola, R. O. Uusitalo, and M. Weckström, "Transfer of graded potentials at the photoreceptor-interneuron synapse.," *J. Gen. Physiol.*, vol. 105, no. 1, pp. 117–148, 1995.

[218] M. Stopfer, S. Bhagavan, B. H. Smith, and G. Laurent, "Impaired odour discrimination on desynchronization of odour-encoding neural assemblies.," *Nature*, vol. 390, no. 6655, pp. 70–74, 1997.

[219] C. M. Hodges and L. L. Wolf, “Optimal foraging in bumblebees: Why is nectar left behind in flowers?,” *Behav. Ecol. Sociobiol.*, vol. 9, no. 1, pp. 41–44, 1981.

[220] C. Ma, S. Kessler, A. Simpson, and G. Wright, “A Novel Behavioral Assay to Investigate Gustatory Responses of Individual, Freely-moving Bumble Bees (Bombus terrestris),” *J. Vis. Exp.*, no. 113, pp. 1–7, 2016.

[221] T. A. Christensen and J. G. Hildebrand, “Male-specific, sex pheromone-selective projection neurons in the antennal lobes of the moth Manduca sexta,” *J. Comp. Physiol. A*, vol. 160, no. 5, pp. 553–569, 1987.

[222] N. T. Davis and J. G. Hildebrand, “Neuroanatomy of the sucking pump of the moth, Manduca sexta (Sphingidae, Lepidoptera),” *Arthropod Struct. Dev.*, vol. 35, no. 1, pp. 15–33, 2006.

[223] S. R. Olsen and R. I. Wilson, “Lateral presynaptic inhibition mediates gain control in an olfactory circuit,” *Nature*, vol. 452, no. 7190, pp. 956–960, 2008.

[224] M. Stopfer, V. Jayaraman, and G. Laurent, “Intensity versus identity coding in an olfactory system,” *Neuron*, vol. 39, no. 6, pp. 991–1004, 2003.

[225] R. I. Wilson and G. Laurent, “Role of GABAergic inhibition in shaping odor-evoked spatiotemporal patterns in the Drosophila antennal lobe.,” *J. Neurosci.*, vol. 25, no. 40, pp. 9069–79, 2005.

[226] Q. Liu, X. Yang, J. Tian, Z. Gao, M. Wang, Y. Li, and A. Guo, “Gap junction networks in mushroom bodies participate in visual learning and memory in Drosophila,” *Elife*, vol. 5, no. MAY2016, pp. 1–18, 2016.